The Thesis Committee for Mitchel Joseph Bartolo
Certifies that this is the approved version of the following thesis:

Mechanisms of Ligand Removal and Competition in Aluminum Salt Coagulation Systems: Insights Using ATR-FTIR Spectroscopy

APPROVED BY
SUPERVISING COMMITTEE:

Lynn E. Katz, Co-Supervisor

Desmond F Lawler, Co-Supervisor

Mechanisms of Ligand Removal and Competition in Aluminum Salt Coagulation Systems: Insights Using ATR-FTIR Spectroscopy

by

Mitchel Joseph Bartolo, B.S.

Thesis

Presented to the Faculty of the Graduate School of

The University of Texas at Austin

in Partial Fulfillment

of the Requirements

for the Degree of

Master of Science in Engineering

The University of Texas at Austin

May 2016

Acknowledgements

I would first like to thank my co-advisors, Dr. Lynn Katz and Dr. Desmond Lawler for granting me the opportunity to fulfill my goal of obtaining a graduate degree from a prestigious research institution. Beyond the fact that they are both leaders in our field, these professors are the most personable, genuine, and supportive advisors I could ask for and the passion that they express for their work in water inspires me every day. I would also like to thank Dr. Satish Myneni, for without his expertise and collaboration, we would not have gained the invaluable spectroscopic insights that we did. Katherine, Mark, Isababella, Ki, and Jon: this project was a team effort and I truly appreciate the work that all of you have contributed. I'd like to thank my family for their endless support and the bond of brotherhood that followed me to Austin. Lastly, my time here would not have been as memorable as it was without the amazing family we call EWRE. I will forever cherish the lifelong friendships that I have established during my time in this program.

Abstract

Mechanisms of Ligand Removal and Competition in Aluminum Salt Coagulation Systems: Insights Using ATR-FTIR Spectroscopy

Mitchel Joseph Bartolo, M.S.E.

The University of Texas at Austin, 2016

Co-Supervisors: Lynn E. Katz and Desmond F. Lawler

Fluoride, while beneficial in moderate to low doses, has detrimental health effects associated with chronic exposure to elevated concentrations from sources such as drinking water. Natural organic matter (NOM) is ubiquitous in many drinking water sources and can contribute to the formation of carcinogenic disinfection by-products (DBPs). In an era marked by increasing concerns for drinking water quality and increased costs to produce high quality drinking water, small water systems (SWSs) are the most vulnerable due to their lack of financial and operational resources. Aluminum salt coagulation processes have the potential to remove both fluoride and NOM, and would be advantageous to a SWS since the technology has been widely used for decades. However, the removal mechanisms and interactions among competing contaminants remain poorly understood. This study aims to elucidate the mechanisms of removal and better understand the competition that occurs in a coagulation system by using a combination of spectroscopic insights at the solid surfaces and macroscopic insights from aqueous removal levels.

Attenuated total reflectance Fourier transform infrared spectroscopy provided insights at the solid-aqueous interface where it was concluded that sulfate and pyromellitate (an NOM surrogate) adsorb via outer-sphere complexation while fluoride, silicate, and carbonate create inner-sphere surface complexes. It was also evident that silicate accumulated and polymerized at the aluminum hydroxide surface with time. Both fluoride and pyromellitate exhibited greater removal efficiencies in waters containing sulfate versus chloride, suggesting that sulfate has a higher affinity for the surface than chloride. Fluoride and pyromellitate removals were also reduced at the higher pH of 7.5 due to increased aluminum solubility and competition with inner-sphere complexed carbonate. Pyromellitate removal is significantly impacted by the presence of fluoride whereas fluoride removal is marginally impacted by the presence of pyromellitate. This was explained by the inner-sphere complex that fluoride forms in comparison to the weaker electrostatic interaction of pyromellitate. Silicate was observed to reduce fluoride and pyromellitate removals both initially and with time due to competition for surface bonding sites. Over time, the accumulation and polymerization of silicate is believed to be responsible for desorption of fluoride and pyromellitate.

Table of Contents

List of Tables

List of Figures

Chapter 1: Introduction

1.1 Background and Motivation

Much like liberty, property, and education, the United Nations explicitly recognizes access to clean drinking water as a basic human right (United Nations, 2010). The removal of pathogens, particles, and chemical substances that constitute threats to human health, as well as aesthetics, are the main objectives in drinking water treatment. Only upon the completion of these objectives can a drinking water be deemed safe and clean in accordance with this human right. Fluoride is a chemical constituent of drinking water that is both naturally occurring in source waters and added by municipalities. At low quantities, fluoride is an essential nutrient for the strengthening of dental enamel and bones during mineralization (Meenkashi and Maheshwari, 2006; Mohapatra et al., 2009). However, chronic exposure to excessive fluoride concentrations in drinking water can lead to the discoloration of teeth and the embrittlement of teeth and bones resulting in the conditions known as dental and skeletal fluorosis (Eklund et al., 1987; Meenkashi and Maheshwari, 2006; Mohapatra et al., 2009). These elevated fluoride concentrations are endemic to more than 20 countries of varying development status including the United States (U.S.), India, Argentina, China, Canada, Turkey, and numerous African nations (Ayoob and Gupta, 2006; Meenkashi, 2006). Within the US, enforceable regulation of fluoride in drinking water began in 1987 when the United States Environmental Protection Agency (USEPA) finalized a maximum contaminant level (MCL) of 4.0 mg/L under the Safe Drinking Water Act (SDWA). While the MCL was enacted to protect against the more crippling effects of skeletal fluorosis, a non-mandatory secondary maximum contaminant level (SMCL) of 2.0 mg/L was put forth to abate the more

cosmetically problematic dental fluorosis (USEPA, 2003). In 2003 and 2010, the USEPA included fluoride in their Six-Year Reviews of 71 national primary drinking water standards (NPDWRs) to determine whether the current MCL needs revision (USEPA, 2003; USEPA, 2010). In each of these reviews, the impacts of fluoride on dental and skeletal health were noted; however, further dose-response assessment was deemed necessary before any revisions to the MCL would occur (USEPA, 2010).

In light of these detrimental health effects, many technologies have been used for the removal of fluoride from drinking water. Membrane techniques include reverse osmosis (RO), nanofiltration, dialysis, and electro-dialysis (ED) (Meenkashi and Maheshwari, 2006; Mohapatra et al., 2009). Adsorption-based techniques such as activated alumina columns and ion-exchange onto various synthetic resins are prevalent. Coagulation and precipitation processes that employ coagulants such as lime, alum, and other aluminum salts are also widely accepted for fluoride removal; however, their ability to meet lower regulatory standards is uncertain (Meenkashi and Maheshwari, 2006; Mohapatra et al., 2009; Srimurali et al., 1997).

Many drinking water treatment plants in the U.S. rely on these latter coagulation processes in their conventional treatment trains for particle and natural organic matter (NOM) removal. NOM is problematic in drinking water due to its contribution to taste and odor issues as well as the more serious concern of disinfection by-product (DBP) formation. In chlorine-disinfected drinking waters, chlorine and NOM can react to form DBPs in a number of ways (Matilainen et al., 2010; Singer, 1994; Westerhoff et al., 2004). The problem is exacerbated with natural waters containing bromide, another halogen that can contribute to DBP formation (Singer, 1994; Westerhoff et al., 2004). DBPs have been linked to several forms of cancer, with chronic exposure and more acute reproductive and developmental harm expected at higher concentrations (Boorman et al.,

1999; Singer et al., 1995; Westerhoff et al., 2004). Other inorganic anions that are ubiquitous in surface waters such as sulfate, silicate, and carbonate are known to compete with fluoride and NOM in removal processes (Meenkashi and Maheshwari, 2006; Mohapatra et al., 2009; Croue et al., 1999; Korshin et al., 1997). The current understanding of the interactions among fluoride, NOM, and inorganic ions in the context of drinking water is deficient.

In the likely event that the USEPA resolves to lower the MCL for fluoride, affected small water systems (SWSs) will likely face the greatest challenge in meeting new MCLs. More than 94 percent of the nation's public water systems (PWS) serve fewer than 3,300 persons, and these SWSs lack the financial and operational capacities required for more advanced, costly fluoride removal processes such as RO, ED, and ion-exchange (USEPA, 2015; Meenkashi and Maheshwari, 2006). Therefore, the coagulation process offers a potentially viable solution for fluoride removal with virtually no changes to conventional treatment infrastructure and minimal changes to plant operation. However, a mechanistic understanding of the interactions that occur during the simultaneous removal of fluoride, NOM, and other ions present in the source water is currently lacking. Due to the public health concerns of NOM and fluoride in drinking water, it is essential to fully comprehend the competitive removal mechanisms at play in these systems to better inform the design and operating guidelines of coagulation processes.

1.2 Objectives of this Study

The goal of this work was to further investigate the specific removal mechanisms of NOM and other inorganic ions at the solid-aqueous interface in an aluminum salt

coagulation treatment scheme. The coagulation treatment process was simulated at the laboratory scale with batch reactor jar tests. These jar tests were administered over a set of prescribed synthetic water conditions with varied ligand compositions. Analyses of the chemical makeup of both the aqueous supernatants and the settled solids elucidated the ligand removal mechanisms in the system. The overall objectives of this investigation are summarized as follows:

1. Elucidate the adsorption mechanisms of various ligands in synthetic drinking water matrices with *in situ* Attenuated Total Reflectance-Fourier Transform Infrared Spectroscopy (ATR-FTIR) analysis of settled precipitates from jar tests containing varying ligand mixtures and aged for varying lengths of time,
2. Investigate competition among ligands based on the individual adsorption mechanisms by using the findings from ATR-FTIR and the macroscopic aqueous removal levels, and
3. Investigate the impact of precipitate aging on ligand competition and ligand removal using the findings from ATR-FTIR and the macroscopic aqueous residuals.

The remainder of this document explains how these objectives were accomplished and is organized into five chapters. Chapter 2 is comprised of a detailed literature review which covers relevant background information spanning from the health impacts of these compounds to prior findings on ligand removal mechanisms, coordination chemistry, and solids analyses. Chapter 3 illustrates the methodology and materials used in these experiments while Chapter 4 includes a thorough account of the results and discussion. A conclusion of findings and a discussion of future work are covered in Chapter 5.

Chapter 2: Literature Review

2.1 Fluoride, DBPs, and Public Health

Fluoride and DBPs in drinking water present significant risks to public health. In an era marked by increasing concerns for drinking water quality and increased costs to produce high quality drinking water, SWSs are the most vulnerable due to their lack of financial and operational resources. Both fluoride and DBPs have the potential to be removed in a conventional aluminum salt coagulation scheme, which could be operationally and financially advantageous for small systems. A review of the public health implications of fluoride and DBPs are offered in the following two sections.

2.1.1 Fluoride Human Health Impacts

The dichotomous public health history of fluoride makes it a unique constituent of concern in public drinking water systems. Fluoride has long been touted as a promoter of dental health. Dental caries, the demineralization of teeth due to acid production of mouth bacteria, is one of the most prevalent, yet preventable, chronic diseases worldwide (Featherstone, 1999; Selwitz et al., 2007). Found in dental products as well as food and beverages, fluoride acts topically by inhibiting acid demineralization, enhancing remineralization at the tooth surface, and inhibiting bacterial enzymes (Ayoob and Gupta, 2006; Featherstone, 1999). Tooth enamel is similar in nature to hydroxyapatite [$Ca_{10}(PO_4)_6(OH)_2$], but is highly substituted with carbonate in the place of phosphate and sodium or magnesium in the place of calcium. These substitutions make the enamel much more susceptible to acid demineralization (Featherstone, 1999). Negatively charged fluoride ions in saliva can adsorb to enamel surfaces, attracting phosphate and calcium ions as well. The localization of these ions on enamel surfaces promotes remineralization of a more hydroxyapatite-like structure. Beyond this, fluoride can substitute for hydroxyl

anions creating fluorapatite [$Ca_{10}(PO_4)_6(F)_2$], a mineral much more resistant to acid decay. Fluoride can also decrease acid production in bacteria by inhibiting enzymatic activity (Ayoob and Gupta, 2006; Featherstone, 1999). For these reasons drinking water fluoridation, which began in the U.S. in 1945, has been described as one of the ten most important public health advances of the 20th Century (Mullen, 2005).

The above benefits, however, depict only half of the fluoride story. The advantages of enamel hardening and decay prevention occur in the concentration range slightly lower than 1.0 mg/L up to around 1.5 mg/L fluoride (Fawell et al., 2006; Mohapatra et al., 2009; Ayoob and Gupta 2006). At levels above this, dental fluorosis is likely to occur, which is characterized by a hypomineralizations, or the creation of pores within the tooth mineral. This complex biochemical process stems from an altered mineralization environment with excessive fluoride substitution (Aoba and Fejerskov, 2002; DenBesten, 1999). Symptoms of dental fluorosis include enamel discoloration ranging from opaque white, to yellow, and eventually brown and black in more serious cases (Meenkashi and Maheshwari, 2006; Ayoob and Gupta, 2006). Both dose and duration of exposure play into the severity of dental fluorosis, and the dose-response curve is linear, indicating continuous impact of fluoride on tooth enamel (Aoba and Fejerskov, 2002; DenBesten, 1999). Prolonged exposure to higher concentrations (> 4 mg/L) can lead to a more serious form of fluorosis within the bone. Skeletal fluorosis is characterized by abnormal densification, mottling, fracture, and deformation of bone. Much like dental fluorosis, the skeletal condition is due to an increased accumulation of fluoride within the bone, which results in impaired collagen synthesis and the rapid mineralization of denser, yet more brittle, bone structures (Mohapatra et al., 2009; Boivin et al., 1989; Ayoob and Gupta, 2006). Estimates range from 70 to 200 million people that are at risk for both skeletal and dental fluorosis worldwide, with the majority of cases

stemming from water quality issues in China and India (Fawell et al., 2006; Ayoob and Gupta, 2006). Beyond fluorosis, numerous epidemiological studies have been conducted on fluoride-related cancers and the impairment of renal function, child development, and reproduction. However, more research on these conditions and the possible link to fluoride is necessary before any significant conclusions can be met (Fawell et al., 2006).

2.1.2 DBP Human Health Impacts

DBPs share a similar dichotomous nature with fluoride in the sense that their formation stems from the beneficial disinfection of pathogens from drinking water. Like fluoridation, disinfection in drinking water has been recognized as one of the great public health achievements of the 20th century, protecting populations from waterborne pathogens such as typhoid, cholera, and *E. coli*. Chemical disinfectants in the form of chlorine (Cl_2), chlorine dioxide (ClO_2), chloramines (NH_xCl_y) or ozone (O_3) can be added to inactivate harmful pathogens, but each contributes to a unique suite of chemical DBPs (Richardson 2003). Chlorine, present as hypochlorous acid (HOCl) and hypochlorite (OCl^-) in water, can react with NOM in the drinking water to form trihalomethanes (THMs), haloacetic acids (HAAs), and other DBPs of concern (Nietwenhuijsen et al., 2000; Singer, 1994; Westerhoff et al., 2004). Bromide is another commonly found halogen in natural waters that can be oxidized by chlorine and other oxidants to form hypobromous acid (HOBr) or hypobromite (OBr^-), and they react with NOM to form mixed brominated DBPs (Singer, 1994; USEPA, 2006). The hydrophobic portion of NOM, which is mostly comprised of humic and fulvic acids, is characterized by a high aromatic carbon content and is considered to be the largest contributor to DBP formation (Edzwald, 1993; Singer, 1999; Matilainen et al., 2010). Halogenated DBPs have been linked to urinary and digestive cancers as well as negative reproductive and

developmental outcomes (Richardson, 2003; Nieuwenhuijsen et al., 2000; Singer, 1999; USEPA, 2006). In response to a growing concern over these health outcomes, the USEPA enacted a Stage 2 Disinfectants and Disinfection Byproducts Rule in 2006 which set MCLs for total THMs and HAAs and maximum contaminant level goals (MCLGs) for the DBPs chloroform, monochloroacetic acid, and trichloroacetic acid (USEPA, 2006). The background documentation associated with the 2006 Stage 2 USEPA rule cites cancers of the rectum, bladder, kidney, colon, lung, and breast as well as preterm birth, low birth weight, stillbirth, and various birth defects in its summary of relevant epidemiological studies. Table 1 summarizes the USEPA DBP regulations.

Table 1: USEPA Stage 1 and Stage 2 DBP Regulations (Adapted from USEPA 2006).

DBP	**Class**	**MCLG (mg/L)**	**MCL (mg/L)**
Chloroform	THM	0.070	
Bromoform	THM	0.000	
Bromodichloromethane	THM	0.000	
Dibromochloromethane	THM	0.060	
Monochloroacetic acid	HAA	0.070	
Dichloroacetic acid	HAA	0.000	
Trichloroacetic acid	HAA	0.020	
Monobromoacetic acid	HAA	none	
Dibromoacetic acid	HAA	none	
Total Trihalomethanes	THM		0.080
Haloacetic Acids (five)	HAA		0.060

2.2 SMALL WATER SYSTEMS

SWSs are an often overlooked, yet significant, fraction of the nation's public drinking water supply. The definition of a SWS can be nebulous, but the SDWA broadly characterizes small systems as those serving less than 10,000 persons. The SDWA further characterizes small systems as those serving between 3,300 person and 10,000 persons, fewer than 3,000 but above 500 persons, and fewer than 500 but above 25 persons (USEPA, 1998b). The broader definition accounts for more than 92% of the nation's 51,000 community water systems and virtually 100% of the non-community water systems for a total of over 97% of the nation's PWSs (USEPA, 2016). Though they are the most numerous, these systems lack the economy of scale that is inherent in larger systems. Therefore, SWSs have lower financial resources and operating capacities to adapt to more stringent drinking water regulations.

In 1996, Amendments to the SDWA recognized this issue and created what is known as a small system variance (SSV) for systems serving less than 10,000 persons. They allow for compromises with respect to compliance technologies. A compliance technology is a preferred treatment process that is affordable and achieves compliance with the MCL. When compliance technologies are financially unattainable, an SSV allows the SWS to implement a less expensive and less effective variance technology upon approval from the regulating agency (USEPA, 2006). Small systems that are granted a SSV must achieve the maximum reduction that is affordable for the system given its size and source water quality. While still considered protective of public health, systems using these variance technologies do not have to meet MCL requirements for the associated contaminant (USEPA, 1998b). Therefore, states can grant SSVs when it is determined that the system cannot afford to observe an MCL or compliance technology; however, adequate protection of human health must also be ensured (USEPA, 2006).

Currently, SSVs are not permitted for fluoride (USEPA, 1998b; USEPA, 2006) based on a rule that prohibits pre-1986 regulated contaminants from inclusion in these variances (USEPA, 1998b). SSVs for THMs and HAAs are also not permitted since affordable compliance technologies were determined for each of these contaminants (USEPA, 2006).

In 1998, the EPA compiled a report of small system compliance technologies. In the report, coagulation/filtration was listed as an inorganic contaminant removal technology suited for a wide range of water quality. However in all three SWS size classifications, the compliance technologies tabulated for fluoride were activated alumina and reverse osmosis (USEPA, 1998a). The affordable small systems compliance technologies for DBPs include substitution of chloramines for chlorine and UV disinfection (USEPA, 2005). These compliance technologies aim to alleviate the problem of chlorinated DBPs by reducing the availability of reactive chlorine rather than the removal of NOM-based DBP precursors. Since coagulation is a widely applied treatment process, a well-understood aluminum coagulation scheme provides a unique opportunity to affordably address both fluoride and DBP precursors in SWSs. Research is necessary to evaluate the viability of coagulation as an affordable compliance or variance technology for DBP precursors and fluoride for these small systems in the event of regulatory changes.

2.3 Aluminum Coagulation In Drinking Water Treatment

2.3.1 Coagulation, Flocculation, and Particle Stability

Coagulation and flocculation are central to the effectiveness of many drinking water treatment facilities. The contaminants in source water can be present as particles,

converted into particles, and/or attached to particles throughout the treatment train. However, the imprecise use of the terms coagulation and flocculation has generated confusion in the field for quite some time.

Natural waters are considered to be a stable suspension, meaning that the suspended particles do not readily combine or settle. This stability is primarily caused by charges on the particle surfaces which act to repel other particles of like charge. Upon destabilization of these charges, particles can aggregate, grow, and settle (Benjamin and Lawler, 2013). Destabilizing agents, often referred to as coagulants, operate by two mechanisms relevant to this work. Coagulants can provide a source of molecules that exhibit a charge opposite to those found on the particle surfaces. Inorganic metal salts and synthetic polymers are commonly used in this application. These molecules can adsorb to particles, effectively neutralizing the surface charge and eliminating the repulsion (Benjamin and Lawler, 2013). The second mechanism is the formation of metal precipitates which, upon settling, can "sweep" other suspended solids out of the suspension as well. Inorganic metal salts involving iron and aluminum are commonly associated with this mode of destabilization (Benjamin and Lawler, 2013). In this research, we are concerned with the application of these mechanisms with aluminum chloride ($AlCl_3$) and aluminum sulfate ($Al_2(SO_4)_3$, commonly referred to as alum) coagulation. In referring back to the confusion of terms, some consider both the initial chemical addition (destabilization) and particle growth as coagulation (O'Melia, 1972). Others refer to coagulation exclusively as the processes that involve destabilization and precipitation of new solids. Flocculation is most widely used to explain the collisions and aggregation of particles (both precipitated and originally present in the source water) that leads to larger, contaminant-laden solids. In this study, we refer to coagulation as the

chemical addition that leads to destabilization (by any mechanism) and flocculation as defined above.

2.3.2 Fluoride Removal Mechanisms

The coagulation and flocculation process has been widely studied as a means of defluoridation (Boruff et al., 1937; Culp and Stoltenberg, 1958; Sollo et al., 1978; Meenkashi and Maheshwari, 2006; Ayoob et al., 2008; Gong et al., 2012). As early as the 1930s, chemists recognized the effectiveness of aluminum salts, particularly alum, in the removal of fluoride from drinking water (Boruff et al., 1937). Fluoride removal in an aluminum coagulation system can be explained by a somewhat nebulous interplay among three major processes: aqueous complexation, adsorption to precipitates, and coprecipitation. Aluminum and fluoride share a strong affinity for one another and readily form a suite of various soluble complexes (Choi and Chen, 1979; Gong et al., 2012) (Figure 1). Soluble fluoride anions and aluminum-fluoride (AL-F) complexes (collectively referred to as soluble fluoride species) can take part in adsorption and coprecipitation; two processes that can be analyzed as a continuous spectrum rather than two exclusive events. Throughout this spectrum, soluble fluoride species are considered an impurity present during the formation of metal hydroxide precipitates, which in this study is amorphous aluminum hydroxide.

These impurities can undergo adsorption, inclusion, and occlusion with the metal precipitate (Randtke, 1988; Lawler and Kweon, 2003). Adsorption to preformed metal hydroxides (the adsorbent) occurs when a soluble fluoride species (the adsorbate) attaches to the surface in a phenomenon known as surface complexation (Equation 1).

Adsorption: $\equiv \mathbf{AlOH} + \mathbf{F^-} \leftrightarrow \equiv \mathbf{AlF} + \mathbf{OH^-}$ **(1)**

Surface complexation is highly dependent on the adsorbent and adsorbate and can range from formation of weak, electrostatic outer-sphere to strong, specific inner-sphere complexes, discussed in further detail in section 2.4.1 (Stumm, 1995). Fluoride is proposed to take part in the latter of these surface complexation mechanisms by displacing hydroxyl ions and coordinating directly with the metal ion (Ayoob et al., 2008; Agarwal et al., 2003; Barbier and Mazounie, 1984; Wasay et al., 1996).

Inclusion occurs when soluble fluoride species substitute for precipitate ions within the crystal lattice during precipitation, resulting in a mixed Al-F precipitate. Here, the substituting species must have similar dimensions and charge to the displaced species (Randtke, 1988). Fluoride, which has similar size and charge to hydroxyl ions, is proposed to substitute for hydroxyl ions via both adsorption and inclusion (Hu et al., 2004; Ayoob et al., 2008, Alfredo, 2012). Equation 2 offers a proposed coprecipitation reaction in which the mechanism for incorporation of fluoride is inclusion.

Inclusion: $$n\mathrm{Al}^{3+}_{(aq)} + (3n\text{-}m)\ \mathrm{OH}^-_{(aq)} + m\mathrm{F}^-_{(aq)} \leftrightarrow \mathrm{Al}_n\mathrm{F}_m(\mathrm{OH})_{3n-m\ (s)} \qquad (2)$$

Lastly, occlusion can occur when the soluble impurity becomes entrapped within the crystal structure as the precipitate is forming. In this case, the charge and molecular size of the impurity play less of a role (Lawler and Kweon, 2003).

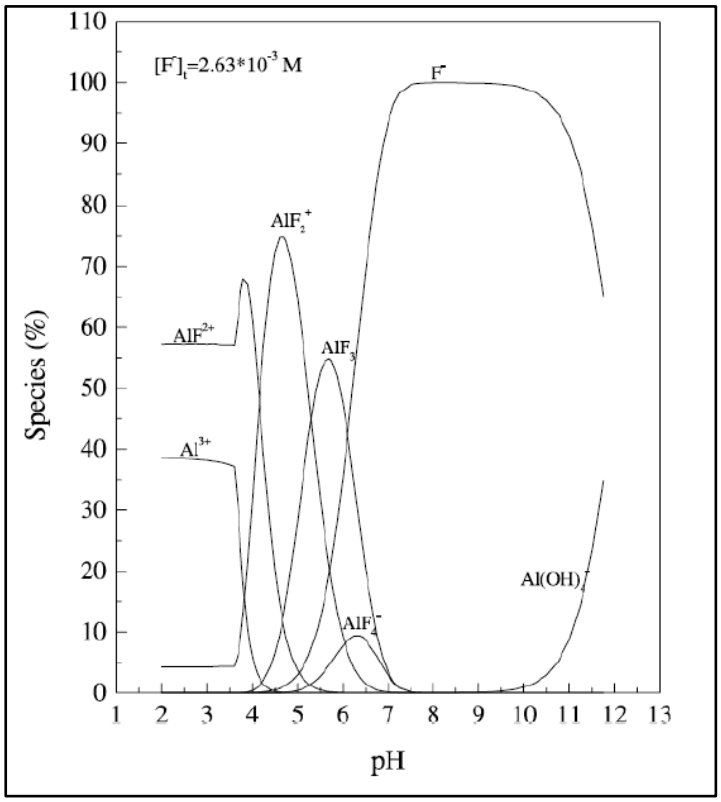

Figure 1: Al-F speciation diagram as a function of pH at 2.63 mM F and 4 mM Al3+ (figure taken from Stewart 2009)

Furthermore, pH is known to be a key parameter in the optimization of fluoride removal. The soluble Al-F complexes that take part in the coprecipitation spectrum (Figure 1) as well as the adsorbent are highly pH dependent. The isoelectric point (or pH of the point of zero charge) for aluminum hydroxides ranges from 8-11.5, which corresponds to a negatively charged surface below this pH and a positively charged surface above it (Kosmulski, 2006). Alfredo (2012) conducted electrophoresis measurements with alum flocs and varied NOM and fluoride, shown in Figure 2. In that study, the isoelectric point of bare aluminum hydroxide flocs was approximately 8 and was lowered upon addition of fluoride and NOM. At low pH values, positively charged

AlF^{2+} and AlF_2^{+} predominate in solution and undergo repulsion with the negatively charged aluminum hydroxide surfaces, resulting in decreased fluoride removals (Choi and Chen, 1979; Gong et al., 2012). At pH values above the isoelectric point, free (uncomplexed) fluoride anions predominate but the aluminum hydroxide surface becomes negatively charged and thus repulsive to the fluoride. It is worth noting that the Al-F interaction is not an electrostatic ion pair reaction as the term "repulsion" might suggest. Nonetheless, like charges of the adsorbent and adsorbate (even with specific bonding interactions) are believed to hinder fluoride removal. Additionally, the high concentration of hydroxide at the higher pH allows these ions to outcompete fluoride for adsorption sites (Choi and Chen, 1979; Gong et al., 2012).

The stability of aluminum hydroxide solid is also a strong function of pH, with maximum aluminum solubility, and therefore decreased fluoride removal, occurring at the pH extremes. As a result, the ideal pH of fluoride removal in aluminum-based coagulation systems tends to fall between pH 6 and 7 (Ayoob et al., 2008; Sollo, 1978; Hu et al., 2004; Boruff et al., 1937; Culp and Soltenberg, 1958; Gong et al., 2012). This pH region encompasses the optimum balance between the interconnected soluble Al-F complexes, aluminum hydroxide solubility, and hydroxide competition.

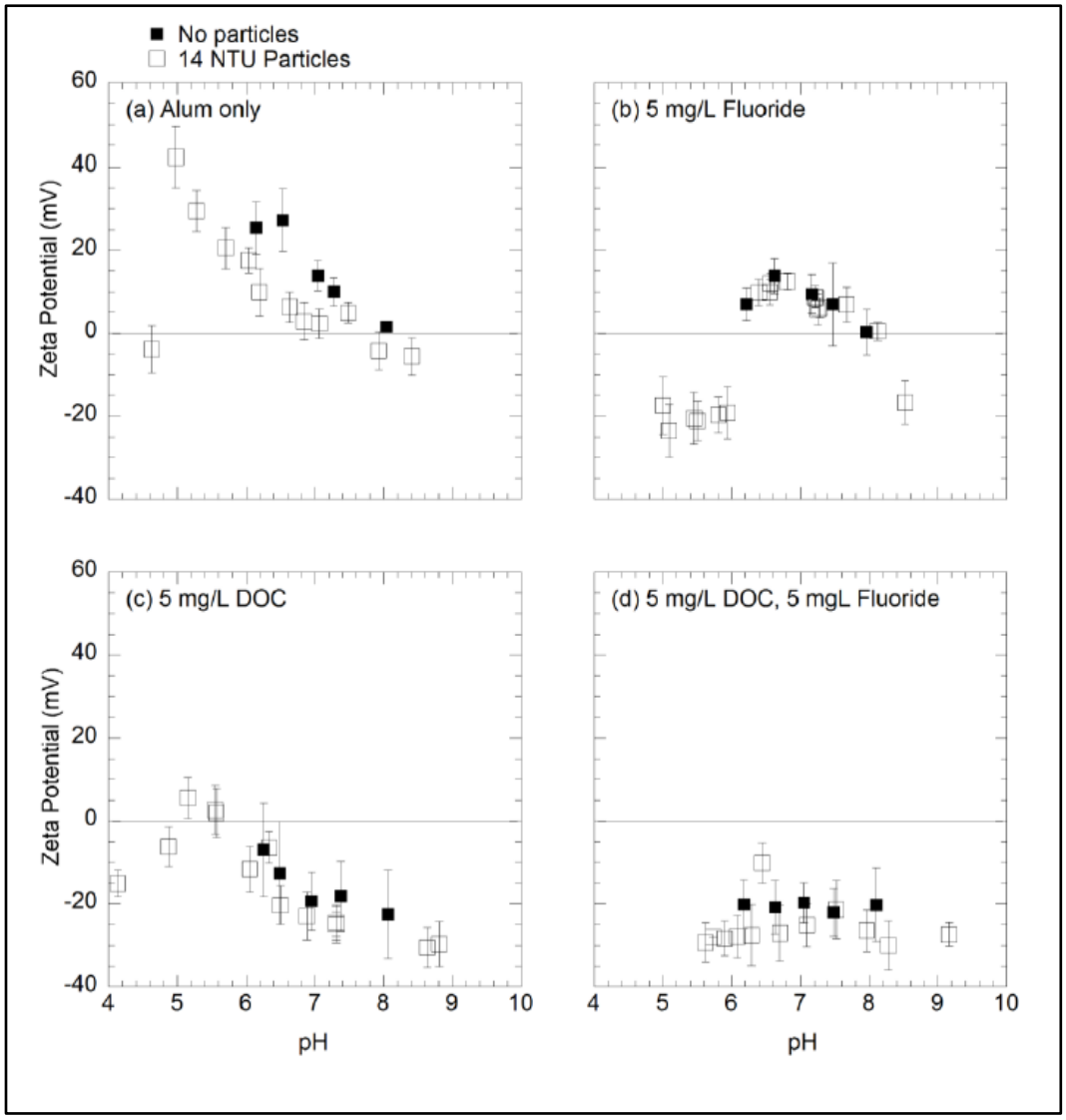

Figure 2: Electrophoresis measurements taken with 20 mg/L alum flocs under varied ligand conditions (figure taken from Alfredo 2012).

2.3.3 NOM Removal Mechanisms

NOM is ubiquitous in natural waters, often responsible for the natural surface charge of particles in source waters. The concentration of dissolved organic carbon (DOC) and ultraviolet-visual spectroscopy (UV-Vis) absorbance is widely used to express NOM levels in natural waters. These complex organic molecules, derived from the decay and metabolism of plants, animals, and microorganisms, include both nonpolar hydrocarbon ends (carbon chains and rings) and highly functionalized polar ends resulting in adsorption to a wide variety of solid surfaces (Benjamin and Lawler, 2013). NOM functional groups include, among others, hydroxyl, carboxyl, and amine groups which contribute to the acidity of basicity of these molecules. The dissociation of these acids (usually carboxyl groups) in the natural pH region contributes to the commonly found negative charge of particles in natural waters (Benjamin and Lawler, 2013).

The characterization of NOM can be made in several different ways, but is commonly made on the basis of hydrophobic and hydrophilic fractions (Edzwald, 1993; Singer 1999; Matilainen et al., 2010). The hydrophobic fraction of NOM is characterized by a higher degree of aromatic carbon rings and encompasses humic acids and fulvic acids, both of which are referred to as humic substances (Edzwald et al., 1993). Singer (1999) concluded that DBP production is directly proportional to the degree of aromatic carbon content in NOM. Numerous studies have shown that coagulation is effective in the removal of these highly aromatic humic substances from natural waters (Singer, 1999; Matilainen et al., 2010; Edzwald and Tobiason, 1999). Table 2 illustrates the breakdown of NOM based on the hydrophobic/hydrophilic fractionation scheme.

Table 2: Characterization of NOM (Adapted from Edzwald 1993 and Edzwald and Tobiason 1999)

Fraction	**Chemical Groups**	**Coagulation Removal Potential**
Hydrophobic		Very good (>50% for alum, slightly greater for ferric)
Acids		
Strong	Humic and fulvic acids, high molecular weight (MW) alkyl carboxylic acids, aromatic acids	
Weak	Phenols, tannins, intermediate MW alkyl carboxylic acids	
Bases	Proteins, aromatic amines, high MW alkyl amines	
Neutrals	Hydrocarbons, aldehydes, high MW methyl ketones and alkyl alcohols, ethers, furans, pyrrole	
Hydrophilic		Poor (<25%)
Acids	Hydroxy acids, sugars, sulfonics, low MW alkyl carboxylic acids	
Bases	Amino acids, purines, pyrimidines, low MW alkyl amines	
Neutrals	Polysaccharides, low MW alkyl alcohols, aldehydes, ketones	

The two most commonly discussed mechanisms of soluble NOM removal in the aluminum coagulation process are charge neutralization and precipitation (CNP) and adsorption (Hundt and O'Melia, 1988; Edwald and Tobiason, 1999; Yan et al., 2008;

Matilainen et al., 2010). Figure 3 illustrates the possible modes of NOM removal. Both mechanisms may begin via complexation of NOM with metal hydrolysis species (Table 3), forming metal-NOM complexes (Matilainen et al., 2010, Yan et al., 2008). In the CNP mechanism (also referred to as direct precipitation), the cationic aluminum species form insoluble complexes with NOM, resulting in an aluminum-NOM mixed precipitate (Yan et al., 2008; Edzwald and Tobiason, 1999). In the adsorption case, charged, soluble metal-NOM complexes (or uncomplexed NOM molecules) adsorb to the surface of existing aluminum hydroxide solids generated from the initial coagulant addition (Hundt and O'Melia, 1988; Edwald and Tobiason, 1999; Yan et al., 2008; Matilainen et al., Hundt and O'Melia, 1988). The bonds that result in this adsorption can vary from weak physical van der Waals interactions to more significant chemical substitution reactions (Hundt and O'Melia, 1988). Chemical adsorption reactions can be divided further into strong inner -sphere complexes and weaker outer-sphere complexes which are discussed in more detail in section 2.4.1.

Table 3: Aluminum hydrolysis and aluminum hydroxide (gibbsite) dissolution (Equilibrium constants from Morel and Hering 1993)

Reaction	**Log K**
$Al^{3+} + H_2O \leftrightarrow AlOH^{2+} + H^+$	-5.0
$Al^{3+} + 2\ H_2O \leftrightarrow Al(OH)_2^+ + 2\ H^+$	-9.3
$Al^{3+} + 3\ H_2O \leftrightarrow Al(OH)_3 + 3\ H^+$	-15.0
$Al^{3+} + 3\ H_2O \leftrightarrow Al(OH)_{3(s)} + 3\ H^+$	-8.5
$Al^{3+} + 4\ H_2O \leftrightarrow Al(OH)_4^- + 4\ H^+$	-23.0

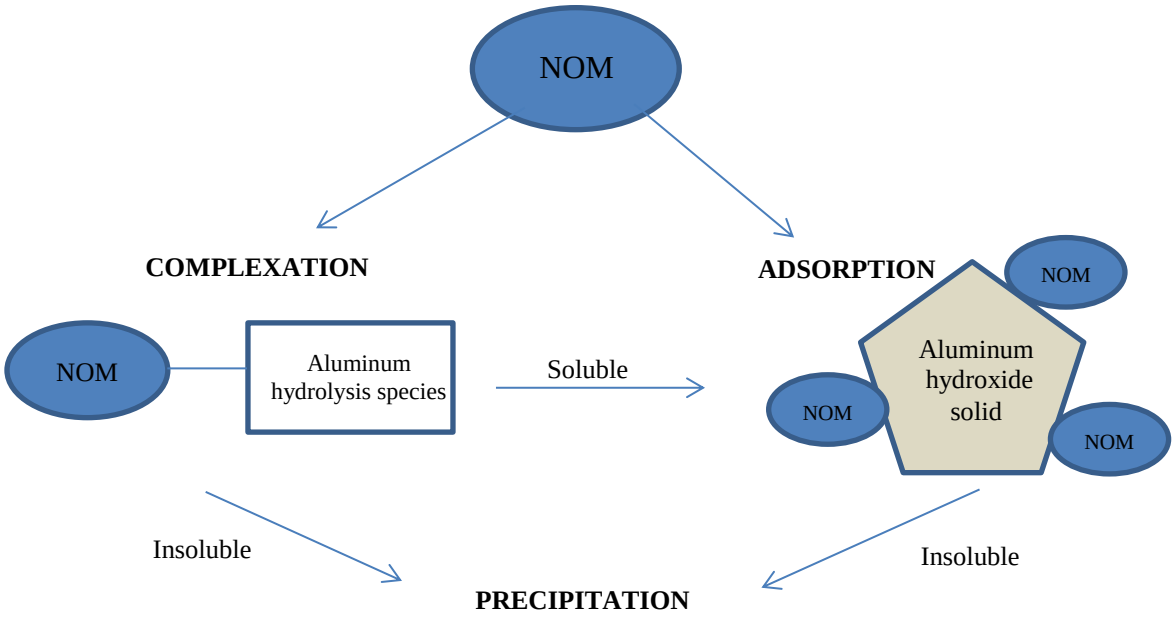

Figure 3: Proposed mechanisms of NOM removal during aluminum coagulation (Adapted from Matilainen et al. 2010)

2.4 Investigations of Metal Oxide Precipitates

2.4.1 Adsorption and Coordination Chemistry

As alluded to in the discussion of NOM and fluoride adsorption, ions can form outer-sphere or inner-sphere interactions with an adsorbent surface. Stumm (1995) discusses coordination types. Outer-sphere complexation is defined as a weak electrostatic interaction between an ion and adsorbent surface in which all spheres of hydration are maintained. Conversely, an inner-sphere complex is characterized by an ion directly coordinating to the adsorbent surface via a specific chemical bond. This chemical bond is covalent in nature and results in what is often referred to as ligand exchange as surface hydroxyl groups are replaced (in the case of metal oxides and hydroxides). When

one adsorbing atom shares electrons with the surface, this is called a monodentate inner-sphere complex (Figure 4). Bidendate ligands have two electron-donating atoms and are one example of a polydentate ligand. Mononuclear and multinuclear (bi- or more) complexes refer to the number of metal atoms that the ligand shares electrons with. Multinuclear complexes can result in bridging of multiple metal or oxygen atoms. Though it can be used to describe any form of adsorbing molecule, a ligand is often more strictly defined as a species that can form covalent bonds with a central metal atom (Morel and Hering, 1993). For the purposes of this study, both outer-and inner-sphere complexing anions and acids will be referred to as ligands.

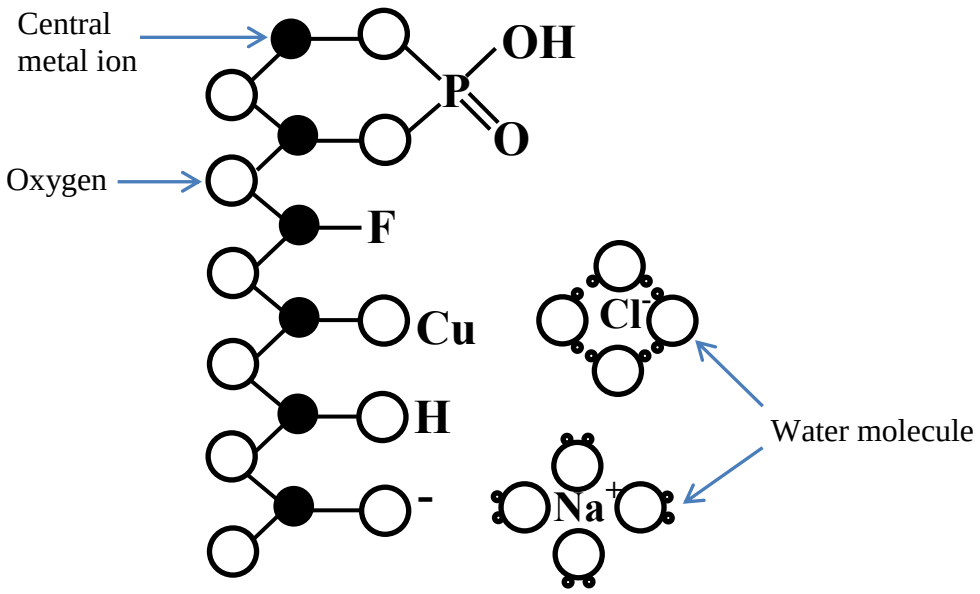

Figure 4: Schematic representation of the various complexation modes. The phosphate, fluoride, and copper are inner-sphere complexes with the surface. The phosphate (binuclear bidentate) and fluoride (mononuclear monodentate) undergo inner-sphere ligand exchange by replacement of the hydroxyl group. Chloride and sodium are outer-sphere complexes with complete spheres of hydration. (Adapted from Stumm 1995)

The type of coordination that a ligand exhibits has important implications for applications involving contaminant removal. Inner-sphere complexes result in much stronger binding to metal surfaces versus outer-sphere complexes due to the covalent nature of the bonds involved. Hayes et al. (1987) discusses the necessity for molecular spectroscopic insights at the interfaces between solids and liquids in order to account for differences between coordination types and to more accurately predict adsorption behavior. Hayes and Katz (1996) note that models that ignore differences between inner-

and outer-sphere complexes have much less success in modeling competitive ligand adsorption. Differences not only occur between inner- and outer-sphere complexes, but within each type of complex as well (Stumm, 1995). Within the inner-sphere realm, multinuclear bidentate ligands can block more surface sites than their mononuclear bidendate or monodentate counterparts, which mitigates subsequent surface reactivity.

Mononuclear ligands are believed to enhance dissolution of the metal hydroxide solid by bringing the electron density of the central metal into the coordination sphere of the ligand and facilitating its detachment. Conversely, binuclear complexes are inert when it comes to this dissolution reaction due to the larger energy required to simultaneously detach two central metal ions (Bondietti et al., 1993). Thus, binuclear complexes can inhibit dissolution by occupying multiple sites that could otherwise be occupied by (mono- or bidentate) mononuclear ligands. This interpretation is supported by multiple studies including Bondietti et al. (1993) who found that EDTA-promoted dissolution was greatly inhibited by binuclear complexed phosphate, arsenate, and selenite. Even the presence of outer-sphere adsorbed species can affect dissolution. Johnson et al. (2004) found that outer-sphere adsorbed pyromellitate sterically protects aluminum oxides from attack by protons. Given the implications that arise from the various coordination complexes, it is important to understand the specific mechanisms at play. Much of the research that exists on coordination chemistry has focused on well-defined metal oxide and metal hydroxide surfaces. The coordination chemistry of nebulous amorphous solids, that result from the aluminum salt coagulation process in water treatment, remains poorly understood and is the main thrust of this study.

2.4.2 *Ex Situ* Analyses of Precipitates

X-ray diffraction (XRD), scanning electron microscopy with energy-dispersive electron microscopy (SEM/EDX), and X-ray photoelectron spectroscopy (XPS) are all spectroscopic methods that can provide microscopic insights that aid in identifying the impacts of aging and ligand substitution on precipitated solids. However, these analyses are often *ex situ,* requiring vacuum freeze-drying at low temperature and pressure. Therefore the solid-aqueous interface at which the coordination of ligands is taking place is often compromised in these studies. Nonetheless, these analyses still provide vital insights about the system.

The crystalline structure of a solid has tremendous implications on its solubility, surface charge, surface area and other characteristics which together have a tremendous impact on contaminant removal potential (Sposito, 1996). XRD is an analytical tool that identifies minerals by matching sample diffraction peaks with tabulated, defined peaks of known minerals. Amorphous solids are characterized by broad, low-intensity peaks while crystals produce sharp, intense peaks at well-defined diffraction angles (Ryland, 1958). Hsu and Bates (1964) used XRD analysis to determine the structure of various sulfate and chloride-based aluminum hydroxide precipitates. It was concluded that bayerite, nordstrandite, and gibbsite peaks became sharper and larger with age over the course of a month, indicating a transition from amorphous to crystalline structure. Martinez and McBride (1998) investigated the crystallinity of ferrihydrite with varied aging periods. They identified broad, amorphous peaks of 1- and 9-line ferrihydrite. However, broad peaks occurring at positions that correspond to goethite, hematite, and lepidocrocite tended to sharpen slightly with age. Despite the fact that the timescales of mineral ageing in the above investigations are much longer than the residence times that precipitates

experience in a drinking water treatment plant, they still provide relevant details about structural transitions.

In addition to age, the presence of inorganic ionic impurities can impact crystallinity. Cornell (1988) studied the coprecipitation of ferrihydrite in the presence of the trace metals Co^{2+}, Cu^{2+}, Mn^{2+}, Ni^{2+}, and Zn^{2+} where it was concluded that hematite, goethite, and/or substituted spinel products could be formed but were dependent on the specific ionic impurity. Moreover, Co^{2+}, Cu^{2+}, Mn^{2+}, and Si^{4+} have all been shown to retard the rate of ferrihydrite transformation to more crystalline phases (Anderson and Benjamin, 1985; Cornell and Giovanoli, 1987; Cornell and Giovanoli, 1988; Cornell and Giovanoli, 1989).

XPS provides information on both the bonding energies and stoichiometric ratios of elements near the surface. In the study by Gong et al. (2012), aluminum flocs were analyzed with XPS in a coagulation (coprecipitation) scheme and an adsorption scheme in the presence of fluoride. The binding energies of the coprecipitated flocs were different for the base aluminum hydroxide flocs and aluminum hydroxide flocs with adsorbed F. This indicated strong Al-F complexation and incorporation of F into the solid to form a mixed coprecipitate. Alfredo (2012) investigated binding energies and stoichiometric ratios in alum precipitates with and without fluoride present and in coprecipitated and adsorption-only schemes. Al:O ratios were highest in the base aluminum hydroxide case and decreased with the addition of fluoride in both the adsorption and coprecipitation cases. As more fluoride was added in the coprecipitation cases, the O:F ratios decreased, indicating an inner-sphere ligand replacement reaction and/or replacement of hydroxyls for fluoride in the coprecipitate. A slight increase in fluoride binding energies from the adsorbed case to the coprecipitate case indicated that a fluoride coprecipitate with replacement of hydroxyls was likely forming in this process. The deeper penetration

depths of SEM/EDX spectra further supported these findings by reporting the highest Al:F ratio, indicating that fluoride was indeed incorporated into the bulk solid rather than solely adsorbing to the surface.

Organic impurities can also impact solid structure. Alfredo (2012) performed XRD on alum precipitates in the presence of organic acids and fluoride; a lack of defined features confirmed the amorphous nature of the resulting solids. Yu et al. (2007) studied the effects of organics and aging on aluminum precipitates from $AlCl_3$ with XRD, concluding that aluminum precipitated in the presence of tannate resulted in a decreased crystallinity and increased surface area. Increased aging time only improved the crystallinity in organic-free systems. The crystallinity of aluminum hydroxide precipitates is also known to decrease in the presence of fulvic and humic acids (Kodama and Schnitzer, 1980; Singer and Huang, 1990). Guan et al. (2007) used XPS on precipitated aluminum hydroxides in the presence of different organic acids. Shifts in the binding energies of non-adsorbed organic solids (sodium salicylate and sodium benzoate) compared to the spectra of aluminum hydroxides with adsorbed organics were attributed to different modes of complexation with the surface. Specifically, a decrease in the binding energy of salicylate upon complexation was attributed to the binding of phenol groups with aluminum, and an increase in the binding energy of adsorbed salicylate was explained by complexation with carboxylic moieties. To further investigate complexation at the solid-aqueous interface, *in situ* spectroscopic methods are needed.

2.4.3 *In Situ* Precipitate Wet Analysis

Where the above analyses fall short is their inability to capture the binding environment that is present in an aqeous system. By removing water from the system, one loses vital information about these amorphous solid complexes. In contrast, FTIR

spectroscopy can be conducted in the presence of water. ATR-FTIR requires minimal solid sample preparation compared to conventional infrared spectroscopy, allowing the user to examine precipitate solids *in situ*. Infrared (IR) spectroscopy has long been utilized as a tool for surface characterization, with early fingerprinting work done by organic chemists in the 1930s (Larkin, 2011). The way in which substances absorb and transmit IR radiation is unique to the molecular component of that substance. Absorption of IR radiation induces a change in molecular dipole moments, thus changing the vibrational energy levels of the affected molecules (Potts, 1963; Larkin, 2011). These vibrational changes include symmetric and asymmetric stretching as well as in-plane and out-of-plane bending (Larkin, 2011). These various infrared vibrations or bands are often denoted with different ν values, i.e. ν_1, ν_2, ν_3.

ATR is a non-destructive sampling method that allows the user to probe the aqueous/mineral interface *in situ* (see section 3.2.4 for more details on the method). Rather than transmission through the sample, ATR-FTIR is a reflectance technique with a depth of penetration ranging on average from 0.5 to 3 micrometers (Bruker, 2011). For this reason, it provides an excellent characterization of solid surfaces through the recognition of various functional groups. The magnitude of absorbance is proportional to the abundance of the recognized substances, whereas shifts in peak wavenumber provide information about bonding and coordination changes. Often, comparisons are made between pure, non-adsorbed samples and samples that have been adsorbed to precipitated solids.

Guan et al. (2006, 2006(b), 2007) and Nordin et al. (1997, 1998) have done extensive work on the adsorption of model organic acids to aluminum hydroxide surfaces with ATR-FTIR. As discussed in section 2.3.3, NOM encompasses a wide variety of large, complex structures. However, the functionality of NOM has been fairly well

defined with aromatic carboxyl and phenolic groups having the most important roles in DBP formation and adsorption onto metal hydroxides (Singer, 1999; Snoeyink and Jenkins, 1980). Therefore, the use of well-defined low molecular weight (LMW) organic acids can aid in the elucidation of adsorption mechanisms to solids (Guan et al., 2007).

In addition to NOM, competing inorganic ligands are of great concern in these systems and have also been characterized on surfaces using ATR-FTIR spectroscopy. Multiple charged species in solution can result in neutral, competitive, or promotive adsorption effects on one another (Wijnja, 1999; Davis and Kent, 1999). Several studies have investigated the adsorption of inorganic and organic ligands independently and in competition to understand these effects. Carbonate, arguably the most important and prevalent oxyanion species in natural waters, is thought to undergo inner-sphere monodentate complexation and compete with other anions such as acetate and hydroxide on the surface (Su and Suarez, 1997). Wijnja (1999) concluded that inner-sphere monodentate carbonate complexes promote the adsorption of outer-sphere adsorbed sulfate and selenate. The organics acetate and formate also promoted adsorption whereas oxalate and citrate exhibited competitive effects. This difference is because multicarboxylic acids are known to have a higher adsorption affinity than monocarboxylic acids, thus competing with other high-affinity oxyanions such as silicates. Hu et al. (2015) investigated the competitive adsorption of silicate and arsenate with *in situ* ATR-FTIR, concluding that inner-sphere coordinated silicate that undergoes polymerization is not easily desorbed and negatively impacts the adsorption capacity of inner-sphere coordinating arsenate. In an FTIR study by Tang et al. (2009), fluoride adsorption to granular ferric hydroxide was proposed as inner-sphere complexation based on observed changes in hydrogen bonding and surface hydroxyl groups. Major anions in solution were found to decrease fluoride adsorption from greatest to least effect as

follows: $H_2PO_4^-$, HCO_3^-, SO_4^{2-}, and Cl^-. $H_2PO_4^-$ was found to have the largest impact on fluoride removal due to competition for inner-sphere ligand exchange, while Cl^- had the least effect due to weak outer-sphere complexation. Table 4 and Table 5 summarize organic acid adsorption mechanisms and inorganic adsorption mechanisms reported in the literature, respectively.

Table 4: Proposed modes of adsorption for various LMW organic acids

Organic Acid	pH	Mode of Adsorption	Adsorbent	Study
Phthalate	5, 7, 9	Outer-sphere	Freeze-dried amorphous $Al(OH)_3$ precipitates ($AlCl_3$-derived)	Guan et al., 2006
Phthalate	3.7, 5.3, 6.5	Inner-sphere and Outer-sphere (outer-sphere dominates at lower ionic strength)	Boehmite (γ–ALOOH)	Nordin et al., 1997
Salicylate	5, 7	Inner-sphere monodentate with bridging	Freeze-dried amorphous $Al(OH)_3$ precipitates ($AlCl_3$-derived)	Guan et al., 2007
Salicylate	2, 5, 7	Inner-sphere monodentate	α–Al_2O_3 (corundum), γ–Al_2O_3, δ–Al_2O_3	Biber and Stumm, 1994
Pyromellitate	5, 7, 9	Outer-sphere (pH 5), inner-sphere (pH 7, 9	Freeze-dried amorphous $Al(OH)_3$ precipitates ($AlCl_3$-derived)	Guan et al., 2006
Pyromellitate	4.4, 7.0, 8.1	Outer-sphere	Boehmite (γ–ALOOH)	Nordin et al. 1998

Table 5: Proposed modes of adsorption for various inorganic ligands

Inorganic	pH	Mode of Adsorption	Adsorbent	Study
Carbonate	5.1, 6.2, 7.2	Inner-sphere monodentate	γ–Al_2O_3	Wijnja and Schulthess, 1999
Carbonate	4.1, 4.2, 4.3, 6.0, 7.8	Inner-sphere monodentate	Air-dried amorphous $Al(OH)_3$ precipitates ($AlCl_3$-derived)	Su and Suarez, 1997
Sulfate	4.4, 6.4	Predominately outer-sphere (small fraction inner sphere at pH<6)	γ–Al_2O_3	Wijnja and Schulthess, 2000
Sulfate	3, 3.1, 3.6, 4.1, 4.6, 5.2, 6.8	Outer-sphere	α–Al_2O_3, γ–Al_2O_3, $Al(OH)_3$	Muller and Lefevre, 2011
Silica (Sodium Silicate)	7.0, 8.3, 9.3, 10.2, 11.2	Inner-sphere (bidentate, polymerization at low pH and high Si concentrations)	Magnetite paste (from $FeCl_2$ and $FeCl_3$)	Yang et al., 2008
Silica (Silicic acid)	4.0	Inner-sphere bidentate (polymerization at higher Si concentrations)	Freeze-dried two-line ferrihydrite ($Fe(NO_3)_3$-derived)	Swedlund et al., 2009
Fluoride	2.1, 4.6, 6.3	Inner-sphere	Granular ferric hydroxide	Tang et al., 2009
Fluoride	2, 6, 7, 9	Inner-sphere	γ–Fe_2O_3 nanoparticles	Jayarathna et al., 2015

Despite this breadth of research on aluminum-ligand interfaces, information regarding the interaction of ligands and freshly precipitated aluminum hydroxides in a drinking water coagulation basin is still lacking. Much of the literature relies on well-characterized aluminum oxides or hydroxides or aged precipitates. Thus, this study is relevant in that it fulfills a need for an *in situ* FTIR study that elucidates the interactions among ligands and freshly precipitated aluminum hydroxide.

Chapter 3: Research Approach and Methodology

3.1 Research Approach

The removal of fluoride and NOM via aluminum salt coagulation involves a complex interplay of removal mechanisms among many molecules. Aluminum hydrolysis and complexation with NOM and fluoride can occur followed by subsequent coprecipitation and adsorption. Within the realm of adsorption, the various modes of coordination to the aluminum surface have implications for competition with other ligands, many of which are not target contaminants but are still ubiquitous in natural waters.

To understand the mechanisms that dictate ligand removal at the solid surface, an experimental matrix of jar tests was designed to gain optimal insights about the interaction of selected ligands and the aluminum hydroxide surface independently and in various ligand mixtures. The pH values of the solutions were also varied between 6.5, the known point of minimum aluminum solubility and maximum fluoride removal, and 7.5, which is higher than optimal but within the range of water treatment operations. The species varied included fluoride, carbonate, sulfate, silicate, and the LMW organic acids pyromellitic acid, phthalic acid, and salicylic acid. As discussed in section 2.4.3, LMW organic acids can be useful in determining the coordination mechanisms of NOM based on well-characterized functional groups. Molecules with aromatic rings, phenolic groups, and carboxyl groups appear to be the most relevant in terms of both DBP formation potential and similarity to the adsorption mechanisms of NOM to metal oxides. Phthalic acid, salicylic acid, and pyromellitic acid are all single-ring aromatic hydrocarbons with varied phenolic group and carboxylic group quantity and position. Alfredo (2012) chose these model compounds for the following reasons. Salicylic acid is commonly found in natural waters and exhibits a unique ortho positioning of the carboxylic and phenolic

groups which have been shown to enhance removal on metal oxide surfaces (Evanko and Dzombak, 1998). Phthalic acid has shown evidence of chelation at oxide surfaces which has important implications for ligand competition (Lindegren and Persson, 2010). Lastly, pyromellitic acid and other benzenepolycarboxylic acids are recognized in the literature to closely mimic humic acid behavior (Evanko and Dzombak, 1998; Glaser et al., 1998; Schnitzer and Calderoni, 1985). The structures and corresponding pKa values of these organics are offered in Table 6.

Table 6: NOM surrogates used in this study (Adapted from Alfredo 2012)

Name	Structure	pKa
Pyromellitic Acid	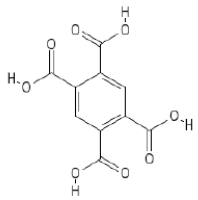	1.52, 2.95, 4.65, 5.89
Salicylic Acid	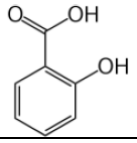	2.88, 13.56
Phthalic Acid	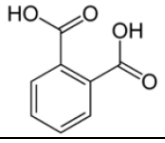	2.87, 5.23

The experimental design was as follows:

1. Conduct a set of jar tests (batch reactors that undergo pre-defined rapid mix, slow mixing and settling periods) with varying initial ligand

concentrations over the course of one week and repeat over a total of 4 weeks resulting in identical reactor conditions with precipitates aged from 0-3 weeks.

2. During week 4, collect precipitates and supernatant samples from the jars on the same weekday that each test was initiated. Collect the ATR-FTIR spectra of the solid samples and preserve supernatant solutions to obtain macroscopic removal data.
3. Use the ICP, UV-Vis, and fluoride-selective electrode to gain information about ligand concentrations removal during the course of the jar tests and aging process.

All tests were done in carefully prescribed synthetic waters. Although unrealistic in terms of the timescales that settled solids might experience in a drinking water treatment plant, aging of the settled solids was employed as a tool to better understand how the various ligands interact over time. Thus, we gain insight as to how each ligand was initially attached to the solid surface

3.2 METHODOLOGY

A variety of ligands were investigated for their impacts on the formation of aluminum hydroxide precipitates and competitive ligand removal during coagulation. Researchers have found that sulfate salts have a catalytic effect on the formation of solids in comparison to chloride or nitrate salts (Hundt and O'Melia, 1988). Figure 5 illustrates the decrease in aluminum solubility due to sulfate commensurate with this hypothesis; these results provided motivation for including both chloride and sulfate in this study. Chloride, sulfate and the organic acids salicylic acid, phthalic acid and pyromellitic acid

were studied for their impact on removal in the short time periods associated with the coagulation process. The precipitates formed in these systems were characterized immediately after the coagulation and settling process (a little over one hour) as well as over a three week period following the coagulation process to investigate changes in the ligand-surface interface over time.

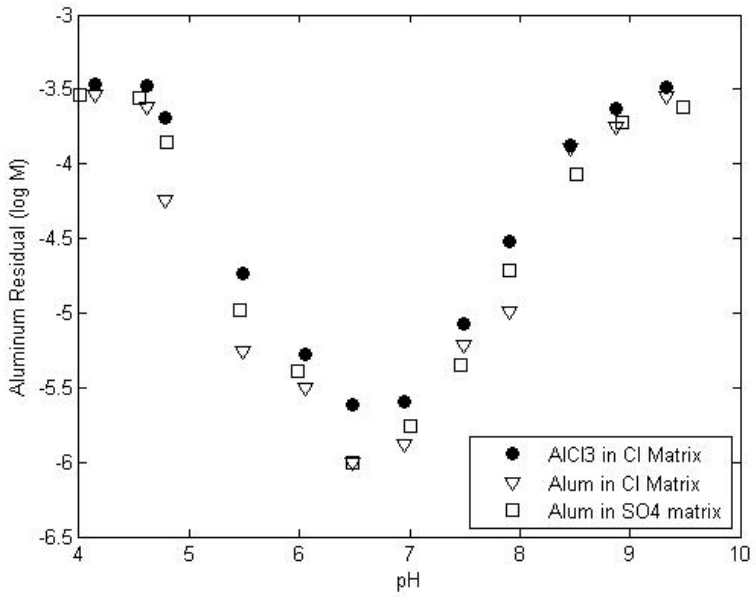

Figure 5: Aluminum solubility differences between chloride and sulfate synthetic waters (total Al= 0.34 mM)

3.2.1 Synthetic Waters and Stock Solutions

All reagents used in this investigation were of analytical grade or higher. Two synthetic waters were used in this study: a chloride salt synthetic water and a sulfate salt synthetic water. Alum was the coagulant used in sulfate water tests and $AlCl_3$ was the coagulant used in chloride water tests. Sulfate is an important oxyanion in natural waters

and also results from the addition of alum. Synthetic waters were created to simulate natural source waters, yet with carefully controlled and well-defined compositions. Both the alkalinity and hardness of each synthetic water was 3 meq/L. Ionic strength of the synthetic waters was initially 0.014 M and varied up to 0.016 M depending on the amount of NaOH and HCl needed to reach the target pH. The total concentrations of each anionic ligand species (when present in a reactor) is displayed in Table 7.

Table 7: Total dissolved concentrations of each anion species (when present).

Species	**Concentration (mg/L)**	**Concentration (mmol/L)**	**Source**
Fluoride	5.0 (as F)	0.26	Sodium fluoride
Pyromellitate	5.0 (as C)	0.042	Pyromellitic acid
Salicylate	5.0 (as C)	0.045	Salicylic acid
Phthalate	5.0 (as C)	0.039	Phthalic acid
Sulfate	548	5.7	Alum, calcium sulfate, sodium sulfate, sulfuric acid
Carbonate*	180 (as CO_3^{2-})	3.0	Sodium bicarbonate
Silicate	20 (as SiO_2)	0.29	Sodium metasilicate
Chloride	340	9.6	Aluminum chloride, calcium chloride, sodium chloride, hydrochloric acid

*Reflects the concentration of carbonate added to the system. The actual concentration varies slightly since the system is open to the atmosphere

Each synthetic water was made with ultrapure, filtered water (Thermo Scientific Nanopure) in 4 L batches. The chloride matrix was made by the addition of calcium chloride dihydrate to provide hardness and control ionic strength ($CaCl_2 \cdot 2\ H_2O$, ACS, Fisher Scientific), sodium bicarbonate for alkalinity ($NaHCO_3$, ACS, Fisher Scientific), sodium chloride for ionic strength (NaCl, ACS, Fisher Scientific), and 1N hydrochloric acid diluted from concentrated hydrochloric acid for stability and prevention of immediate aluminum nucleation upon coagulant addition (36.5%-38% HCl, GR, ACS, EMD Chemicals). The sulfate matrix was composed of sodium bicarbonate for alkalinity, anhydrous calcium sulfate for hardness and ionic strength ($CaSO_4$, Spectrum Chemical), anhydrous sodium sulfate for ionic strength (Na_2SO_4, ACS, Fisher Scientific), and 1N sulfuric acid diluted from concentrated sulfuric acid for stability and prevention of immediate aluminum nucleation upon coagulant addition (95%-98% H_2SO_4, GR, ACS, EM Science).

Ligands were dosed from pre-made stock solutions of various strengths. Alum was dosed from a 13.31 g/L stock solution made from aluminum sulfate hydrate powder ($Al_2(SO_4)_3 \cdot (H_2O)_{14\text{-}18}$, 98%, Aldrich Chemical Company). The alum stock was acidified to 4% by volume with 1 N HCl to aid in the dissolution of the alum powder. A 6.04 g/L aluminum chloride stock was produced with anhydrous aluminum chloride powder ($AlCl_3$, reagent grade, Alfa Aesar). Each organic acid stock was 1000 mg/L as carbon including pyromellitic acid ($C_{10}H_6O_8$, 96%, Alfa Aesar), salicylic acid ($C_7H_6O_3$, AR, Mallinckrodt), and phthalic acid ($C_8H_6O_4$, 99.5%, ACS, Alfa Aesar). Fluoride was dosed from a 1000 mg/L as F solution made from sodium fluoride (NaF, ACS, Fisher Scientific). Silicate stock was prepared with 1000 mg/L as SiO_2 (+/- 5 mg/L as SiO_2) silica standard (sodium metasilicate nonahydrate, $Na_2O_3Si \cdot 9H_2O$, analytical reagent grade, Ricca Chemical Corporation).

3.2.2 Jar Tests

Jar tests were used to simulate the physical and chemical processes that a natural water would experience in the coagulation and flocculation basins of a drinking water treatment plant. During each jar test set, a total of seven jars were subjected to the jar testing process as follows: First, 200 mL of synthetic water were poured into each custom-built, rectangular, polycarbonate jar and the ligands silicate, organic acid, and fluoride were dosed accordingly. During the rapid mixing period, jars were subjected to 300-400 rpm stirring and dosed to create a 200 mg/L alum (or the equivalent aluminum dose for $AlCl_3$) concentration in the jar. Although a 200 mg/L dose may be excessive for the operations of most drinking water treatment plants, this dose was necessary to create sufficient solids for FTIR analysis and was determined in previous studies to exhibit excellent removals of fluoride and NOM (Alfredo, 2012; Stehouwer, 2014). Dosing the ligands in this order, rather than after the precipitation of alum, is more representative of the actual conditions in a drinking water treatment plant and allows for the complex spectrum of coprecipitation to occur. 1 N HCl and 1 N NaOH were used to adjust the solution to the target pH, 6.5 or 7.5. Orion 8175BNWP Ross Sure-Flow and Orion 8102BNUWP Ross Ultra pH probes (Thermo Scientific) were used for all pH measurements. Once the desired pH was reached, slow-mixing was provided by a Phipps and Bird PB-700 Jar tester at approximately 20 rpm. This value was determined by previous researchers to provide a mean velocity gradient, G, of about $15s^{-1}$ (Cornwell and Bishop, 1983). Following 30 minutes of slow-mixing, the jars were removed from the jar tester and allowed to settle quiescently for 40 minutes. During rapid mixing, settling, and sampling, the jars were open to the atmosphere. Once a jar was placed on the jar tester for slow-mixing, the entire process was repeated for the subsequent jar resulting in a

staggered start format, carefully monitored with a timer. Table 8 shows the weekly jar test regimen repeated over the course of 4 weeks.

Table 8: Jar test conditions which were repeated over the course of 4 weeks.

Sample #	Coagulant	pH	Organic Acid	Fluoride	Buffer	SiO2
1	Alum	6.5	None	None	Carbonate	None
2	Alum	6.5	None	5 mg/L F	Carbonate	None
3	Alum	6.5	5 mg/L C Pyromellitic	None	Carbonate	None
4	Alum	6.5	5 mg/L C Salicylic	None	Carbonate	None
5	Alum	6.5	5 mg/L C Phthalic	None	Carbonate	None
6	Alum	6.5	5 mg/L C Pyromellitic	5 mg/L F	Carbonate	None
7	Alum	6.5	5 mg/L C Salicylic	5 mg/L F	Carbonate	None
8	Alum	6.5	5 mg/L C Phthalic	5 mg/L F	Carbonate	None
9	Alum	6.5	None	None	Carbonate	20 mg/L
10	Alum	6.5	None	5 mg/L F	Carbonate	20 mg/L
11	Alum	6.5	5 mg/L C Pyromellitic	None	Carbonate	20 mg/L
12	Alum	6.5	5 mg/L C Pyromellitic	5 mg/L F	Carbonate	20 mg/L
13	Alum	7.5	None	None	Carbonate	None
14	Alum	7.5	None	5 mg/L F	Carbonate	None
15	Alum	7.5	5 mg/L C Pyromellitic	None	Carbonate	None
16	Alum	7.5	5 mg/L C Pyromellitic	5 mg/L F	Carbonate	None
21	$AlCl_3$	6.5	None	None	Carbonate	None
22	$AlCl_3$	6.5	None	5 mg/L F	Carbonate	None
23	$AlCl_3$	6.5	5 mg/L C Pyromellitic	None	Carbonate	None
24	$AlCl_3$	6.5	5 mg/L C Pyromellitic	5 mg/L F	Carbonate	None
25	$AlCl_3$	7.5	None	None	Carbonate	None
26	$AlCl_3$	7.5	None	5 mg/L F	Carbonate	None

3.2.3 Analysis of residual aqueous phase concentrations

Following each jar test, a small amount of solution was filtered through a 0.45 micron syringe filter and used for immediate fluoride analysis. All filtration was conducted with the same syringe filter type (0.45 micron, 25 mm, nylon membrane,

VWR). Suspensions that were subjected to aging were transferred to sealed polyethylene bottles and stored quiescently. After aging, additional solution (supernatant) was filtered and preserved for fluoride, aluminum, silica, and UV-Vis analysis. When possible, samples were kept at 4°C until the macroscopic analyses were complete (temperature variations may have occurred during short-term transit of samples).

Residual fluoride concentrations were made with a fluoride ion selective electrode (Thermo Scientific, Orion Ionplus Sure-Flow, Solid State, Combination). Prior to analysis, filtration and storage at 4°C were the only preservation measures used. All fluoride samples were contained in plastic labware to avoid the risk of sorption to vessel surfaces. Every fluoride sample and standard was diluted 1:1 using Total Ionic Strength Adjustment Buffer with CDTA (Orion, TISAB II) to provide ionic strength and pH consistency, as well as to chelate any residual aluminum that could interfere with the electrode. Readings of relative millivolts (RmV) were translated to mg/L concentrations using linear standard curves of RmV versus the base 10 logarithm of the standard concentrations. A standard curve was created from premade 0.5, 1.0, 2.0, 3.0, and 6.0 mg/L samples prepared from dilutions of a 1000 mg/L fluoride stock before each set of fluoride measurements. During sample measurements, re-zeroing every 2-4 samples and the re-measurement of standards was done to account for any electronic drift over time. The method detection limit for this particular fluoride probe was reported at 0.02 mg/L (Thermo Scientific, 2011).

Aluminum and silicate samples were preserved prior to analysis by acidification with trace metals grade nitric acid (67%-70% HNO_3, OmniTrace, EMD) in addition to filtration and refrigeration. 200 µL of acid were used for each filtered 10 mL sample. Residuals were analyzed using inductively coupled plasma optical emission spectroscopy (ICP-OES, Varian 710-ES with Autosampler). Combined aluminum (aluminum nitrate,

$Al(NO_3)_3$, analytical reagent grade, Ricca Chemical Corporation) and silica (Sodium metasilicate nonahydrate, $Na_2O_3Si \cdot 9H_2O$, analytical reagent grade, Ricca Chemical Corporation) standards were made from 1000 mg/L (+/- 5 mg/L) ICP/AA standard solutions and acidified to 2% nitric acid by volume. Aluminum wavelengths were set at 237.312 nm, 308.215 nm, and 396.152 nm, while the silicon wavelengths were 250.690 nm, 251.611 nm, and 288.158 nm. Therefore, no interference between elements was expected. Standard calibration curves were made prior to each sample analysis and the 250.690 nm (R^2=0.9996) and 396.152 nm (R^2=0.9988) wavelengths were chosen based on best fit for the silica and aluminum standard curves, respectively.

Organic acid samples were preserved by filtration and storage at 4°C until analysis. Residual organic concentrations were measured with UV-Vis absorbance at various wavelengths with an Agilent 8453 spectrophotometer and in 1 cm quartz cuvettes. Stehouwer (2014) identified optimal wavelengths for each LMW organic by scanning for regions of highest absorbance. Table 9 lists the wavelengths used for each organic in this study, based on the aforementioned investigation. Protonation state of the organic acid can affect the molar absorptivity of the compound and thus the overall UV-Vis absorbance; therefore, samples were acidified immediately before analysis with 5 µL of 1 N hydrochloric acid per 1 mL sample (0.5% by volume) to ensure that speciation was consistent across samples. Seven-point standard curves made in the appropriate synthetic matrix were used to relate absorbance and concentration in each organic acid analysis.

Table 9: UV-Vis wavelengths for residual organic acid analysis

Organic Acid	Wavelength (nm)
Pyromellitic	294
Salicylic	296
Phthalic	277

3.2.4 *In situ* ATR-FTIR analysis of precipitates

Precipitates were analyzed with FTIR after 40 minutes of quiescent settling for the non-aged samples and after 1-3 weeks of aging in sealed polyethylene jars for the remaining samples. Once settling and/or aging was complete and supernatant samples were withdrawn, a portion of the remaining supernatant was poured off and the remaining liquid-solid mixture was transferred into 50 mL polypropylene centrifuge tubes. The liquid-solid mixtures were centrifuged at 3000 rpm for 10 minutes. The instrument used to collect the infrared spectra was a Bruker Optics IFS 66v/S FTIR with a broad band mercury cadmium telluride detector at an aperture setting of 5mm. The ATR attachment used was a Specac Golden Gate with a diamond crystal and self-leveling pressure anvil. Prior to each sample spectrum, air was used as the background to correct for any spectral contributions inherent in the instrument setup. Ultrapure water spectra were recorded for subsequent water subtractions. Supernatant from centrifuged solids was decanted and a small mass of wet, amorphous solid was placed on the ATR crystal (Figure 6). Dry laboratory air was blown over each sample for 1 minute to remove excess bulk water and thus reduce spectral interference. Drying was vital since water absorbs around 1600 cm^{-1} near the regions of LMW organic acid absorbance. After the partial bulk water removal, uniform pressure was applied to the sample to ensure proper contact with the crystal by applying force from the adjustable ATR attachment onto a centrifuge cap resting on a

silica microscope slide (Figure 7). Each IR run consisted of 200 scans over the range of 500 cm^{-1} to 4000 cm^{-1}.

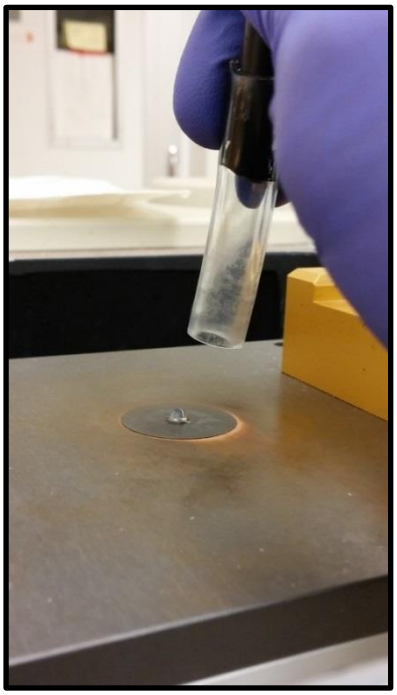

Figure 6: Amorphous solid sample on the ATR crystal undergoing partial drying of bulk water.

Figure 7: Method used to apply uniform pressure and achieve adequate crystal contact

Initially, the sample spectra were recorded with Bruker Opus Spectroscopy software, however all subsequent spectral analysis was done in MATLAB (Version R2015b, MathWorks). The initial step in spectral analysis was subtraction of the bulk water absorbance. Bulk water, both in the solid samples and ultrapure water samples, absorbed strongly at 3300 cm^{-1} and 1640 cm^{-1} which agrees well with the literature

(Bertie et al., 1989; Kanno et al., 2014). Subtraction of the bulk water was accomplished by subtracting the ultrapure water spectrum from each raw, solids spectrum. However, because the amount of residual bulk water varied slightly among the samples, different subtraction factors were required for each sample. Equation 3 describes the bulk water subtraction process.

$$\boldsymbol{c = r - fw} \quad \textbf{(3)}$$

where:

c *are the absorbance values of the corrected spectrum*,

r *are the absorbance values of the raw sample spectrum*,

w *are the absorbance values of the ultapure water spectrum,* and

f *is the water subtraction factor*

The selection of each subtraction factor involved a delicate balance: inadequate subtraction resulted in an overshadowing of nearby features, whereas excessive subtraction resulted in negative peaks and feature losses. The magnitudes of the 3300 cm^{-1} and 1640 cm^{-1} peaks were used to assess the quality of the subtraction. This process is illustrated in Figure 8. After proper bulk water subtraction, the spectra were smoothed using a built-in Savitsky-Golay filter in MATLAB. The polynomial order was set at 2 and the frame size varied between 21, 31 and 51 depending on the noise of the spectra. Higher polynomial orders and lower frame sizes correspond to less filtering, thus the aforementioned parameters were chosen to optimize the elimination of noise without losing key features. Figure 9 displays the impacts of the filtering process.

To aid in the identification of peaks, the MATLAB "findpeaks" function was used with a minimum prominence level set at 0.003 absorbance units to avoid the

identification of trivial features. Peak magnitude is indicative of the amount of adsorbed species, however, absolute peak magnitude can vary with the degree of contact between the sample and ATR crystal (Shimadzu, 2016). Therefore, comparisons using peak to peak ratios of a target feature to another prominent feature (such as sulfate) are implemented to correct for these variations in crystal contact. Deconvolution of peaks was performed with OriginPro 8.5 (OriginLab) using a nonlinear multiple peak fit.

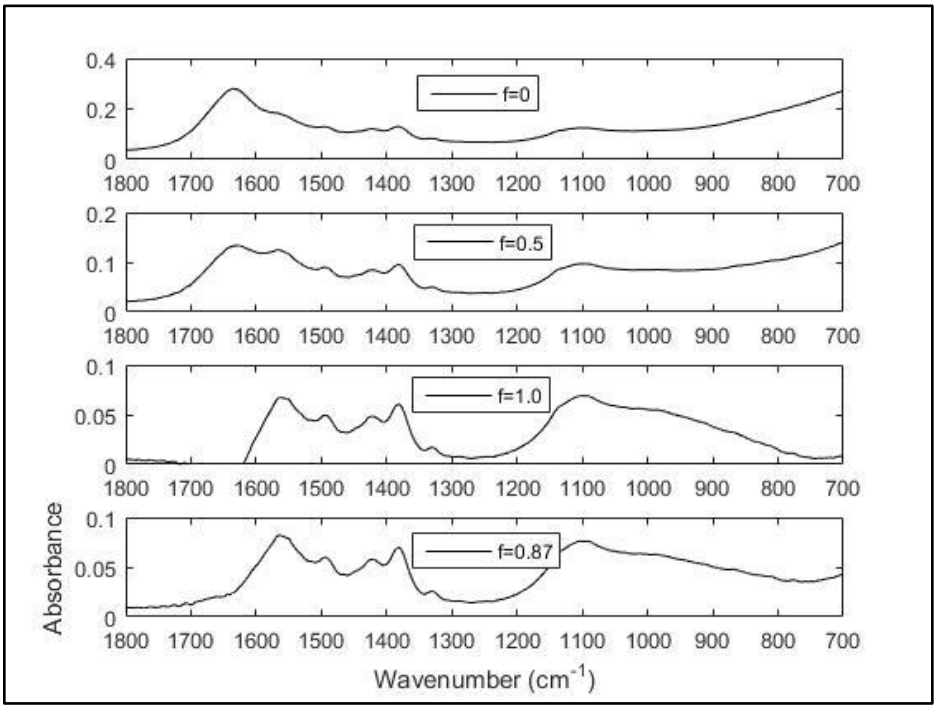

Figure 8: The impacts of water subtraction on a sample spectrum. f=0.87 provides the ideal subtraction magnitude.

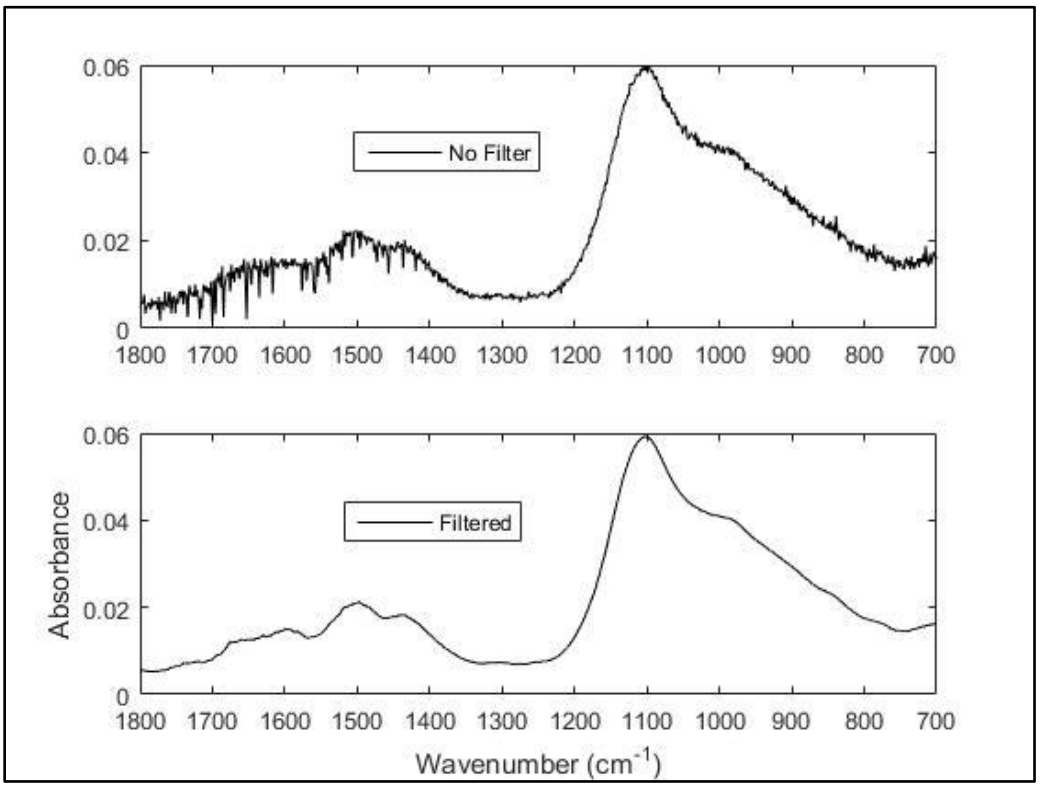

Figure 9: The effects of filtering on a sample spectrum with an excessively noisy signal. The filter used was a Savitsky-Golay with polynomial degree 2 and frame size 51

Chapter 4: Results and Discussion

This chapter presents the results of the investigation investigating the effect of ligands on alum coagulation precipitates in three main sections. The first section introduces each ligand and its respective mechanism of adsorption to the aluminum hydroxide surface as informed by the *in situ* FTIR findings. Secondly, analysis of ligand removal from aluminum coagulation jar tests conducted in the multi-ligand systems is discussed in combination with the spectroscopy data to understand competitive adsorption among the ligands. Lastly, insights from the varied levels of aging are discussed.

4.1 *IN SITU* FTIR RESULTS: INNER- VS. OUTER-SPHERE COMPLEXATION

4.1.1 Fluoride adsorption mechanism

Like other monatomic ions in solution such as chloride, fluoride ions are infrared inactive due to a lack of dipole moment. Therefore, changes in fluoride spectral features upon complexation with a surface are impossible to identify directly since no fluoride ion features exist. However, the FTIR detection and mechanistic identification of fluoride adsorption is often inferred by observing shifts in surface bound hydroxyl groups (OH) and surface water hydrogen bonding (Jayarathna et al., 2015; Tang et al. 2009). Jayarathna et al. (2015) noted that surface OH groups experiencing hydrogen bonds with adjacent outer-sphere coordinated water molecules contributed to a broad peak in the region around 3400 cm^{-1} in the spectrum of bare metal oxide. When fluoride was adsorbed, a dip was observed around 3400 cm^{-1} and new, defined peaks appeared at slightly higher wavenumbers. It was concluded that fluoride was taking part in ligand exchange with OH at the surface, resulting in a decreased signal of the hydrogen bonded OH around 3400 cm^{-1}. Vithanage et al. (2012) also attributed peaks near 3400 cm^{-1} to

OH coordination to trivalent cations such as aluminum and iron; thus, decreases in IR absorbance in this region may indicate the replacement of these OH groups by fluoride.

In Figure 10, FTIR spectra of precipitates from the sulfate matrix with and without fluoride and at pH 6.5 are shown. Focusing on the OH region near 3400 cm^{-1}, it is evident that, upon fluoride addition, there is a shift of the larger wavenumber peak to a higher frequency; this result agrees well with findings by Vithanage et al. (2012) where metal-OH and metal-O vibrations were observed to shift to higher frequencies after disruption by inner-sphere fluoride adsorption. In Figure 10, the prominent negative peak spanning from 3200 to about 3400 cm^{-1} may be due to the reduction in signal from hydrogen bonded and trivalent coordinated OH groups caused by ligand exchange of these groups with fluoride. Based on these observations, it is likely that fluoride replaces OH and coordinates with aluminum to form inner-sphere monodentate complexes, a widely accepted hypothesis as discussed in Chapter 2. Because the 3400 cm^{-1} region where the hydroxyl ligand exchange occurs is highly sensitive to the water subtraction, the impact of varied water subtraction factors (r) is shown in Figure 11. The above hydroxyl ion observations in the 3400 cm^{-1} region were not sensitive to r.

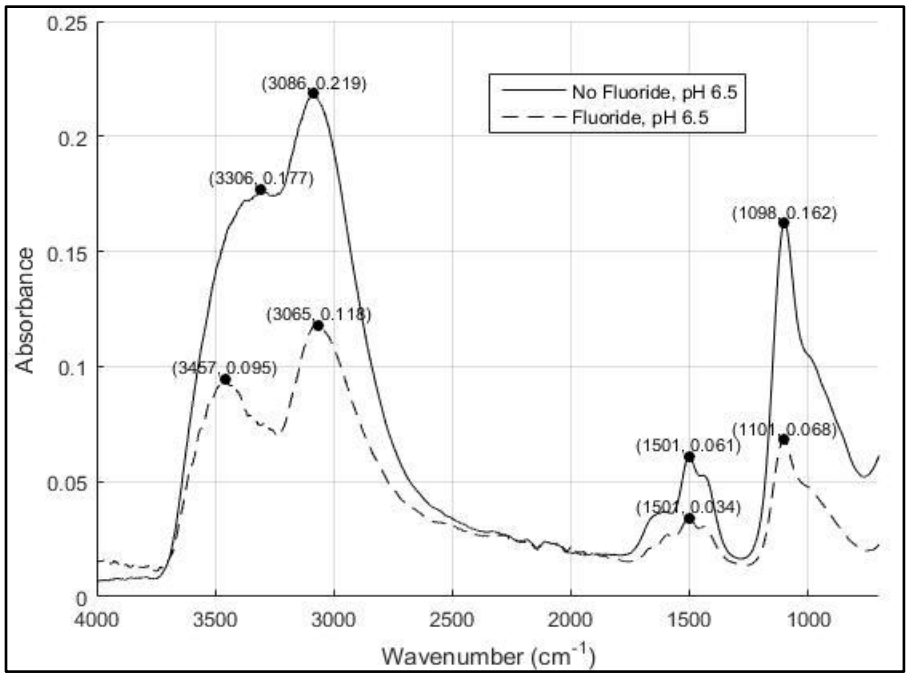

Figure 10: ATR-FTIR spectra comparing the precipitates with and without fluoride in sulfate matrices, both at pH 6.5. No additional ligands present

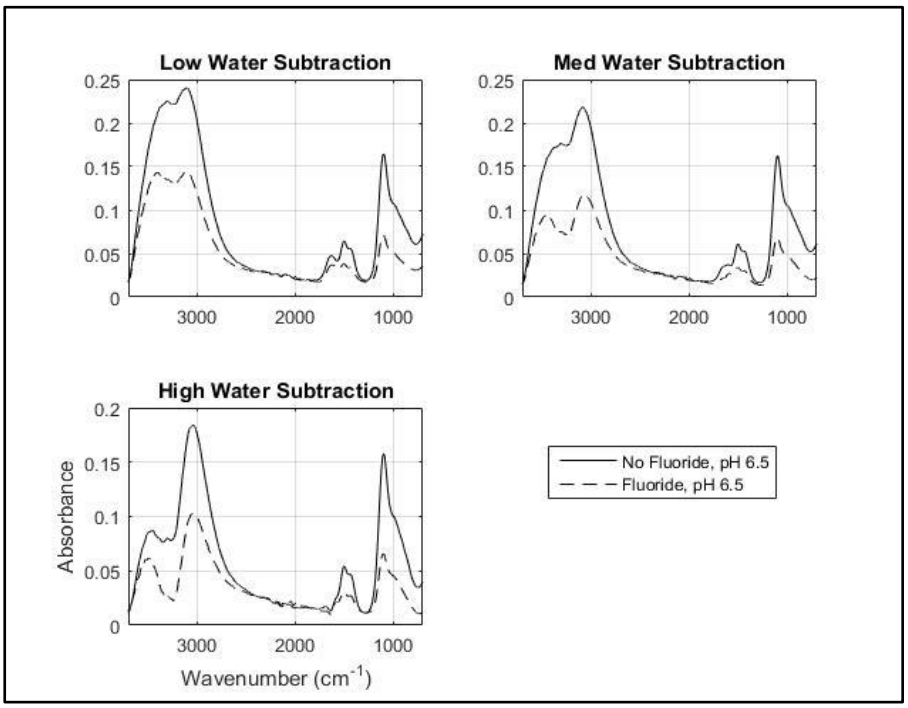

Figure 11: ATR-FTIR spectra comparing the precipitates with and without fluoride in sulfate matrices and varied water subtraction factors, all at pH 6.5.

4.1.2 Carbonate adsorption mechanism

Carbonate was present in every reactor as the main source of alkalinity and buffering, much like natural systems. As a multiprotic acid-base system, the distribution of carbonate species is strongly dependent on pH as illustrated in Figure 12 and Figure 13. In both open and closed systems at pH 6.5, we expect large amounts of both carbonic acid (H_2CO_3*) and bicarbonate (HCO_3^-), with slight dominance by the bicarbonate species. At pH 7.5, bicarbonate dominates in the open and closed systems.

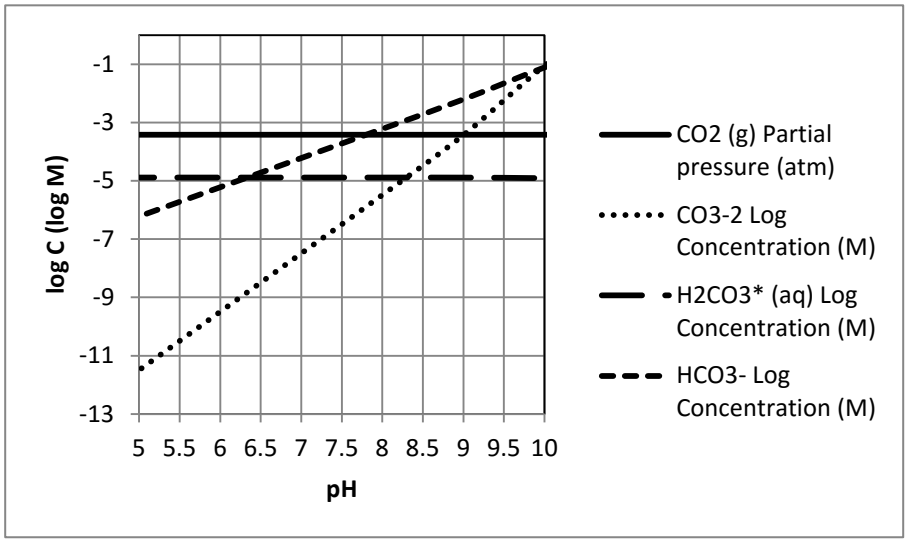

Figure 12: Carbonate speciation at 3 mM open to the atmosphere calculated in Visual MINTEQ

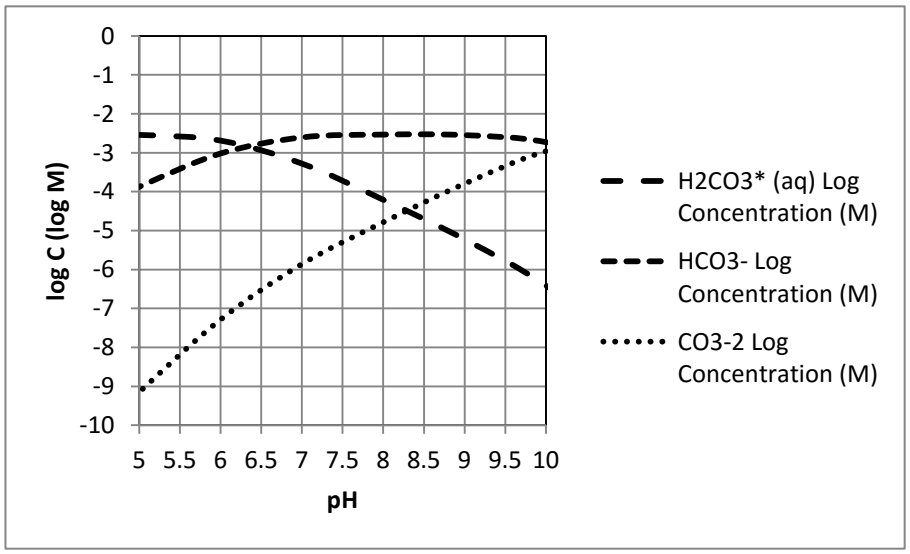

Figure 13: Carbonate speciation at 3 mM closed to the atmosphere calculated in Visual MINTEQ

The determination of surface coordination type relies on IR comparisons between carbonate adsorbed to the amorphous aluminum hydroxide surface and non-adsorbed carbonate in solution. In Figure 14, three peaks are apparent in the samples containing carbonate and sulfate (from alum) at pH 6.5 and at pH 7.5. The prominent feature at 1100 cm^{-1} can be attributed to sulfate and is discussed in more detail in the subsequent section, 4.1.3. However, the features at 1500 cm^{-1} and 1435 cm^{-1} result from carbonate coordination to the surface (Wijnja and Schulthess, 1998; Su and Suarez, 1997).

Table 10: FTIR vibrations of HCO_3^- in solution

HCO_3^- Vibration	Group/Type	Wavenumber in Solution (cm^{-1})
ν_1	C-OH stretch	1010
ν_2	CO_2 symmetric stretch	1360, 1310
ν_3	CO_3 symmetric in-plane bend	<800
ν_4	CO_2 asymmetric stretch	1670, 1605
ν_5	CO_3 asymmetric in-plane bend	<800
ν_6	CO_3 out-of-plane bend	840

Table 11: FTIR vibrations of CO_3^{2-} in solution and changes upon surface coordination

CO_3^{2-} Vibration	Group/Type	Wavenumber in Solution (cm^{-1})	Change Upon Coordination
ν_1	Symmetric stretch	1050-1070	None
ν_2	Out-of-plane bend	890	None
ν_3	Asymmetric stretch	1380-1390	Splitting into 2 distinct bands (1200-1455 cm^{-1} and 1450-1800 cm^{-1})

In solution, the family of carbonate species can exhibit various fundamental vibration modes which have been referred to as ν_1 through ν_5 and assigned as shown in Tables 10 and 11 above (Su and Suarez, 1997). In a solution containing the free, planar, tetratomic HCO_3^- ion, ν_1 represents the stretching of a C-OH group (1010 cm^{-1}), ν_2 is the symmetric stretching of CO_2 (1360 and 1310 cm^{-1}), ν_3 is a symmetric in-plane bending of CO_3 (<800 cm^{-1}), ν_4 is asymmetric stretching of CO_2 (1670 and 1605 cm^{-1}), ν_5 is an asymmetric in-plane bending of CO_3 (<800 cm^{-1}), and ν_6 is an out-of-plane bending of CO_3 (840 cm^{-1}) (Su and Suarez, 1997). In the work of Wijnja and Schulthess (1999), similar features were identified, but slightly different ν assignments were used. In solutions containing free trigonal planar CO_3^{2-} anions, expected vibrational modes are a ν_1 symmetric stretching (1050-1070 cm^{-1}), ν_2 out-of-plane bending (890 cm^{-1}), and ν_3 asymmetric stretching (1380-1390 cm^{-1}) (Su and Suarez, 1997; Wijnja and Schulthess, 1999).

When CO_3^{2-} undergoes inner-sphere coordination with a metal surface, the ν_3 asymmetric stretching feature splits into 2 distinct bands due to a disruption of the trigonal planar molecular symmetry. These two bands are the result of symmetric and asymmetric stretching of the unbound (in reference to the surface) oxygens (Villalobos

and Leckie, 2001). The free CO_3^{2-} ν_3 peak is situated around 1390 cm^{-1} and splits into two peaks that straddle the original aqueous peak once adsorbed to the surface. The degree of this splitting, $\Delta\nu_3$, indicates the denticity of the inner-sphere complex. Wijnja and Schulthess (1999) examined complexation with aluminum oxide surfaces and listed $\Delta\nu_3$ values in the range of 79-160 cm^{-1} as monodentate complexes, 300-395 cm^{-1} as bidentate, and values above this as bridging complexes.

Despite the fact that HCO_3^- is the dominant species in solution at the pH values in this study, CO_3^{2-} was the main adsorbed species identified. HCO_3^- can be identified by its distinct ν_4 doublet around 1670 and 1605 cm^{-1} which is only vaguely present, if at all, in the spectra where carbonate species are present. This observation is consistent with both Wijnja and Schulthess (1999) and Su and Suarez (1997) where the only adsorbed species identified was CO_3^{2-} despite operating in pH regions where HCO_3^- dominates.

A comparison of the absorbance intensities between features can be used as a proxy for the relative amount of adsorption of a given species to the surface. When comparing changes in carbonate to sulfate absorbance ratios for selected features (e.g., CO_3^{2-} at 1500 cm^{-1} to SO_4^{2-} at 1100 cm^{-1}) from experiments conducted at pH 6.5 versus 7.5 in Figure 14, it is evident that relatively more adsorption of carbonate occurs in the pH 7.5 case (the ratio of CO_3^{2-} peak absorbance to the SO_4^{2-} peak absorbance is 0.38 for pH 6.5 and 0.51 for pH 7.5). This result may be due to a higher CO_3^{2-} content in the more basic solution, ultimately resulting in more adsorption of CO_3^{2-} to the surface.

CO_3^{2-} features were the primary focus of this study since no prominent HCO_3^- vibrations were detected. In particular, an emphasis was placed on the ν_3 feature around 1390 cm^{-1}, since a splitting of this vibration informs the type of complex forms. The 1500 and 1435 cm^{-1} peaks in Figure 14 are attributed to a splitting of the 1390 cm^{-1} CO_3^{2-} ν_3 feature, which is indicative of inner-sphere coordination of CO_3^{2-}. The $\Delta\nu_3$ values in our

spectra ranged from 65-105 cm^{-1}, consistent with monodentate complexation (see Table 14). Su and Suarez (1997) obtained $\Delta\nu_3$ values of 64-75 cm^{-1} from various concentrations of total carbonate adsorbing to amorphous aluminum hydroxides and reached the same conclusion of inner-sphere monodentate complexation. Since carbonate is either naturally present or added to control alkalinity in coagulation systems, inner-sphere surface complexation of carbonate is likely to impact the removal of other ligands in water treatment systems.

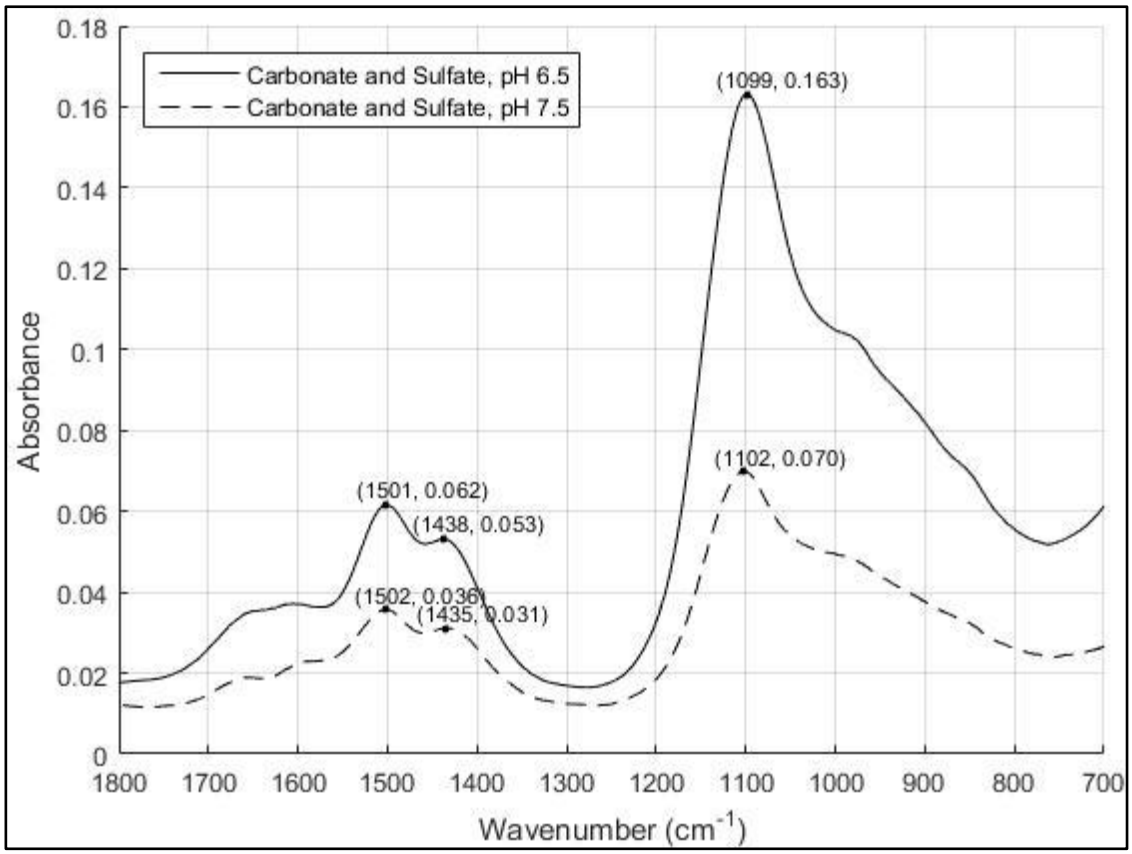

Figure 14: ATR-FTIR spectra comparing the non-aged precipitates with carbonate in the sulfate matrix at pH 6.5 and pH 7.5. No additional ligands present. Values in parentheses are (wavenumber, absorbance).

4.1.3 Sulfate adsorption mechanism

Sulfate is present in the experiments conducted in sulfate matrices and is not present in the chloride matrix tests. The total sulfate concentration in these waters results from the addition of alum coagulant, sodium and calcium salts (for hardness and ionic strength), and sulfuric acid (to prevent instantaneous aluminum precipitate nucleation upon coagulant addition) summing to a total concentration of approximately 5.7 mM. In solution, the free sulfate ion (SO_4^{2-}) exhibits a tetrahedral symmetry. This tetrahedral symmetry results in a pronounced peak at around 1100 cm^{-1} due to the ν_3 asymmetric stretching of S-O (Hug, 1997; Peak et al., 1999; Muller and Lefevre, 2011; Wijnja and Schulthess, 2000). ν_1 is a symmetric S-O stretching that also results from free tetrahedral SO_4^{2-} in solution and occurs around 980 cm^{-1}; however, this vibrational mode is IR inactive and can only be visualized with Raman spectroscopy (Hug, 1997; Muller and Lefevre, 2011). In Figure 15, a prominent peak occurs at 1100 cm^{-1} in the sulfate matrix, but is absent in the sample taken from the chloride matrix. Due to the IR similarities that the adsorbed samples in this study share with the known IR features of sulfate in solution, it is concluded that sulfate is not directly coordinated with the metal surface, but adsorbs via outer-sphere complexation. In the event that inner-sphere complexation was occurring in this study, the tetrahedral symmetry of the SO_4^{2-} ion in solution would be disrupted upon coordination to a metal-oxide surface, resulting in a split of the 1100 cm^{-1} ν_3 vibrational band and the appearance of the previously IR-inactive ν_1 peak at around 980 cm^{-1} (Hug, 1997; Peak et al., 1999, Muller and Lefevre, 2011). Because the 1100 cm^{-1} peak persists throughout our sulfate samples, it is evident that the SO_4^{2-} symmetry with its waters of hydration is not disrupted and outer-sphere complexation is the main mechanism of adsorption. This observation held for all ligand combinations with sulfate present. It is plausible that a small fraction of sulfate is undergoing inner-sphere

complexation, as concluded in the work of Peak et al. (1999) and Wijnja and Schulthess (2000), however, outer-sphere complexation is the dominant mechanism under the conditions examined in this study.

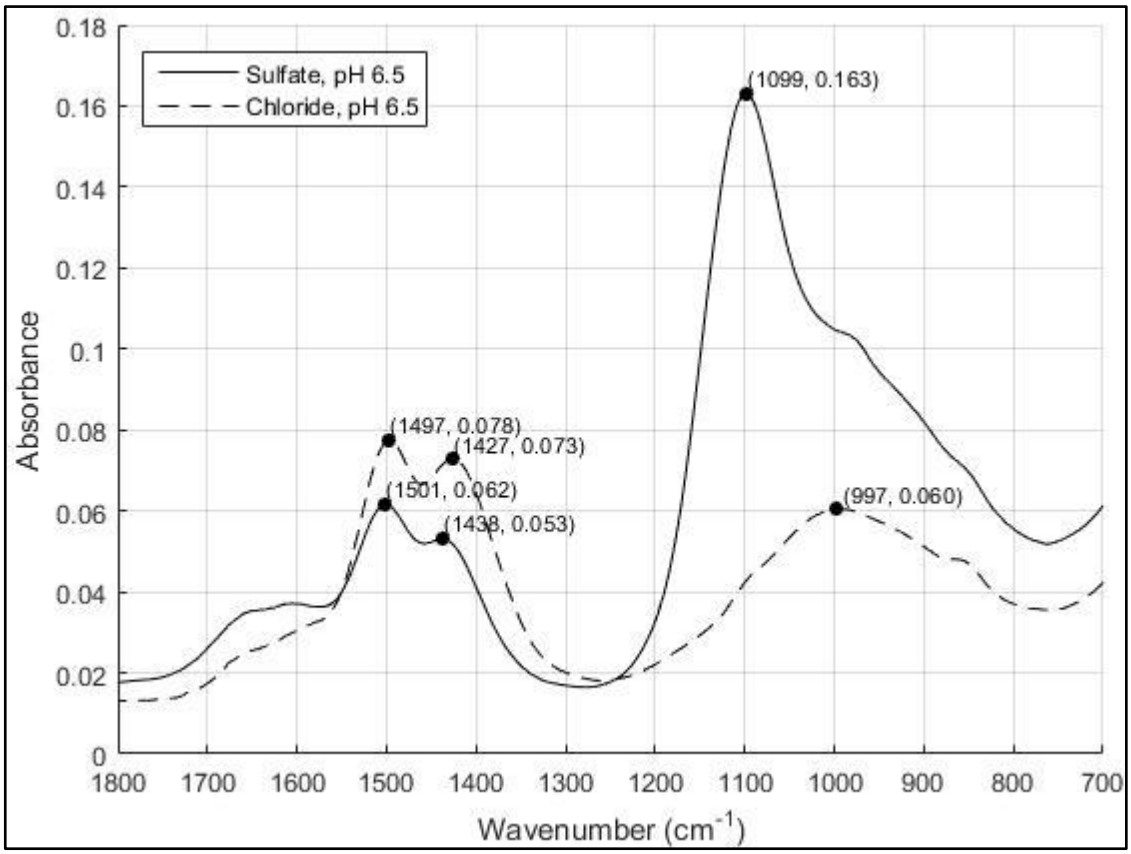

Figure 15: ATR-FTIR spectra comparing the non-aged precipitates in the sulfate matrix to those in the chloride matrix, both at pH 6.5. No additional ligands present. Values in parentheses are (wavenumber, absorbance).

4.1.4 NOM surrogate adsorption mechanism

The three LMW organic acids employed as NOM surrogates in this study were pyromellitic acid, salicylic acid, and phthalic acid. These aromatic carboxylates exhibit several features in the 1300 to 1700 cm^{-1} range depending on the number and types of functional groups present (Nordin et al., 1998). In Figure 16, spectra of the freshly precipitated aluminum hydroxides with pyromellitate, phthalate, and salicylate in sulfate matrices at pH 6.5 are compared to the precipitates with carbonate in the sulfate matrix at the same pH. In the adsorbed pyromellitate spectrum, 5 pronounced features are observed in the 1300-1700 cm^{-1} range, typical of these compounds. While similar fingerprints in that infrared region are expected for salicylate and phthalate, no vibrations that would suggest a significant presence of these organics was observed in those spectra. Rather, the spectra of salicylate and phthalate more closely resemble the case in which no organics were present, showing features that suggest inner-sphere carbonate adsorption, as discussed in section 4.1.2. The absence of carboxylate features and appearance of carbonate in this infrared region holds for all experiments containing salicylate and phthalate. These spectra suggest that pyromellitate removal on the aluminum hydroxide surface was more significant than salicylate and phthalate removals, which is consistent with previous NOM surrogate removal results (Figure 17) and the removal data in this study which is discussed in further detail in section 4.2.2 (Stehouwer, 2014; Alfredo, 2012).

For the remainder of this investigation, the central NOM surrogate of concern will be pyromellitic acid. Focusing on the mechanism of pyromellitic acid removal on aluminum hydroxides provides valuable insight towards real NOM systems since pyromellitic acid is the largest and most carboxylate functionalized LMW acid in this study, most closely characterizes humic acid, and exhibited the closest removal patterns

to real NOM in previous jar test studies (Figure 17:) (Evanko and Dzombak, 1998; Glaser et al., 1998; Schnitzer and Calderoni, 1985).

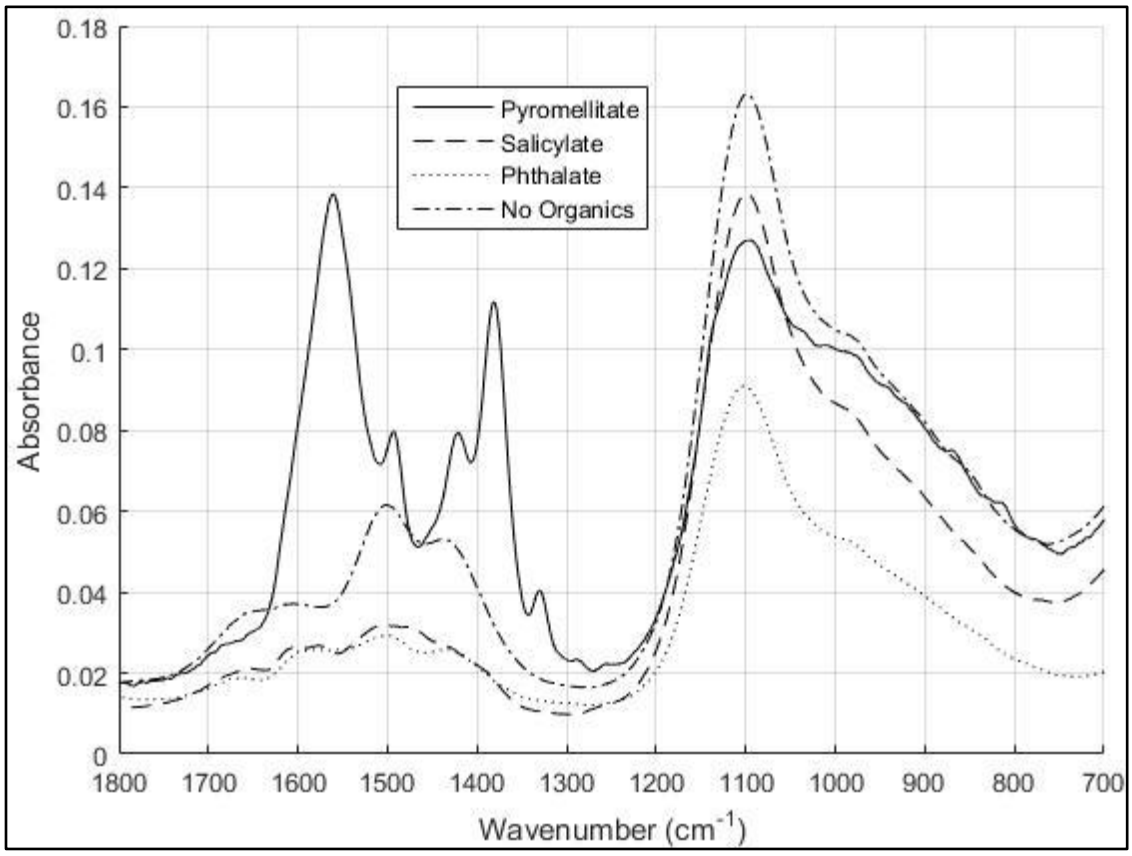

Figure 16: ATR-FTIR spectra comparing the non-aged precipitates in the sulfate matrix to the non-aged precipitates in the presence of the three LMW organic acids in the sulfate matrix, all at pH 6.5. No additional ligands present.

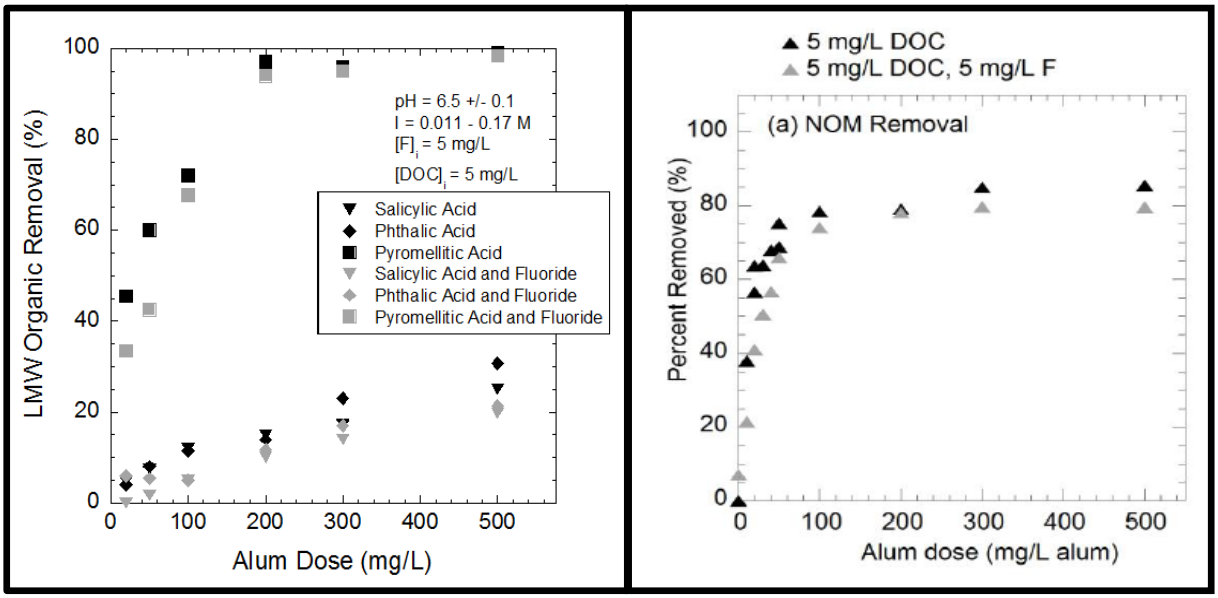

Figure 17: Comparison of NOM surrogates and actual NOM removals in synthetic water jar tests (Stehouwer 2014 and Alfredo 2012)

Fully deprotonated pyromellitate (Pyr^{4-}) in solution exhibits a total of six bands related to its aromaticity and carboxylate functional groups. Pyr^{4-}, the dominant species at the pH values in this study (see Table 6) has a planar aromatic ring with 4 perpendicular carboxylate groups (Nordin et al., 1998). These include a strong asymmetric C-O stretching around 1560 cm^{-1}, three symmetric C-O stretching vibrations around 1410, 1375, and 1325 cm^{-1}, a 1490 cm^{-1} in-plane vibration of the aromatic group, and a minor peak around 1135 cm^{-1} attributed to aromatic C-H bending (Nordin et al., 1998; Johnson et al., 2004; Guan et al., 2006). In Figure 18 the spectra of pyromellitate in a sulfate matrix and a chloride matrix both match closely with aqueous Pyr^{4-} with prominent vibrations at 1560, 1490, 1420, 1380, and 1330 cm^{-1}. Only in the chloride matrix can we see the small aromatic C-H bending at 1137 cm^{-1}. This same feature is manifested as a shoulder of the dominant 1100 cm^{-1} sulfate peak in the sulfate matrix spectrum. Addition

of other ligands such as fluoride and silicate do not disrupt these vibrational signatures. Much like sulfate, the nearly identical resemblance of the adsorbed pyromellitate spectra to aqueous deprotonated Pyr^{4-} spectral features means that, in this study, Pyr^{4-} is present on the amorphous aluminum hydroxide surfaces with its symmetry and waters of hydration intact. Therefore, pyromellitate is proposed to undergo outer-sphere complexation with the amorphous aluminum hydroxide flocs in this study. Outer-sphere complexation of pyromellitate has been previously proposed to occur on freeze-dried amorphous aluminum hydroxide at pH 5 (Guan et al., 2006), boehmite at pH 4.4-8.1 (Nordin et al., 1998), and corundum at pH>5 (Johnson et al., 2004).

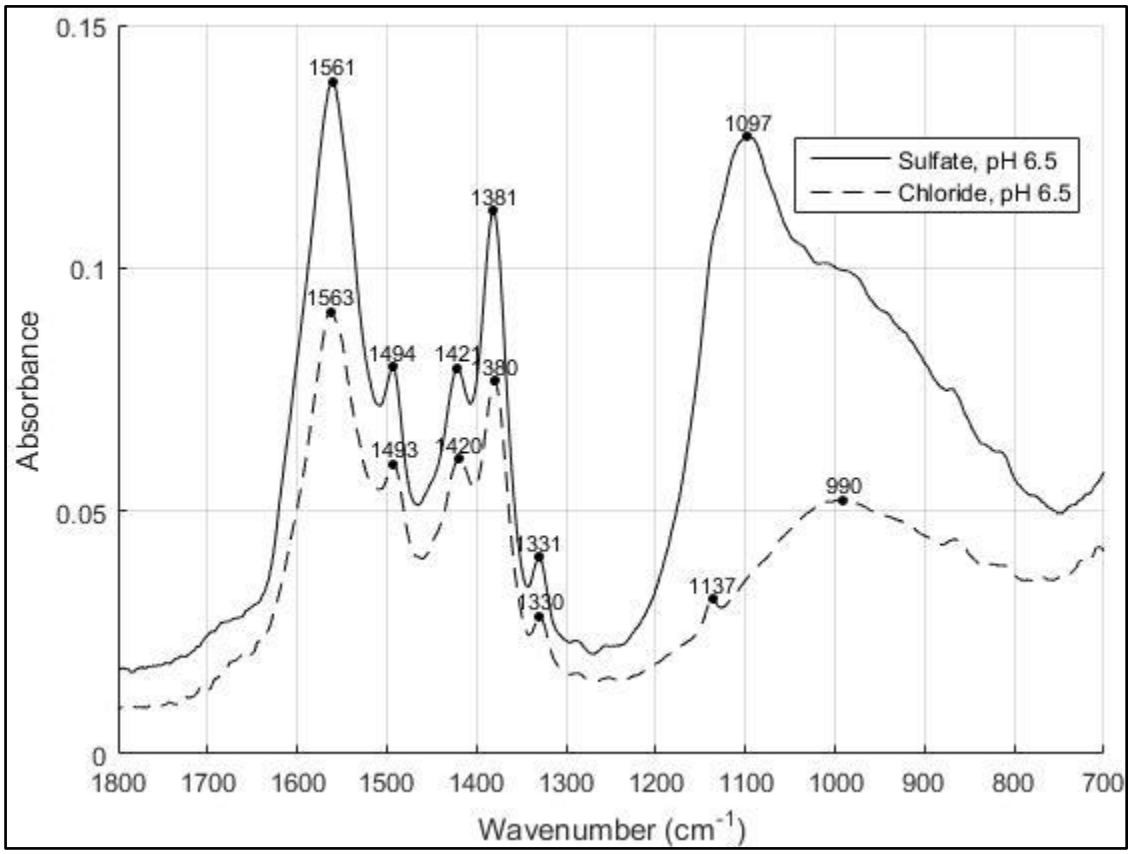

Figure 18: ATR-FTIR spectra comparing the non-aged precipitates with pyromellitate in sulfate and chloride matrices, both at pH 6.5. No additional ligands present.

4.1.5 Silicate adsorption mechanism

The goal of the FTIR analysis with respect to the silicate systems was determination of coordination type as well as to provide evidence of polymerization. The distribution of silicate species in solution at the total silica concentrations used in this study is shown in Figure 19. At a pH of 6.5 where the silicate ligand experiments were performed, the dominant species in solution is expected to be silicic acid ($Si(OH)_4$). Swedlund et al. (2009) conducted an FTIR study of the characterization silicic acid

adsorption to iron oxide surfaces. The structure of monomeric silicic acid can be approximated by tetrahedral symmetry with IR Si-O vibrations (an IR-inactive ν_1 symmetric stretch and an IR-inactive ν_3 asymmetric stretch) visible in the region between 800 and 1000 cm^{-1}. Upon inner-sphere coordination of the tetrahedron to a metal surface, symmetry is lowered, causing the ν_1 stretch to become active and the ν_3 stretch to split into two distinct bands. Bands around 890, 945, and 1020 cm^{-1} have been attributed to Si-O and Si-OH stretching vibrations of aqueous $SiO(OH)_3^-$ and $Si(OH)_4$ monomers from a sodium metasilicate solution (Yang et al., 2008).

Monomeric silicate species can also link to form dimers, trimers, and more complex polymers characterized with FTIR by Si-O-Si linkages (around 985 to 1080 cm^{-1}) and a migration of Si-O vibrations to higher frequencies (Gaggiano et al., 2013; Yang et al., 2008; Swedlund et al., 2009; Hu et al., 2015). A monomer has four non-bound oxygens (NBO) and the number of NBO decreases as silicates link with one another during polymerization. The number of NBO dictates where the FTIR vibration of the molecule occurs.

Table 12 summarizes the important silicate vibration assignments.

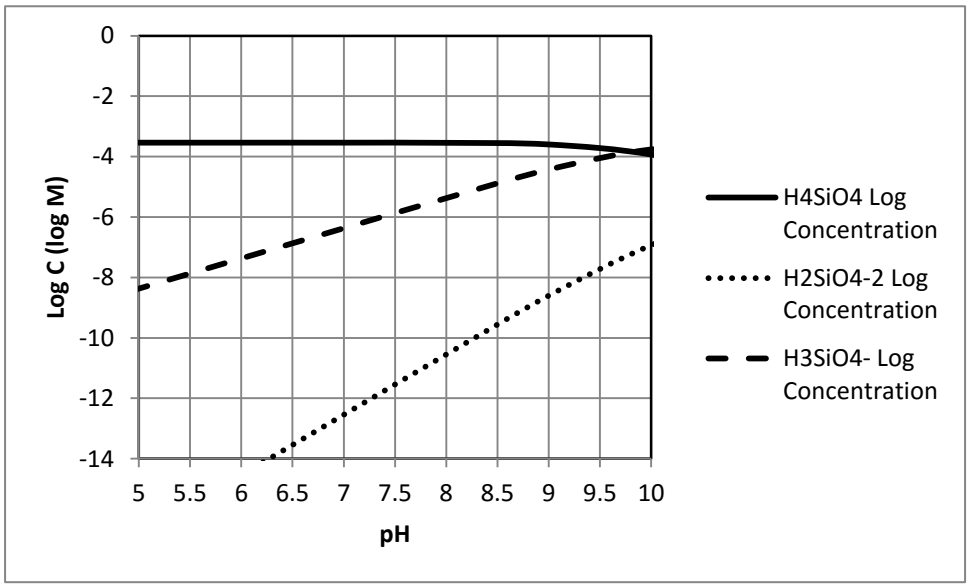

Figure 19: Silicate speciation with a total Si concentration of 0.29 mM calculated in Visual MINTEQ

Table 12: Silicate FTIR vibration assignments (Adapted from Gaggiano et al. 2013)

Silicate Feature	**Wavenumber cm^{-1}**	**This Study**
Si-O bending	800	insignificant/masked
Si-O (4NBO) stretching	850-855	masked
Si-O (3NBO) stretching	898-920	masked
Si-O (2NBO) stretching	938-953	masked
Si-O (1NBO) stretching	1040-1050	masked
Si-O-Si	985-1003	980-1000 cm^{-1}, grows with age
Si-OH	1093-1120	masked

Figure 20 shows the ATR-FTIR spectra of various aged precipitates in a sulfate matrix and in the presence of silicate ligands (in addition to the ever-present carbonate). In the infrared region shown, two sets of prominent peaks appear for each spectrum. The higher wavenumber feature around 1100 cm^{-1} is attributed to the outer-sphere complexed sulfate, as discussed in section 4.1.3. The second prominent vibration, occurring in the range of 980 to 1000 cm^{-1}, is attributed to Si-O-Si linkages.

An important aspect of these spectra is the relative growth of the Si-O-Si peak over time. When observing changes in the ratio of sulfate absorbance at 1100 cm^{-1} to silicate absorbance at 1000 cm^{-1}, a clear trend of increasing relative silicate intensity with time is observed for all four ligand conditions (Figure 21). Sulfate is used as a normalizing factor since the absolute peak magnitudes of silicate and sulfate vary between samples due to variations in diamond contact, but the amount of sulfate on the surface is assumed to be constant. It may be argued that a decrease in sulfate adsorption may be responsible for the decreasing sulfate to silicate peak ratios. However, carbonate to sulfate (or pyromellitate to sulfate) ratios between the silicate experiments and non-silicate analogues agree quite well, indicating that sulfate adsorption has not drastically changed at the surface in the presence of silicate (Figure 22). Therefore, the assumption that sulfate adsorption remained stable and that an increase in silicate adsorption with time was responsible for the trends observed is reasonable.

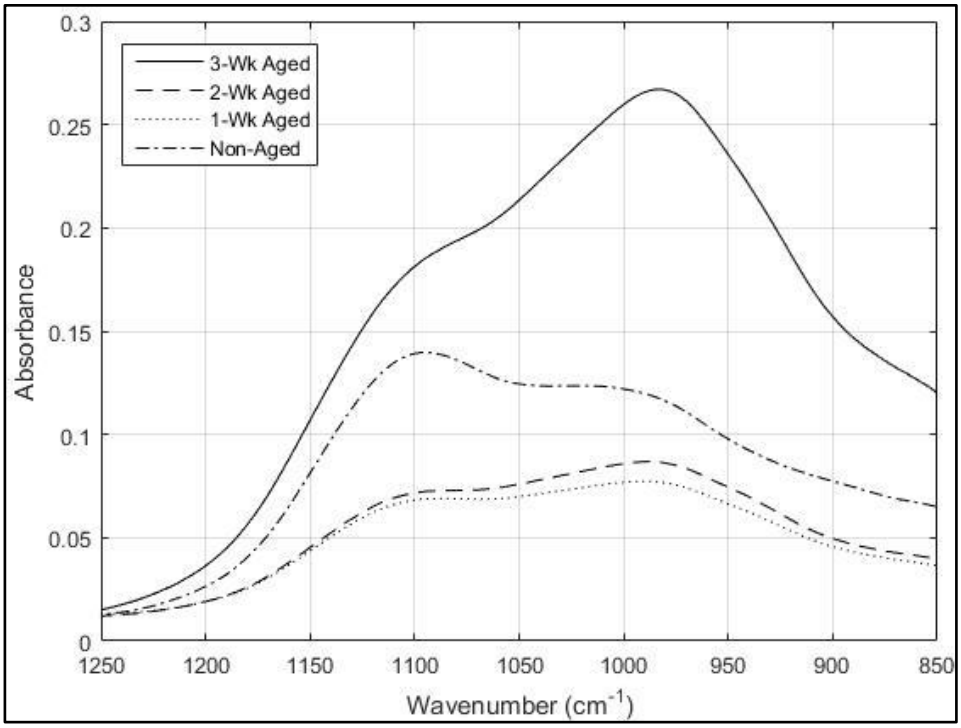

Figure 20: ATR-FTIR spectra comparing precipitates in sulfate matrices with silicate over time, all at pH 6.5. No additional ligands present.

Based on the presence of this prominent Si-O-Si peak in the 980 to 1000 cm^{-1} range and its growth with time, it appears that silicate adsorbed to the aluminum hydroxide and accumulated at the surface over time, undergoing polymerization in the process. Due to the crowding of features in the region of silicate and sulfate adsorption, deconvolution of the signal was done with a multiple peak fitting tool (Figure 23). In the multiple peak fit, previously masked Si-O vibrations in the region around 900 cm^{-1} can be observed. Additionally, it is again evident that the vibration of the Si-O-Si linkage becomes more prominent with time supporting the case for polymerization at the surface. Gaggiano et al. (2013) suggested that in the first stages of silicate adsorption to alumina,

small anions such as monomers and dimers attach to the surface followed by a deposition of larger particles and further polymerization of the deposited silicates at the surface with time.

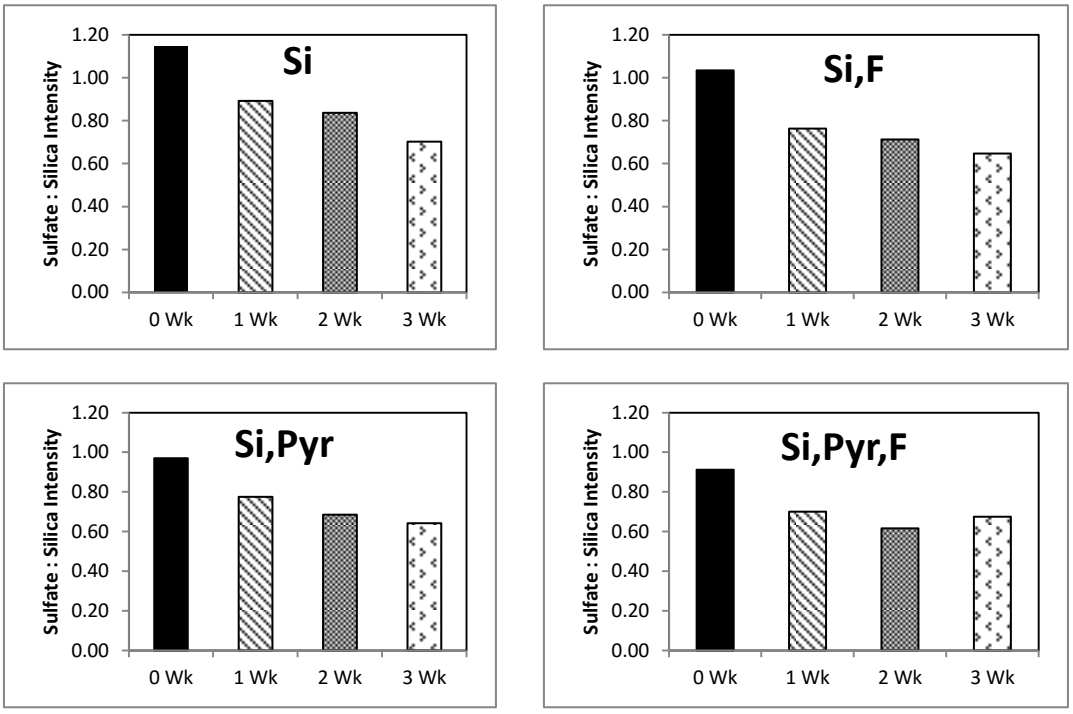

Figure 21: Sulfate to silicate peak ratios for all precipitates with silicate present. Abscissa values refer to time of aging. Ratios correspond to the spectra in Figure 19.

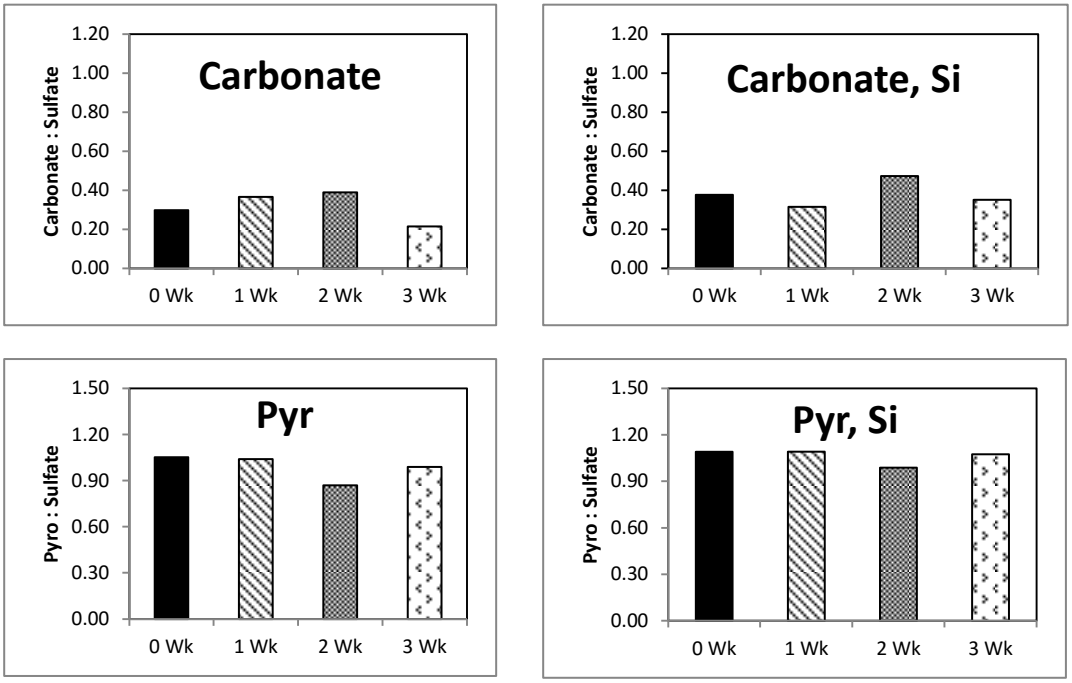

Figure 22: Carbonate to sulfate and pyromellitate to sulfate peak ratios comparing samples with solely carbonate or pyromellitate to those with added silicate. All at pH 6.5

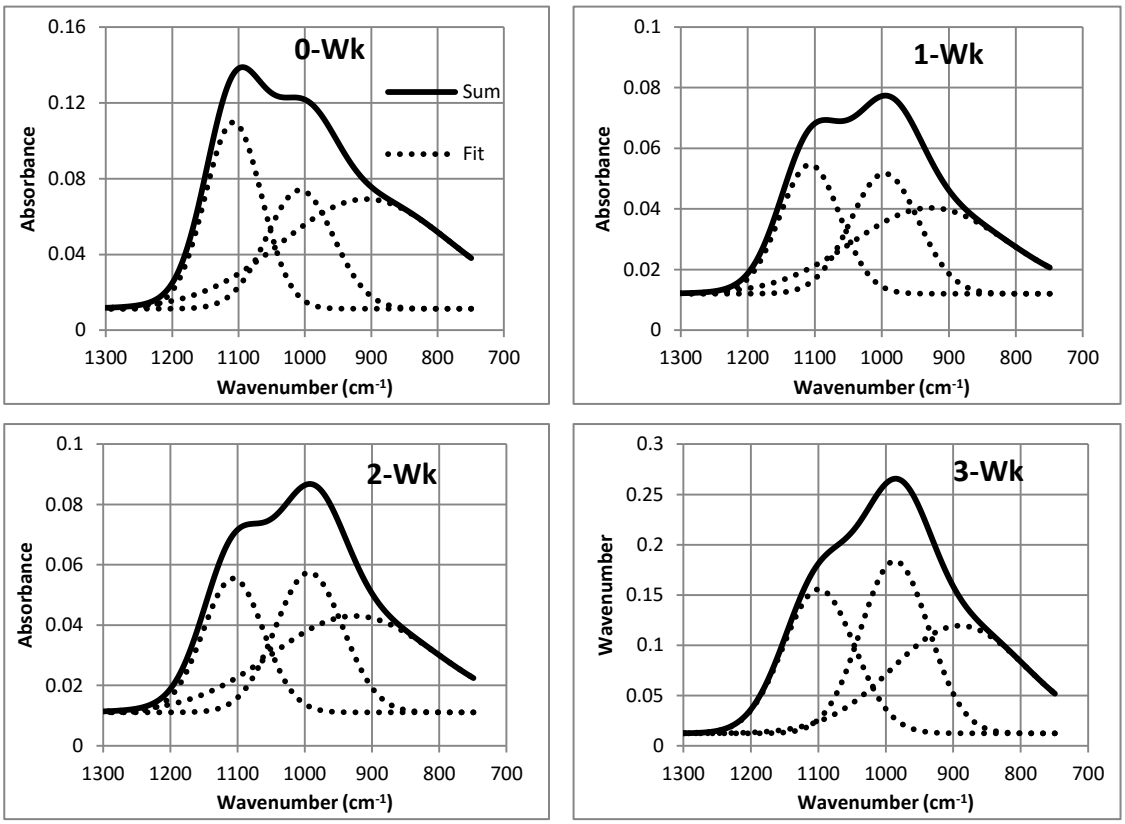

Figure 23: Deconvolution of the silicate IR region for precipitates with silicate in a sulfate matrix over time

Due to the dominance of the Si-O-Si and sulfate features in this infrared region, it is difficult to identify vibrational fingerprints such as a ν_3 splitting that would provide further insights toward the type of coordination that is occurring at the surface. Further deconvolution of these spectra or further investigations in the absence of sulfate would be appropriate to identify these features. However, the presence of polymerization at the surface strongly suggests that a significant inner-sphere interaction is occurring. Previous investigations have identified accumulation and polymerization of silicates on metal

oxide surfaces with inner-sphere adsorption as the proposed mechanism of coordination (Yang et al., 2008; Swedlund et al., 2009; Hu et al., 2015).

4.1.6 Summary

With ATR-FTIR spectroscopy, microscopic insights about ligand complexation to the surface of the aluminum hydroxide flocs can be made *in situ*. Table 13summarizes the spectroscopic findings in this section.

Table 13: Ligand surface complex conclusions from ATR-FTIR data

Ligand	Proposed surface complex in this study	Reasoning
Carbonate	Inner-sphere monodentate	Coordination results in disruption of symmetry: ν_3 splitting
Sulfate	Outer-sphere	No disruption of symmetry, therefore no vibrational shifts from aqueous spectrum
Pyromellitate	Outer-sphere	No vibrational shifts from aqueous spectrum
Fluoride	Inner-sphere monodentate	Disruption of trivalent and hydrogen-bonded hydroxyl groups in the presence of fluoride
Silicate	Inner-sphere with accumulation and polymerization over time	Gradual increase in the intensity of Si-O-Si peaks over time

4.2 LIGAND COMPETITION

The following results and discussion draw from both the FTIR spectroscopic data and macroscopic aqueous residual data. This section includes interactions involving fluoride and NOM surrogates in the non-aged experiments. The impacts of aging are discussed in section 4.3.

4.2.1 Interactions involving fluoride

The understanding of interactions among ligands can often be explained based on differences in binding mechanisms and affinity. One prominent observation with fluoride was the impact of sulfate and chloride on fluoride removals. Both chloride and sulfate concentrations are relatively high in the synthetic water composition after dosing with aluminum salt coagulants (3.0 mM and 5.7 mM, respectively). In Figure 24: (bottom), it is apparent that fluoride removals are reduced in the sulfate synthetic water versus the chloride synthetic water. Comparison of the spectroscopic results for the two systems (Figure 24, top) indicate that the 1100 cm^{-1} peak, indicative of outer-sphere SO_4^{2-} ,is absent from the chloride matrix spectrum. Although it was not covered in the FTIR analysis in this study because of its IR inactivity, chloride is believed to undergo outer-sphere complexation as well (Tang et al., 2009). Therefore, even though fluoride is an inner-sphere complex and both chloride and sulfate are outer sphere complexes, there appears to be competition between these outer sphere complexes and fluoride for surface sites during precipitation. Moreover, sulfate competes more effectively with fluoride than chloride does, suggesting that sulfate has a higher affinity for the aluminum surface relative to chloride. Some studies have shown that sulfate adsorption is a spectrum of inner-sphere and outer-sphere adsorption, and thus it is possible to have a combination of both mechanisms at play with one as the dominant mechanism that is apparent in the spectra (Wijnja and Schulthess, 2000; Peak et al., 1999). However, further investigations

at lower sulfate concentrations need to be conducted to determine whether inner-sphere sulfate complexes that may be present are responsible for reducing the ligand exchange of fluoride for hydroxyl groups within the precipitating aluminum hydroxide phase.

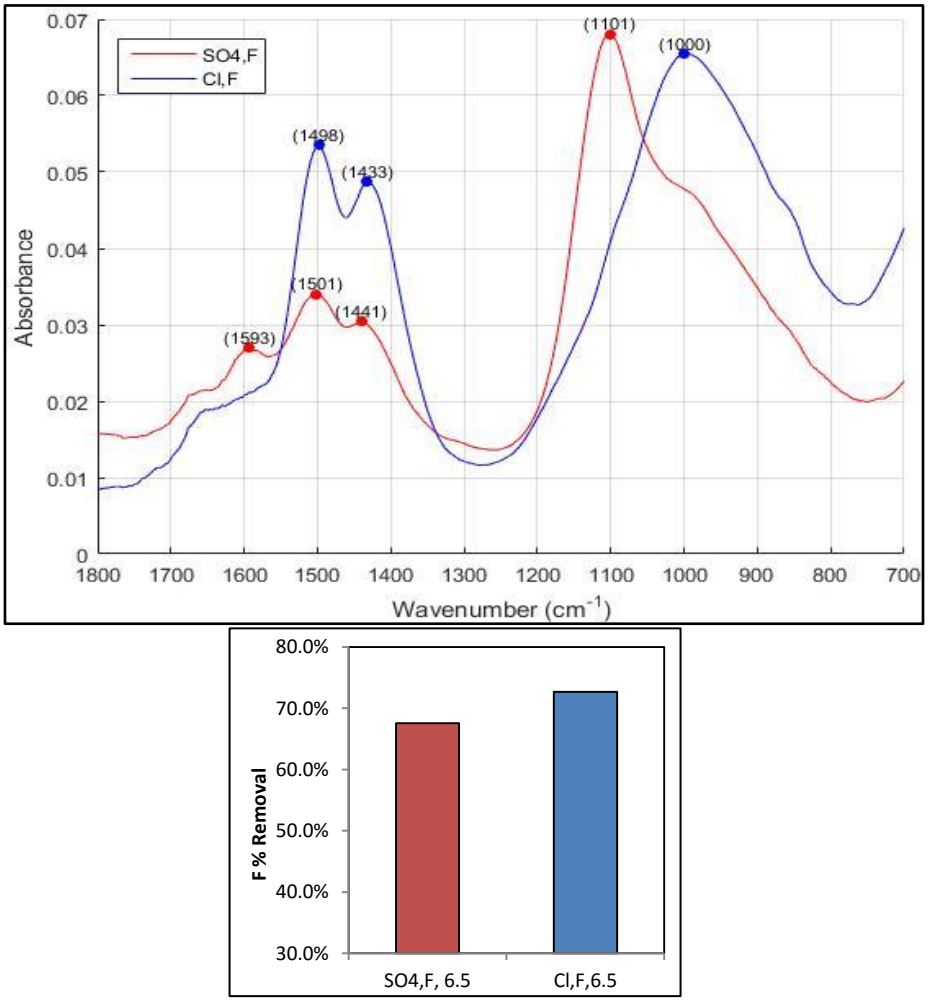

Figure 24: ATR-FTIR spectra comparing the precipitates with fluoride in the sulfate matrix and chloride matrix, both at pH 6.5, no additional ligands present (top) and corresponding fluoride percent removals (bottom)

The pH of the reactor also had a significant impact on the removal efficiency of fluoride. In Figure 25, fluoride removal is significantly reduced from the pH 6.5 to the pH 7.5 experiment. Consistent with the work of Alfredo (2012) and Stehhouwer (2014), this decrease in fluoride removal is expected because the system is less oversaturated with respect to aluminum hydroxide; and so there is less opportunity for fluoride coprecipitation (see Figure 5). In addition, fluoride removal may be decreased at the higher pH of 7.5 due to competition for inner-sphere adsorption with carbonate. This result agrees well with carbonate speciation, indicating a higher fraction of CO_3^{2-} at the higher pH value (Figure 12 and Figure 13). The inner-sphere carbonate becomes more effective at outcompeting fluoride for specific surface sites at this pH due to its larger abundance. Bhatnagar et al. (2012) and Tang et al. (2009) found that carbonate and phosphate hinder fluoride adsorption on alumina and ferric oxide due to competition for active surface sites via inner-sphere coordination with the metal oxide. Our findings are consistent with this previous work.

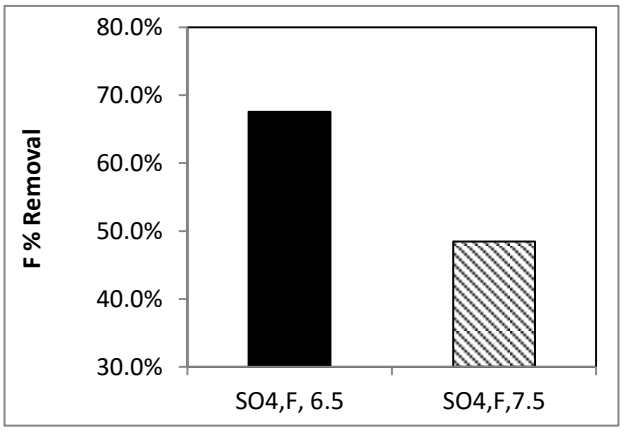

Figure 25: Fluoride percent removal from the reactor with fluoride at pH 6.5 and pH 7.5, both in the sulfate matrix

Fluoride was also inherently linked to trends in the soluble aluminum residuals. In Figure 26, the presence of fluoride is seen to increase the concentration of soluble aluminum in the reactor, regardless of the other ligand combinations present. The experiments without fluoride had a mean aluminum concentration of $10^{-6.032}$ M, whereas those with fluoride exhibited a mean aluminum concentration of $-10^{-5.440}$ M. In referring back to the Al-F speciation diagram (Figure 1), fluoride can form many soluble complexes with aluminum. These Al-F complexes increase the total aluminum solubility in solution. In the absence of F, there is a greater degree of supersaturation with respect to aluminum hydroxide (Figure 5). The role of fluoride in elevated aluminum residuals was also noted in the work of Alfredo (2012) and Stehouwer (2014).

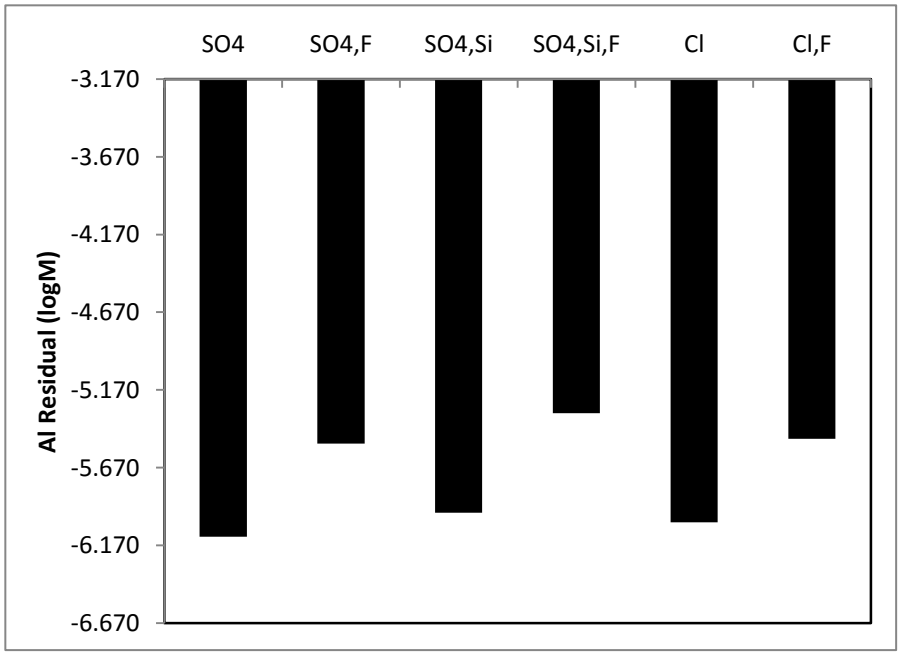

Figure 26: Aluminum residuals for various jars with and without fluoride all at pH 6.5. $\mu_{No\ F} = 10^{-6.032}$ M and $\mu_F = 10^{-5.440}$ M. Initial Al added throughout the study was $10^{-3.17}$ M.

Another notable observation was the decrease in fluoride removal due to competition with silicate. As shown in Figure 27, fluoride removal is decreased by the addition of silicate, and silicate removal is decreased by the addition of fluoride. Both fluoride and silicate were found to adsorb to the aluminum hydroxide surface via inner-sphere complexation in the FTIR results. The macroscopic observation of mutually decreased removals in the presence of one another agrees well with the theory that fluoride and silicate compete with one another for specific surface sites on the metal surface.

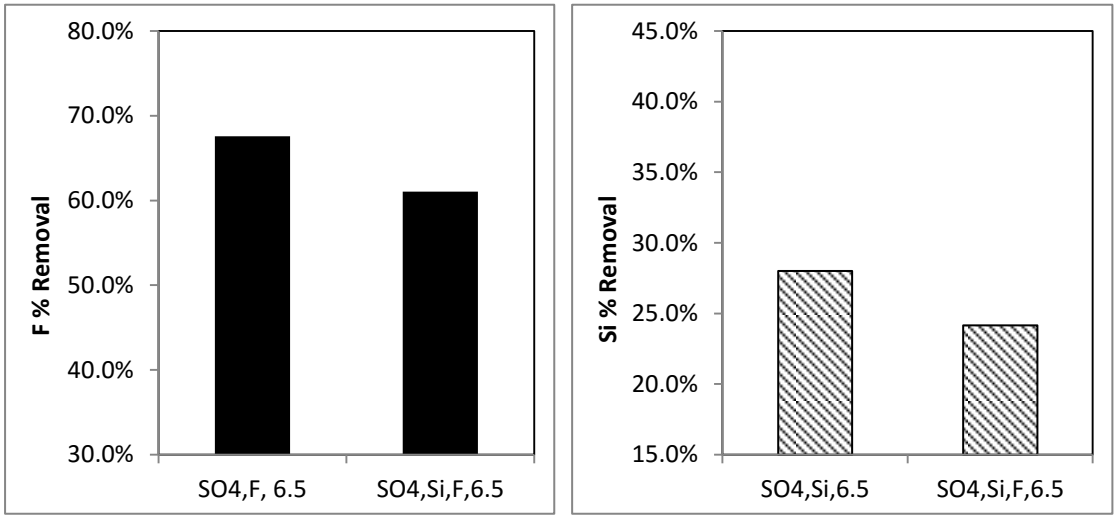

Figure 27: Fluoride percent removal from reactors with and without silicate, both in sulfate matrices and at pH 6.5 (left) and silicate percent removal from reactors with and without fluoride, both in sulfate matrices and at pH 6.5 (right)

4.2.2 Interactions involving NOM surrogates

In section 4.1.4, it was concluded that the absence of aromatic carboxylate features in the salicylate and phthalate reactors was due to the lack of adsorption of these compounds to the surface, which led to low removals from the solution. The percent removals of pyromellitate and salicylate in Figure 28 indicate a very high removal of pyromellitate and low removal of salicylate. This difference is further supported by the salicylate spectrum which lacks the carboxylate features exhibited by the pyromellitate spectrum; these features would be indicative of significant salicylate adsorption to the surface. Because the salicylate spectrum more closely resembles carbonate, it is concluded that carbonate is outcompeting salicylate (and phthalate, not shown) for adsorption to the surface. Carbonate is expected to compete strongly for adsorption due to its ability to form inner-sphere complexes with the surface. In contrast to phthalate and salicylate, the presence of carboxylic pyromellitate features in the IR spectra indicate that it has formed surface complexes and has a higher affinity for the surface than the other LMW organics. This affinity is likely due to the larger number of electronegative carboxylic groups on pyromellitate versus the other organics (Table 6).

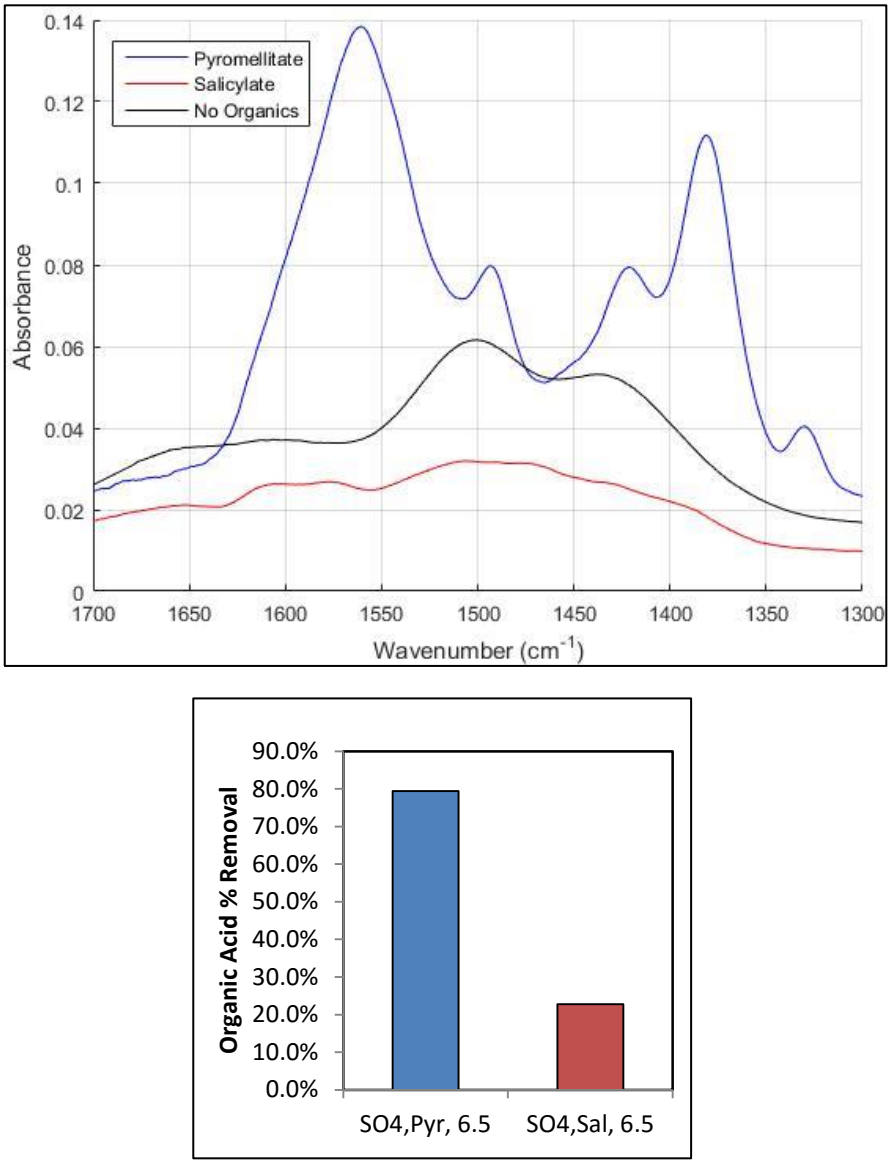

Figure 28: ATR-FTIR spectra comparing the precipitates with pyromellitate, salicylate and no organics, all at pH 6.5, no additional ligands present (top) and corresponding pyromellitate and salicylate percent removals (bottom)

Focusing now on pyromellitate as the model organic, sulfate decreases the removal of pyromellitate compared to the chloride matrix (Figure 29, bottom). The FTIR spectra also demonstrated the negative impact of sulfate on pyromellitate removal similar to its effect on fluoride. In Figure 29 (top), the outer-sphere adsorbing SO_4^{2-} vibration at 1100 cm^{-1} is apparent only in the sulfate spectrum and the series of vibrations attributed to outer-sphere pyromellitate in the 1300-1600 cm^{-1} region are apparent in both spectra. Sulfate, chloride, and pyromellitate are all outer-sphere complexes, and it was evident that each exhibits a different affinity for the solid surface. Chloride has a much weaker electrostatic interaction with the precipitated aluminum hydroxide than sulfate based on the reduced competition it exhibited with pyromellitate. Because pyromellitic acid is displacing chloride and sulfate (albeit to varied degrees), pyromellitate has the strongest electrostatic interaction with the surface of these three species.

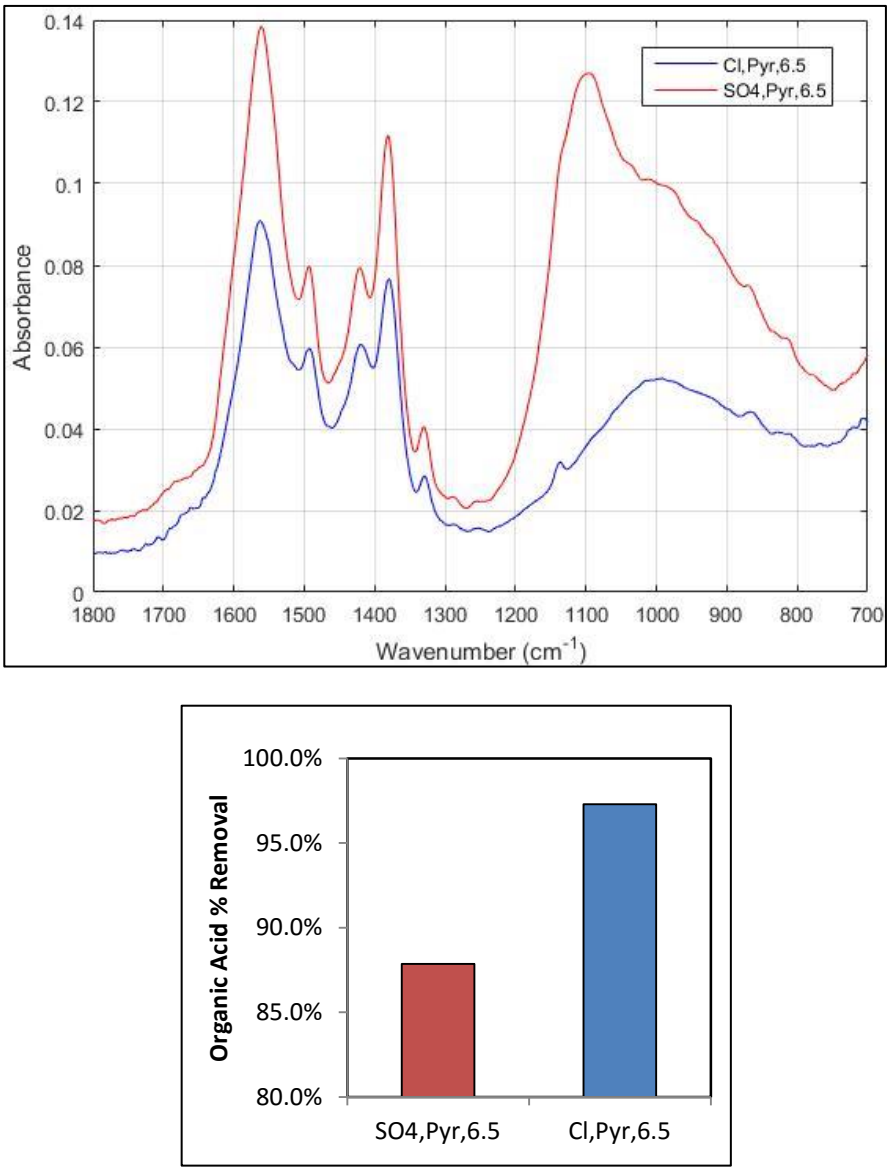

Figure 29: ATR-FTIR spectra comparing the precipitates with pyromellitate in chloride and sulfate matrices, both at pH 6.5, no additional ligands present (top) and corresponding pyromellitate percent removals (bottom)

Similar to fluoride, the reactor pH also contributed to changes in pyromellitate removal. At the higher pH of 7.5, pyromellitate removal was greatly reduced (Figure 30). The explanations of decreased aluminum solubility and increased competition by carbonate at pH 7.5 that were discussed for fluoride in section 4.2.1 are valid in this case as well. However, the magnitude of the decrease in percent removal is much larger in the pyromellitate case than the fluoride case (percent removal reduction of 48.9 for pyromellitate and 19.1 for fluoride). This can be explained in part by an inner-sphere versus inner-sphere competition between fluoride and carbonate and an inner-sphere versus outer-sphere competition between pyromellitate and carbonate. In the latter, pyromellitate is more easily displaced by the more strongly adsorbed carbonate ion.

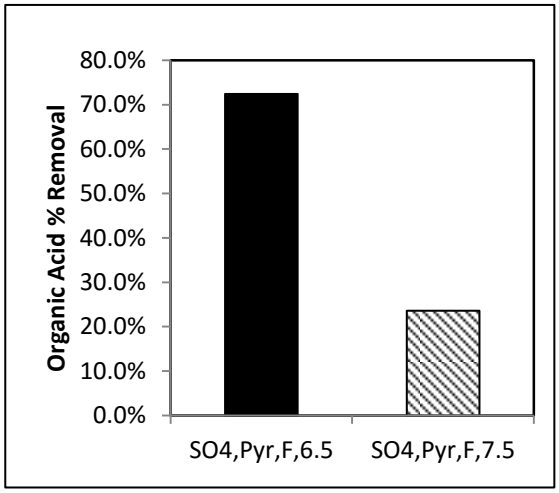

Figure 30: Fluoride percent removal from the reactor with pyromellitate and fluoride at pH 6.5 and pH 7.5, both in the sulfate matrix (Note: UV-Vis data for the reactor with pyromellitate only was n/a)

Silicate was also observed to compete with pyromellitate for removal. The results depicted in Figure 31 make it clear that pyromellitate removal is decreased in the presence of silicate and silicate removal is decreased in the presence of pyromellitate. It is expected that removal of outer-sphere pyromellitate would be reduced due to completion with inner-sphere silicate, but the observation of significantly decreased silicate removal in the presence of pyromellitate was unanticipated. However, as previously discussed, pyromellitate is able to compete well against carbonate, another species that was concluded to coordinate with the surface via inner-sphere complexation. Thus, pyromellitate likely has such a strong electrostatic attraction to the surface that it has the ability to impact the adsorption of these more strongly complexed ligands.

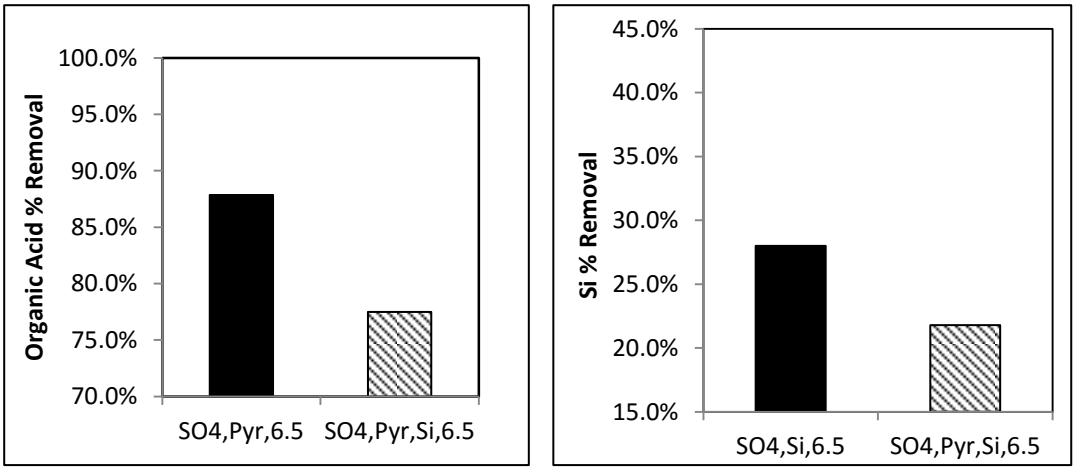

Figure 31: Pyromellitate percent removal from reactors with and without silicate, both in sulfate matrices and at pH 6.5 (left) and silicate percent removal from reactors with and without pyromellitate, both in sulfate matrices and at pH 6.5 (right)

4.2.3 Interactions between fluoride and NOM surrogate

In Figure 32, percent removal data are presented in the context of competition between fluoride and pyromellitate. In the pyromellitate system, it is evident that the presence of fluoride results in competition and decreased pyromellitate removal. Fluoride removal is slightly decreased by the addition of pyromellitate, but this magnitude of reduction is far less significant. It is reasonable to conclude that fluoride removals were less impacted by the presence of pyromellitate compared to pyromellitate removals in the presence of fluoride because fluoride is creating the more significant covalent bond with the surface. The outer-sphere complexed pyromellitate is weakly adsorbed via ion pair interactions with the surface and, therefore, is more easily displaced by fluoride at the surface. The more significant competitive impact of fluoride on pyromellitate was a main conclusion in the work of Stehouwer (2012).

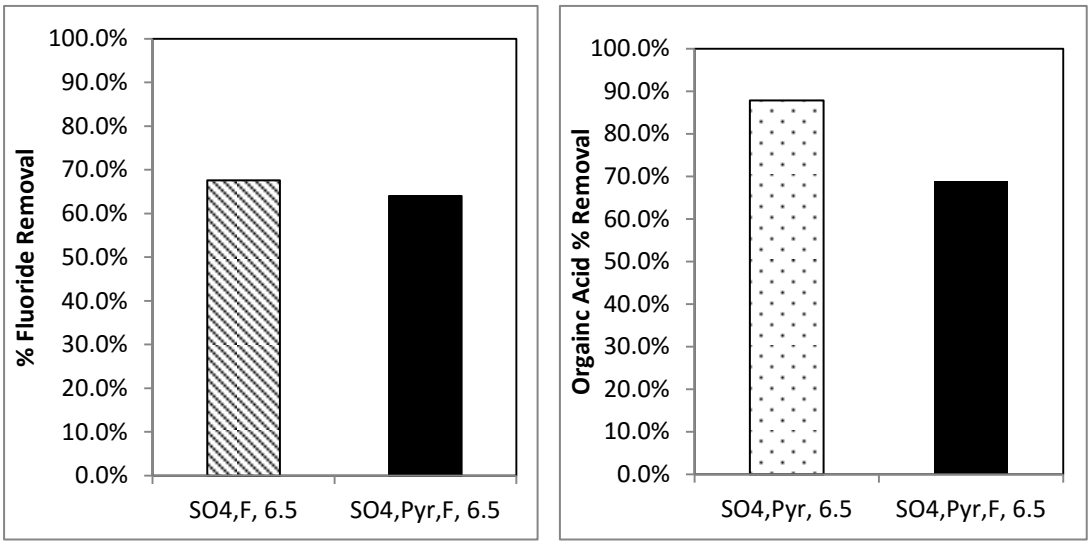

Figure 32: Fluoride percent removal from reactors with and without pyromellitate, both in sulfate matrices and at pH 6.5 (left) and pyromellitate percent removal from reactors with and without fluoride, both in sulfate matrices and at pH 6.5 (right). Solid bar denotes the presence of both fluoride and pyromellitate.

4.3 Ligand Interactions Over Time

The previous section involved a discussion of competition among ligands from the spectroscopic and macroscopic data, but neglected the impacts of aging. The ensuing results and discussion address the insights gained by analyzing these data over the varied aging periods.

Recalling the analysis in section 4.1.2 on the carbonate coordination mechanism, the magnitude of the Δv_3 split was indicative of what type of complex formed. Δv_3values in the range of 70-120 indicate monodentate inner-sphere complexes while larger values show that the carbonate is a bidentate ligand at the surface. In Table 14, Δv_3 values are

provided to compare the sulfate and chloride systems over time. A larger splitting is indicative of a more significant change in molecular symmetry; and thus, more bidentate-like coordination character of the CO_3^{2-} molecule. The largest splitting of the v_3 vibration occurred in the precipitates from the aged chloride systems, indicating that carbonate exhibits a more significant coordination to the surface in these cases. Additionally, the more significant carbonate coordination in the chloride system supports the conclusions in the previous section that sulfate has a stronger electrostatic affinity for the surface. The fact that these larger v_3 splits occurred only in the aged samples suggests that carbonate adsorption increases as the aluminum hydroxide ages (and perhaps becomes less amorphous). Evidence of increased carbonate accumulation at the surface is observed in Figure 33 where carbonate FTIR peaks increase relative to sulfate over time.

Table 14: Δv_3 values from the ATR-FTIR spectra of precipitates with carbonate in both sulfate and chloride matrices over time. No additional ligands present.

Experimental Conditions	**Age**	**v_3**		**Δv_3**
Carbonate and sulfate, pH 6.5	0Wk	1501.3	1437.6	64
	1Wk	1501.3	1443.4	58
	2Wk	1501.3	1434.7	67
	3Wk	1502.2	1438.6	64
Carbonate and sulfate, pH 7.5	0Wk	1502.2	1434.7	68
	1Wk	1500.3	1430.9	69
	2Wk	1502.2	1430.9	71
	3Wk	1502.2	1429.9	72
Carbonate and chloride, pH 6.5	0Wk	1497.4	1427	70
	1Wk	1506.1	1400	106
	2Wk	1501.3	1406.8	95
	3Wk	1498.4	1407.7	91
Carbonate and chloride, pH 7.5	0Wk	1498.4	1423.2	75
	1Wk	1504.2	1399.1	105
	2Wk	1505.1	1400	105
	3Wk	1505.1	1400	105

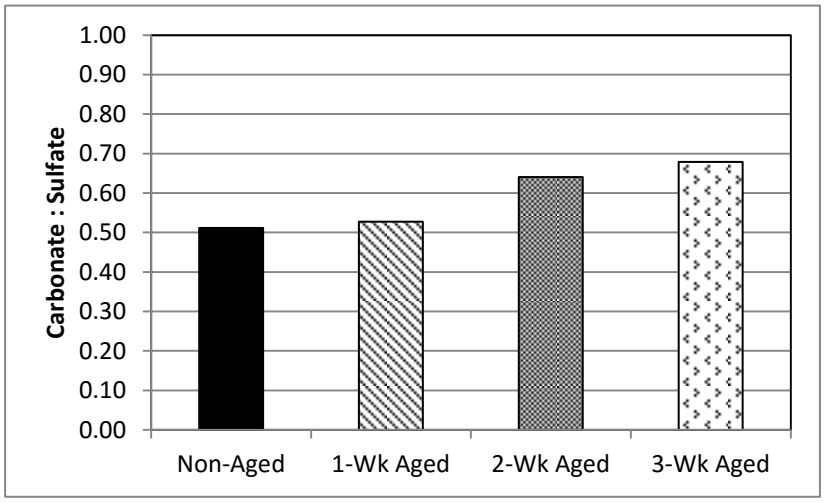

Figure 33: ATR-FTIR peak intensity ratios of carbonate to sulfate for the precipitates in a sulfate matrix at pH 7.5, over time. No additional ligands present.

The accumulation of carbonate at the surface over time is also significant for explaining trends in fluoride and pyromellitate removal. In Figure 34, it is apparent that both fluoride and pyromellitate removals are systematically decreasing with time. Two possible explanations for this decrease in percent removal over time would be aluminum dissociation or desorption of fluoride and pyromellitate in favor of another competing species. However, the aluminum residuals did not reveal any significant trends with time; therefore the hypothesis of aluminum hydroxide dissolution with time is ruled out (Figure 35). The latter hypothesis of desorption with precipitate age can be explained by the accumulation of carbonate with time. Carbonate is highly abundant (initial concentration of 3 mM) and undergoes strong inner-sphere complexation with the surface. Therefore, it

is not unreasonable to identify carbonate as one of the major species associated with the decrease in fluoride and pyromellitate adsorption over time. Fluoride desorption may also be related to an increase in aluminum hydroxide crystallinity over time, but XRD analysis is required to further test this theory.

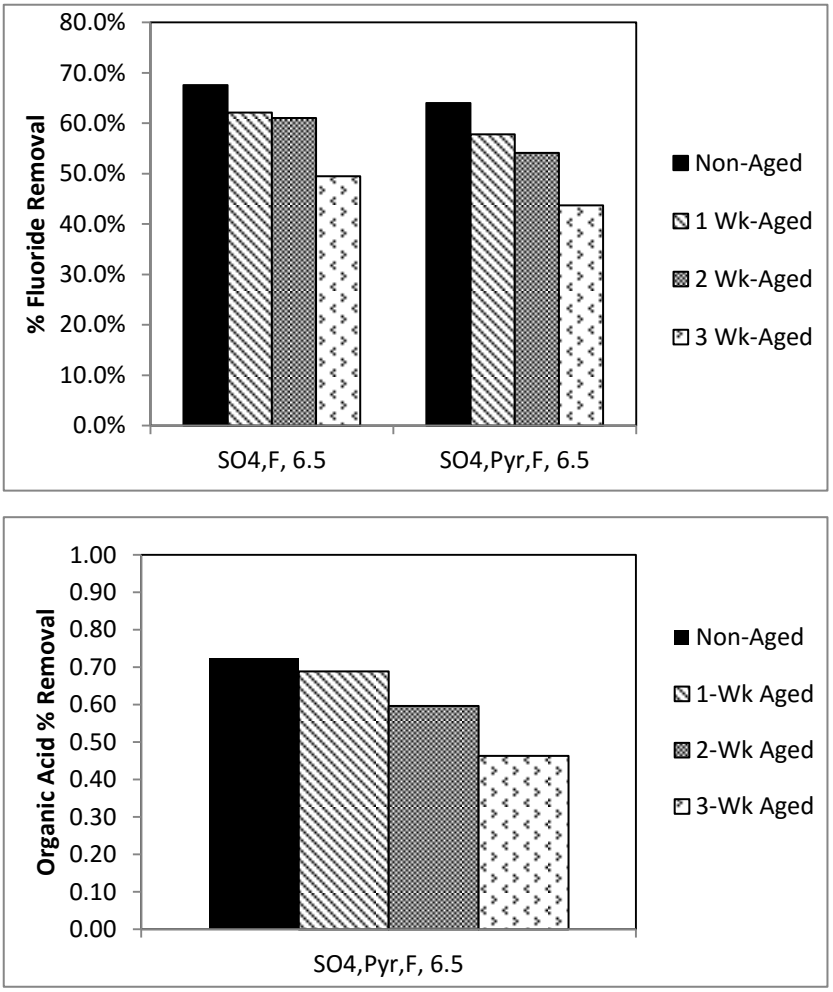

Figure 34: Fluoride percent removal from reactors with and without pyromellitate, both in sulfate matrices and at pH 6.5, over time (top) and pyromellitate percent removal from reactors with fluoride in a sulfate matrix and at pH 6.5, over time (bottom). (Note: some pyromellite removal data was n/a and is therefore omitted)

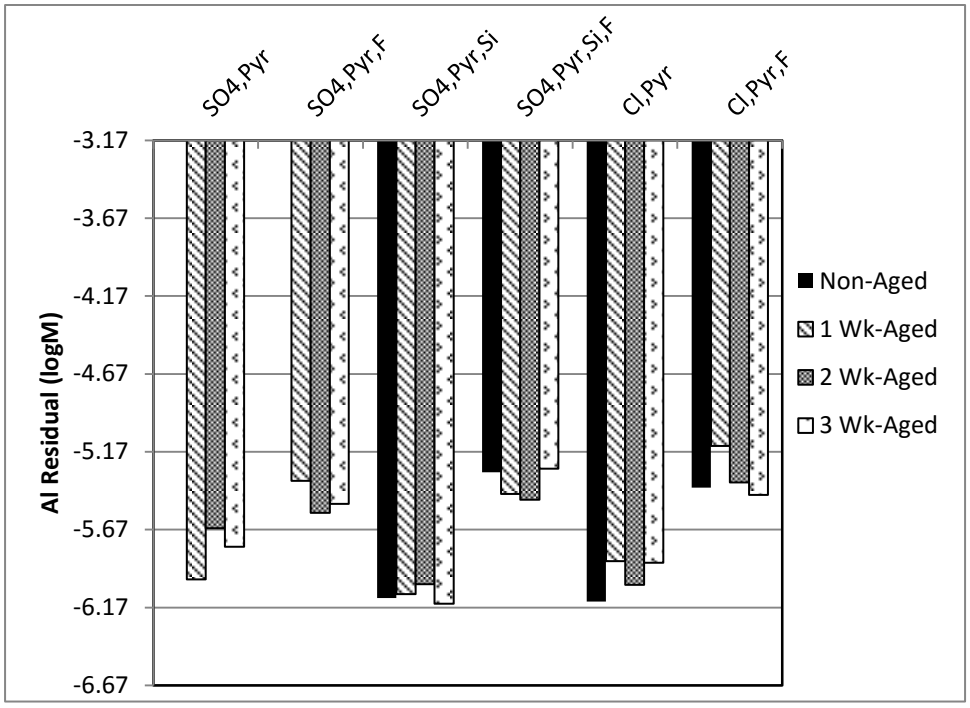

Figure 35: Aqueous aluminum residuals for various ligand combinations over time. All reactors listed were at pH 6.5

While carbonate may be responsible for the observed desorption of fluoride and pyromellitate in silicate-free experiments, strong evidence supports the role of silicate as the competing oxyanion that causes desorption of these other ligands with time. In Figure 36, the spectra from every reactor containing silicate are shown with the respective SO_4^{2-} to Si-O-Si peak intensity ratios. In each experiment containing silicate, it is evident that accumulation and polymerization of silicate is occurring over time as supported by the growth in magnitude of the Si-O-Si features with increased age. In Figure 37, the spectra of the precipitates containing pyromellitate, fluoride and silicate are shown as a function

of varied age with corresponding percent removal data of each ligand below. When all three competing ligands are present, fluoride and pyromellitate removals decease with time as silicate removals increase with time. Since it was established that no time-dependent trends exist for the residual aluminum data, the rise in silicate percent removal and rise in Si-O-Si intensities occurring simultaneously with decreased fluoride and pyromellitate percent removals are strong indicators of desorption by silicate with time. Hu et al. (2015) found that that silicate oligomers and polymers accumulate on the surface of TiO_2 over time, greatly inhibiting the adsorption of arsenic. Luxton et al. (2008) investigated silicate adsorption and polymerization on goethite and concluded that silicate could irreversibly displace and desorb previously equilibrated arsenite. Thus, understanding the role of silicate, a ubiquitous oxyanion in natural water systems, has tremendous implications for the fate of ligands in a coagulation drinking water system.

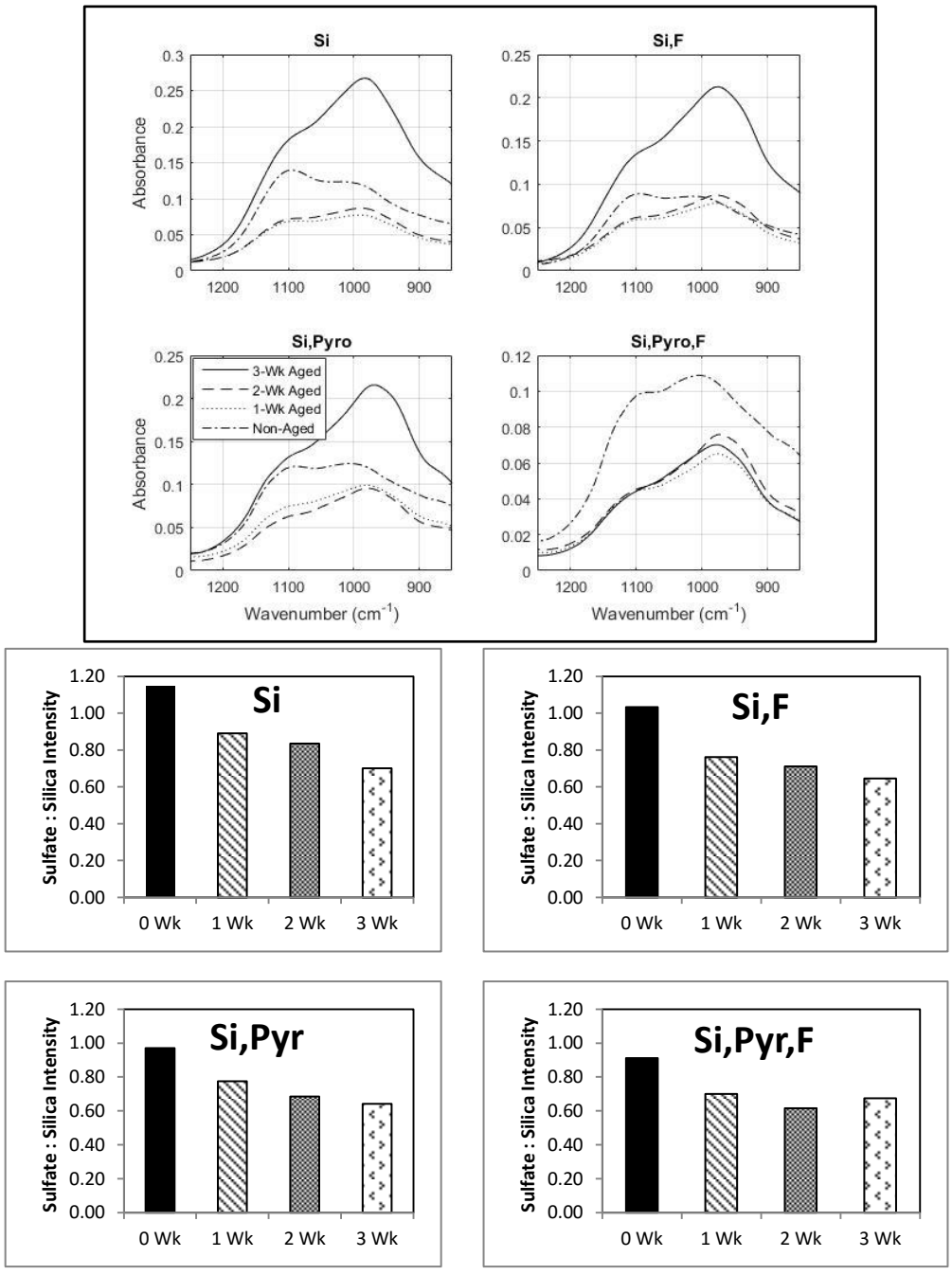

Figure 36: ATR-FTIR spectra comparing precipitates in sulfate matrices with silicate and varied pyromellitate and F over time, all at pH 6.5 (top). Corresponding sulfate to silicate peak intensity ratios (bottom)

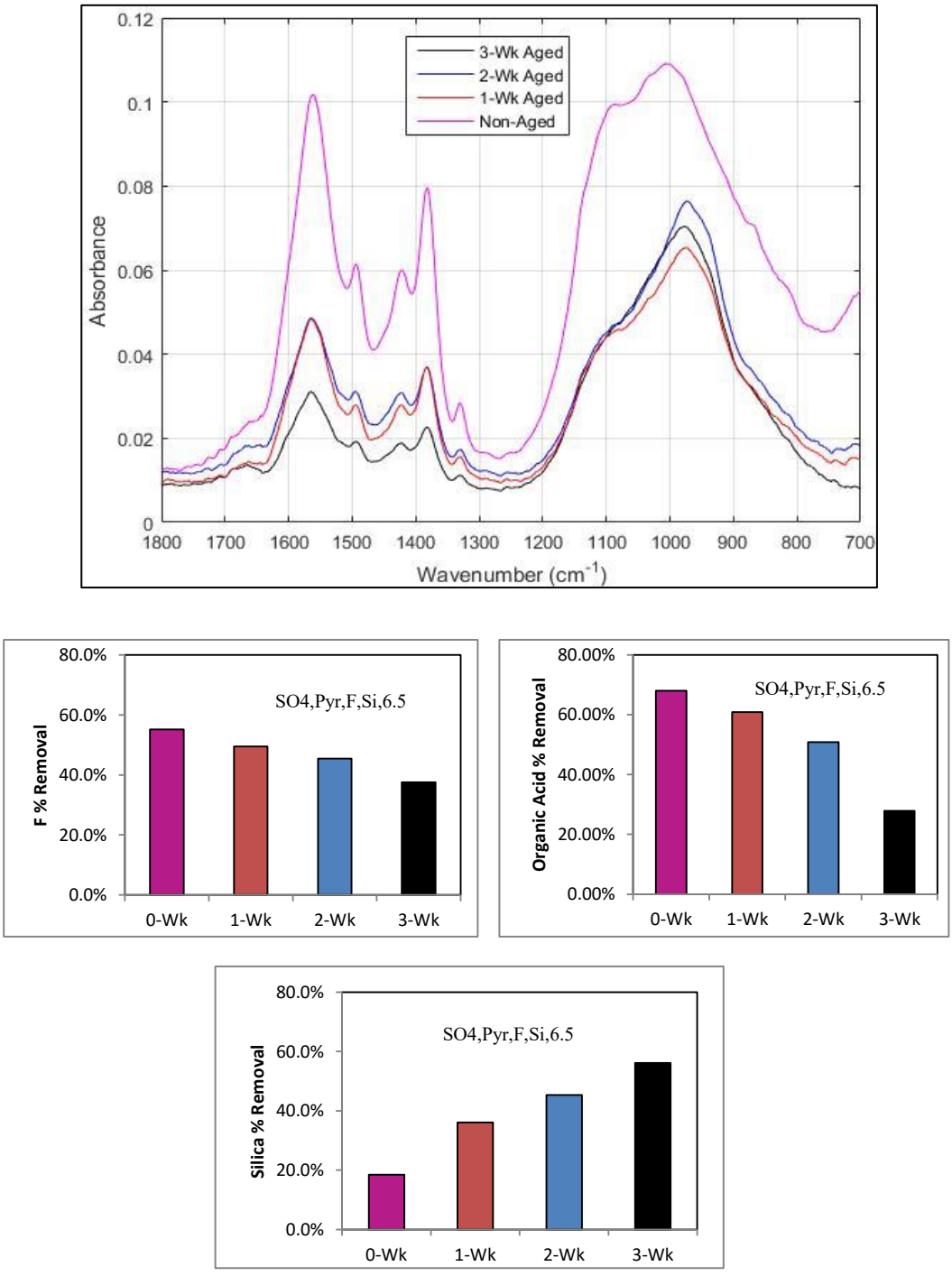

Figure 37: ATR-FTIR spectra comparing the precipitates with pyromellitate, silicate, and fluoride over time, all in sulfate matrices and at pH 6.5 (top) and corresponding, fluoride, pyromellitate, and silicate percent removals (bottom).

Chapter 5: Conclusions

Fluoride and NOM-based DBPs present a significant threat to our basic human right of clean drinking water. The health risks associated with fluoride, HAAs, and THMs have resulted in regulatory scrutiny of these compounds over the past decade resulting in the passage of the Stage 2 Disinfectants and Disinfection Byproducts Rule in 2006 and a potential lowering of the fluoride MCL in the near future. Smaller drinking water systems lack the economy of scale and operational capacity that larger systems have and, therefore, are vulnerable to these contaminants and their tightened regulations. The SWS scale provides a unique opportunity to combat an emerging issue with conventional treatment practices. Aluminum salt coagulation has shown promise in the removal of both NOM and fluoride from natural waters, however, the interactions that occur between NOM, fluoride, and other oxyanions in a coagulation scheme have been inadequately understood.

The experiments in this study were designed to elucidate mechanisms of removal and competitive interactions of the ligands at solid-aqueous interface. Jar tests were conducted to simulate the coagulation-flocculation process at the bench-scale with controlled synthetic water compositions. An assortment of ligand combinations were tested throughout a series of jar tests and aluminum hydroxide precipitates were differentially aged to further probe the mechanisms of ligand attachment. Supernatants from the jar test experiments were analyzed to establish the removal efficiencies of the added ligands. Microscopic insights about the mechanisms of surface complexation for each ligand were informed from *in situ* ATR-FTIR spectroscopy of the aluminum precipitates. Together, these data provide important insights about the interplay of aluminum, fluoride, NOM, and other oxyanions in a drinking water coagulation system.

5.1 CONCLUSIONS

The specific insights gained from the microscopic FTIR data and macroscopic residuals data in this study are summarized in the following list:

1. Analysis of FTIR spectra over a range of mixed ligand/aluminum hydroxide systems and changes in spectra with time elucidated the coordination chemistry of adsorbates. Fluoride, silicate and carbonate were found to adsorb via inner-sphere complexation. Sulfate and pyromellitate sorbed by outer-sphere complexation with the aluminum hydroxide surface in these experiments. Silicate was also observed to accumulate at the surface and polymerize with time.
2. The presence of fluoride resulted in increased aluminum residuals, likely due to the formation of soluble Al-F complexes and disruption of aluminum precipitate growth. These increased soluble aluminum levels are important because a) less aluminum is present for aluminum hydroxide flocs and b) aluminum can be considered a public health threat at high concentrations; it has a SMCL of 0.05 to 0.2 mg/L
3. Fluoride and pyromellitate percent removals are higher in the chloride synthetic water than the sulfate synthetic water. These results suggest that sulfate is a more strongly bound outer-sphere species than chloride, has a higher affinity for the aluminum hydroxide surface than chloride, and is therefore more competitive than chloride during adsorption with other ligands. This interpretation is also supported by the larger splitting of the ν_3 carbonate feature in the chloride matrix, suggesting that carbonate undergoes more bidentate-like coordination in the absence of sulfate.

4. Fluoride and pyromellitate removals are decreased at the higher pH of 7.5 due to the increased solubility of aluminum and the increased fraction of carbonate ions; the latter effect results in more competition for the surface between inner-sphere adsorbing carbonate and fluoride or between carbonate and outer-sphere adsorbing pyromellitate.
5. Fluoride and pyromellitate removals are decreased in the presence of silicate, which forms strong inner-sphere complexes. Fluoride, pyromellitate and silicate all negatively impact the removal of one another. Pyromellitate, which forms outer-sphere complexes, competes well in these mixed ligand systems as evidenced by its impact on silicate removal.
6. Pyromellitate exhibited much higher removals than phthalate and salicylate, as indicated by strong spectroscopic features and low aqueous residuals. This is likely due to its higher degree of functionality in comparison to the other organic acids (four carboxylic groups)
7. Fluoride removal has a greater impact on pyromellitate removal than pyromellitate's impact on fluoride. This result can be explained by the high affinity of fluoride for the aluminum surface resulting in stronger inner-sphere complexation. This high affinity may also create residual soluble Al-F complexes as evidenced by the increased aluminum concentrations in the supernatant when fluoride was present in the reactors. This complexation may cause reduced precipitate formation; however, further precipitate analysis is required to confirm this hypothesis.

8. Fluoride and pyromellitate removals decrease with time. Inner-sphere carbonate and silicate are the likely causes of this reduction in removal with time. This explanation is shown by increasing carbonate FTIR peak intensities with time for the silicate-free experiments. For reactors with silicate, evidence for desorption of fluoride and pyromellitate was provided by increased Si-O-Si peaks and increasing silicate percent removals with time. Inner-sphere adsorption, accumulation and polymerization at the surface by silicate result in desorption of these other ligands.

5.2 FUTURE WORK

While the findings of this research provided a number of insights into the impact of adsorption mechanism on competition among ligands during alum coagulation, there are still many areas to fully address the complex interactions in these systems. Further ATR-FTIR analysis of phthalate and salicylate at higher concentrations than used in this study may help elucidate the coordination mechanisms of these compounds. The absence of carbonate would also help elucidate the coordination of these more weakly adsorbing LMW organics. Experiments at a lower sulfate concentration and over a wider range of pH values may allow determination of the potential role of inner-sphere sulfate complexation. A wider range of pH values is also necessary to investigate the spectrum of coordination types that occur with LMW organic acids in the literature. Silicate ATR-FTIR analyses in the absence of sulfate would help bring clarity in the convoluted IR region where both silicate and sulfate vibrations occur. The pairing of ATR-FTIR with other *ex-situ* microscopic methods such as XRD and XPS can help us attain more

characteristics about the solid such as crystallinity, composition, and bond strength over time and with varied ligand environments to study the aging process. Surface area BET analyses and particle size distributions of flocs under varied ligand conditions can help attain an understanding of the physical changes that the precipitates are experiencing and how these changes might affect adsorption capacity and settling potential. Moreover, similar work with other coagulants such as ferric chloride and to other inorganic pollutants of concern such as manganese, arsenic, and chromium would be very useful. Though the mechanisms at play are intricate and numerous, their understanding is vital in order to offer coagulation as a viable fluoride removal strategy and restore a basic human right of healthy drinking water to many.

References

Adu-Wusu, K., & Wilcox, W. R. (1991). Kinetics of silicate reaction with gibbsite. *Journal of Colloid And Interface Science*, *143*(1), 127–138.

Agarwal, M., Rai, K., Shrivastav, R., & Dass, S. (2003). Deflouridation of water using amended clay. *Journal of Cleaner Production*, *11*(4), 439–444.

Alfredo, K. (2012). *Drinking Water Treatment By Alum Coagulation: Competition Amng Fluoride, Natural Organic Matter, and Aluminum*. Universtity of Texas at Austin.

Aoba, T., & Fejerskov, O. (2002). Dental Fluorosis: Chemistry and Biology. *Critical Reviews in Oral Biology and Medicine*, *13*(2), 155–170.

Ayoob, S., & Gupta, a. K. (2006). Fluoride in Drinking Water: A Review on the Status and Stress Effects. *Critical Reviews in Environmental Science and Technology*, *36*(6), 433–487.

Ayoob, S., Gupta, A. K., Bhakat, P. B., & Bhat, V. T. (2008). Investigations on the kinetics and mechanisms of sorptive removal of fluoride from water using alumina cement granules. *Chemical Engineering Journal*, *140*(1-3), 6–14.

Ayoob, S., Gupta, A. K., & Bhat, V. T. (2008). *A conceptual overview on sustainable technologies for the defluoridation of drinking water*. *Crit. Rev. Env. Sci. Technol.* (Vol. 38).

Barbosa, V. F. F., MacKenzie, K. J. D., & Thaumaturgo, C. (2000). Synthesis and characterisation of materials based on inorganic polymers of alumina and silica: Sodium polysialate polymers. *International Journal of Inorganic Materials*, *2*(4), 309–317.

Benjamin, M. M., & Lawler, D. F. (2013). *Water Quality Engineering: Physical/Chemical Treatment Processes*. Hoboken, New Jersey: John Wiley and Sons Incorporated.

Bertie, J. E., Ahmed, K., & Eysel, H. H. (1989). Infrared Intensities of

Liquids. 5. Optical and Dielectric Constants, Integrated Intensities, and Dipole Moment Derivatives of H20 and D20 at 22. *Journal of Physical Chemistry*, (16), 2210–2218.

Bhatnagar, A., Kumar, E., & Sillanpaa, M. (2011). Fluoride removal from water by adsorption-A review. *Chemical Engineering Journal*, *171*(3), 811–840.

Biber, M. V., & Stumm, W. (1994). An In-Situ ATR-FTIR Study: The Surface Coordination of Salicylic Acid on Aluminum and Iron(III) Oxides. *Environmental Science and Technology*, *28*(5), 763–768.

Boivin, G., Chavassieux, P., Chapuy, M. C., Baud, C. A., & Meunier, P. J. (1989). Skeletal fluorosis: Histomorphometric analysis of bone changes and bone fluoride content in 29 patients. *Bone*, *10*(2), 89–99.

Bondietti, G., Sinniger, J., & Stumm, W. (1993). The reactivity of FE(III) (hydr)oxides: Effects of ligands in inhibiting the dissolution. *Colloids and Surfaces A: Physicochemical and Engineering Aspects*, *79*(2-3), 157–167.

Boorman, G. a. (1999). Drinking water disinfection byproducts: review and approach to toxicity evaluation. *Environmental Health Perspectives*, *107 Suppl* (February), 207–217.

Boruff, C. S., Buswell, a. M., & Upton, W. V. (1937). Adsorption of Fluoride from Salts by Alum Floc. *Industrial & Engineering Chemistry*, *29*(10), 1154–1154.

Bruker Optics. (2011). *Attenuated Total Reflection (ATR) – a versatile tool for FT-IR spectroscopy*.

Choi, W.-W., & Chen, K. Y. (1979). The Removal of Fluoride from Waters by Adsorption. *American Water Works Association*, *71*(10), 562–570.

Cornell, R. M. (1988). The Influence of Some Divalent Cations on the Transformation of Ferrihydrite to More Crystalline Products. *Clay Minerals*, *23*, 329–332.

Cornwell, D. A., and Bishop, M. M. (1983). Determining velocity gradients in laboratory and full-scale systems. *Journal American Water Works Association, 75*(9), 470-475.

Croue, J.-P., Korshin, G. V., & Benjamin, M. M. (2000). *Characterization of Natural Organic Matter in Drinking Water*. American Water Works Association.

Culp, R. L., & Stoltenberg, H. A. (1958). Fluoride Reduction at La Crosse, Kan. *American Water Works Association*, *50*(3), 423–431.

Davis, J. A., & Kent, D. B. (1990). Surface Complexation Modeling in Aqueous Geochemistry. *Reviews in Mineralogy and Geochemistry*, *23*, 177–260.

DenBesten, P. K. (1999). Biological mechanisms of dental fluorosis relevant to the use of fluoride supplements. *Community Dentistry and Oral Epidemiology*, *27*(1), 41–7.

Dimas, D., Giannopoulou, I., & Panias, D. (2009). Polymerization in sodium silicate solutions: A fundamental process in geopolymerization technology. *Journal of Materials Science*, *44*(14), 3719–3730.

Edzwald, J. K., & Tobiason, J. E. (1999). Enhanced coagulation: US requirements and a broader view. *Water Science and Technology*, *40*(9), 63–70.

Edzwlald, J. K. (1993). Coagulation in Drinking Water Treatment: Particles, Organics and Coagulants. *Water Science Technology*.

Eklund, S., Burt, B., Ismail, A. I., & Calderone, J. (1987). High-fluoride drinking water, fluorosis, and dental caries in adults. *Journal of the American Dental Association*, *114*(3), 324–328.

Evanko, C. R., & Dzombak, D. A. (1999). Surface complexation modeling of organic acid sorption to goethite. *Journal of Colloid and Interface Science*, *214*(2), 189–206.

Fawell, J., Bailey, K., Chilton, J., Dahi, E., Fewtrell, L., & Magara, Y.

(2006). *Fluoride in Drinking-water*. World Health Organization.

Featherstone, J. D. (1999). Prevention and reversal of dental caries: role of low level fluoride. *Community Dentistry and Oral Epidemiology*, *27*(1), 31–40.

Gaggiano, R., De Graeve, I., Mol, J. M. C., Verbeken, K., Kestens, L. A. I., & Terryn, H. (2013). An infrared spectroscopic study of sodium silicate adsorption on porous anodic alumina. *Surface and Interface Analysis*, *45*(7), 1098–1104.

Ghernaout, D. (2014). The hydrophilic/hydrophobic ratio vs. dissolved organics removal by coagulation - A review. *Journal of King Saud University - Science*, *26*(3), 169–180.

Glaser, B., Haumaier, L., Guggenberger, G., & Zech, W. (1998). Black carbon in soils: The use of benzenecarboxylic acids as specific markers. *Organic Geochemistry*, *29*(4), 811–819.

Gong, W. X., Qu, J. H., Liu, R. P., & Lan, H. C. (2012). Effect of aluminum fluoride complexation on fluoride removal by coagulation. *Colloids and Surfaces A: Physicochemical and Engineering Aspects*, *395*, 88–93.

Guan, X. H., Chen, G. H., & Shang, C. (2006). Combining kinetic investigation with surface spectroscopic examination to study the role of aromatic carboxyl groups in NOM adsorption by aluminum hydroxide. *Journal of Colloid and Interface Science*, *301*(2), 419–427.

Guan, X. H., Shang, C., & Chen, G. H. (2006b). ATR-FTIR investigation of the role of phenolic groups in the interaction of some NOM model compounds with aluminum hydroxide. *Chemosphere*, *65*(11), 2074–2081.

Guan, X.-H., Shang, C., & Chen, G.-H. (2006c). Competitive adsorption of organic matter with phosphate on aluminum hydroxide. *Journal of Colloid and Interface Science*, *296*(1), 51–58.

Guan, X. hong, Chen, G. hao, & Shang, C. (2007). ATR-FTIR and XPS study on the structure of complexes formed upon the adsorption of simple organic acids on aluminum hydroxide. *Journal of Environmental Sciences*, *19*(4), 438–443.

Hamouda, A. A., & Amiri, H. A. A. (2014). Factors affecting alkaline sodium silicate gelation for in-depth reservoir profile modification. *Energies*, *7*(2), 568–590.

Hayes, K. F., & Katz, L. E. (1996). Chapter 3: Application of X-Ray Absorption. In *The Physics and Chemistry of Mineral Surfaces*.

Hayes, K. F., Roe, A. L., Brown, G. E., Hodgson, K. O., & James, O. (1987). In Situ X-ray Absorption Study of Surface Complexes : Selenium Oxyanions on alpha- FeOOH. *Science*, *238*(4828), 783–786.

Hsu, P. H. (1962). Formation of X-ray Amorphous and Crystalline Aluminum Hydroxides. *Clays and Clay Minerals*, *11*(1), 299–300.

Hu, C. Y., Lo, S. L., & Kuan, W. H. (2005). Effects of the molar ratio of hydroxide and fluoride to Al(III) on fluoride removal by coagulation and electrocoagulation. *Journal of Colloid and Interface Science*, *283*(2), 472–476.

Hu, S., Yan, W., & Duan, J. (2015). Polymerization of silicate on TiO2 and its influence on arsenate adsorption: An ATR-FTIR study. *Colloids and Surfaces A: Physicochemical and Engineering Aspects*, *469*, 180–186.

Hua, G., & Reckhow, D. A. (2007). Comparison of disinfection byproduct formation from chlorine and alternative disinfectants. *Water Research*, *41*(8), 1667–1678.

Hug, S. J. (1997). In Situ Fourier Transform Infrared Measurements of Sulfate Adsorption on Hematite in Aqueous Solutions. *Journal of Colloid and Interface Science*, *188*(188), 415–422.

Hundt, T. R., & O'Melia, C. R. (1988). Aluminum-fulvic acid interactions: mechanisms and applications. *American Water Works Association*, *80*(4), 176–186.

Jayarathna, L., Bandara, A., Ng, W. J., & Weerasooriya, R. (2015). Fluoride adsorption on γ − Fe2O3 nanoparticles. *Journal of Environmental Health Science and Engineering*, *13*(1), 54.

Johnson, S. B., Yoon, T. H., & Brown, G. E. (2005). Adsorption of Organic Matter at Mineral / Water Interfaces . IV . Adsorption of Humic Substances at Boehmite / Water Interfaces and Impact on Boehmite Dissolution. *Interfaces*, (14), 5002–5012.

Jolivet, J. P., Thomas, Y., Taravel, B., Lorenzelli, V., & Busca, G. (1982). Infrared Spectra of Cerium and Thorium Pentacarbonate Complexes. *Journal of Molecular Structure*, *79*, 403–408.

Kanno, C. M., Sanders, R. L., Flynn, S. M., Lessard, G., & Myneni, S. C. B. (2014). Novel apatite-based sorbent for defluoridation: Synthesis and sorption characteristics of nano-micro-crystalline hydroxyapatite-coated-limestone. *Environmental Science and Technology*, *48*(10), 5798–5807.

Kodama, H., & Schnitzer, M. (1980). Effect of fulvic acid on the crystallization of aluminum hydroxides. *Geoderma*, *24*, 195–205. http://doi.org/10.1016/0016-7061(80)90023-3

Korshin, G. V., Benjamin, M. M., & Sletten, R. S. (1997). Adsorption of natural organic matter (NOM) on iron oxide: Effects on NOM composition and formation of organo-halide compounds during chlorination. *Water Research*, *31*(7), 1643–1650.

Kosmulski, M. (2014). The pH dependent surface charging and points of zero charge. VI. Update. *Journal of Colloid and Interface Science*, *426*, 209–212.

Larkin, P. (2011). *Infrared and Raman Spectroscopy: Principles and Spectral Interpretation.* Elsevier Science.

Benjamin, M. M., & Lawler, D. F. (2013). *Water Quality Engineering: Physical/Chemical Treatment Processes*. Hoboken, New Jersey: John Wiley and Sons Incorporated.

Lawler, D.F. and Kweon, J. (2003). *Integrated Water Treatment: Softening and Ultrafiltration*. IWA Publishing.

Lindergren, M. & Persson, P. (2010). Competitive adsorption involving phosphate and benzenecarboxylic acids on goethite—Effects of molecular structures. *Journal of Colloid and Interface Science*, *343*, 263-270.

Luxton, T. P., Eick, M. J., & Rimstidt, D. J. (2008). The role of silicate in the adsorption/desorption of arsenite on goethite. *Chemical Geology*, *252*(3-4), 125–135.

Martinez, C. E., & McBride, M. B. (1998). Coprecipitates of Cd, Cu, Pb and Zn in iron oxides: Solid phase transformation and metal solubility after aging and thermal treatment. *Clays and Clay Minerals*, *46*(5), 537–545.

Matilainen, A., Vepsalainen, M., & Sillanpaa, M. (2010). Natural organic matter removal by coagulation during drinking water treatment: A review. *Advances in Colloid and Interface Science*, *159*(2), 189–197.

Meenakshi, & Maheshwari, R. C. (2006). Fluoride in drinking water and its removal. *Journal of Hazardous Materials*, *137*(1), 456–463.

Mohapatra, M., Anand, S., Mishra, B. K., Giles, D. E., & Singh, P. (2009). Review of fluoride removal from drinking water. *Journal of Environmental Management*, *91*(1), 67–77.

Mullen, J. (2005). History of Water Fluoridation. *British Dental Journal*, *199*, 1–4.

Müller, K., & Lefèvre, G. (2011). Vibrational characteristics of outer-sphere surface complexes: Example of sulfate ions adsorbed onto metal (Hydr)oxides. *Langmuir*, *27*(11), 6830–6835.

National Research Council (NRC). (2006). *Fluoride in Drinking Water: A Scientific Review of EPA's Standards*.

Nieuwenhuijsen, M. J., Toledano, M. B., Eaton, N. E., Fawell, J., & Elliott,

P. (2000). Chlorination disinfection byproducts in water and their association with adverse reproductive outcomes: a review. *Occupational and Environmental Medicine*, *57*(2), 73–85.

Nordin, J., Persson, P., Laiti, E., & Sjoeberg, S. (1997). Adsorption of o-Phthalate at the Water-Boehmite (γ-AlOOH) Interface: Evidence for Two Coordination Modes. *Langmuir*, *13*(15), 4085–4093.

Nordin, J., Persson, P., Nordin, A., & Sjöberg, S. (1998). Inner-Sphere and Outer-Sphere Complexation of a Polycarboxylic Acid at the Water−Boehmite (γ-AlOOH) Interface: A Combined Potentiometric and IR Spectroscopic Study. *Langmuir*, *14*(13), 3655–3662.

Peak, D., Ford, R., & Sparks, D. (1999). An in Situ ATR-FTIR Investigation of Sulfate Bonding Mechanisms on Goethite. *Journal of Colloid and Interface Science*, *218*(1), 289–299.

Potts, W.J. (1963). *Chemical Infrared Spectroscopy: Volume I, Techniques.* New York. John Wiley and Sons Incorporated

Randtke, S.J. (1988). Organic contaminant removal by coagulation and related process combinations. *J. Am. Water Works Assoc.* 80 (5), 40–56.

Richardson, S. D. (2003). Disinfection by-products and other emerging contaminants in drinking water. *Trends in Analytical Chemistry*, *22*(10), 666–684.

Ryland, A. L. (1958). X-Ray Diffraction. *Journal of Chemical Education*, *35*(2).

Safe Drinking Water Act (SDWA) (2002). United States of America.

Safe Drinking Water Act (SDWA) Amendments of 1996 (1996). United States of America.

Schnitzer, M., & Calderoni, G. (1985). Some chemical characteristics of paleosol humic acids. *Chemical Geology*, *53*(3-4), 175–184.

Selwitz, R. H., Ismail, A. I., & Pitts, N. B. (2007). Dental caries. *The Lancet*, *369*, 51–59

Singer, A. and Huang, P.M. (1990). Effects of Humic Acid on the Crystallization of Aluminum Hydroxides. *Clays and Clay Minerals*, *38*(1), 47–52.

Singer, P. (1994). Control of Disinfection By-Products in Drinking Water. *Journal of Environmental Engineering*, *120*(4), 727–744.

Singer, P. C. (1999). Humic substances as precursors for potentially harmful disinfection by- products. *Water Science and Technology*, *40*(9), 25–30.

Snoeyink, V.L. and Jenkins, D. (1980). *Water Chemistry*. New York: John Wiley and Sons

Sollo, F. W., Larson, T. E., Mueller, H. F., & Sollo, B. F. W. (1978). *Fluoride Removal from Potable Water Supplies*. Retrieved from Fluoride Removal from Potable Water Supplies\nweb.extension.illinois.edu/iwrc/pdf/136.pdf

Sposito, G. (Ed.). (1996). *The Environmental Chemistry of Aluminum* (2nd ed.). Lewis Publishers. Retrieved from http://www.cabdirect.org/abstracts/19911956179.html

Srimurali, M., Pragathi, A., & Karthikeyan, J. (1998). A study on removal of fluorides from drinking water by adsorption onto low-cost materials. *Environmental Pollution*, *99*(2), 285–289.

Stehouwer, M. (2014). *Defluoridation and Natural Organic Matter Removal in Drinking Waters by Alum Coagulation*. University of Texas at Austin.

Stewart, T. (2009). Removal of Fluoride from Drinking Water: Alumina Based Adsorption (Term Paper). Institute of Biogeochemistry and Pollutant Dynamics, ETH Zurich, 1-24.

Stumm, W. (1995). The Inner-Sphere Surface Complex. *Aquatic Chemistry*, *244*(244), 1–32.

Su, C., & Suarez, D. L. (1995). Coordination of Adsorbed Boron: A FTIR Spectroscopic Study. *Environmental Science & Technology*, *29*(2), 302–

Su, C., & Suarez, D. L. (1997). In Situ Infrared Speciation of Adsorbed

Carbonate on Aluminum and Iron Oxides. *Clays and Clay Minerals*, *45*(6), 814–825.

Swedlund, P. J., Miskelly, G. M., & McQuillan, A. J. (2009). An attenuated total reflectance IR study of silicic acid adsorbed onto a ferric oxyhydroxide surface. *Geochimica et Cosmochimica Acta*, *73*(14), 4199–4214.

Tang, Y., Guan, X., Wang, J., Gao, N., McPhail, M. R., & Chusuei, C. C. (2009). Fluoride adsorption onto granular ferric hydroxide: Effects of ionic strength, pH, surface loading, and major co-existing anions. *Journal of Hazardous Materials*, *171*(1-3), 774–779.

Thermo Scientific. (2011). *User Guide: Fluoride Ion Selective Electrode*.

U.S. Environmental Protection Agency. (1998a). *Announcement of Small System Compliance Technology Lists for Existing National Primary Drinking Water Regulations and Findings Concerning Variance Technologies* (Vol. 63).

U.S. Environmental Protection Agency. (1998b). *Variance Technology Findings for Contaminants Regulated Before 1996*.

U.S. Environmental Protection Agency. National Primary Drinking Water Regulations; Announcement of the Results of EPA's Review of Existing Drinking Water Standards and Request for Public Comment, Pub. L. No. 40 CFR Part 141 (2002).

U.S. Environmental Protection Agency. (2003). *National Primary Drinking Water Regulations; Announcement of Completion of EPA's Review of Existing Drinking Water Standards*.

U.S. Environmental Protection Agency. (2005). *Economic Analysis for the Final Stage 2 Disinfectants and Disinfection Byproducts Rule*.

U.S. Environmental Protection Agency. National Primary Drinking Water Regulations: Stage 2 Disinfectants and Disinfection Byproducts Rule, Pub. L. No. 40 CFR Parts 9, 141, and 142 (2006). United States of America.

U.S. Environmental Protection Agency. (2010). *National Primary Drinking Water Regulation; Announcement of the results of EPA's Review of Existing Drinking Water Standards and Request for Public Comment and/or Infornmation on Related Issues*.

U.S. Environmental Protection Agency. (2015). *Safe and Sustainable Water Resources: Strategic Research Action Plan 2016-2019*.

United Nations. The human right to water and sanitation, Pub. L. No. 64/292 (2010). Retrieved from http://www.un.org/es/comun/docs/?symbol=A/RES/64/292&lang=E

Venyaminov SYu, & Prendergast, F. G. (1997). Water (H2O and D2O) molar absorptivity in the 1000-4000 cm-1 range and quantitative infrared spectroscopy of aqueous solutions. *Analytical Biochemistry*, *248*(2), 234–245.

Villalobos, M., & Leckie, J. O. (2001). Surface Complexation Modeling and FTIR Study of Carbonate Adsorption to Goethite. *Journal of Colloid and Interface Science*, *235*(1), 15–32.

Vithanage, M., Jayarathna, L., Rajapaksha, A. U., Dissanayake, C. B., Bootharaju, M. S., & Pradeep, T. (2012). Modeling sorption of fluoride on to iron rich laterite. *Colloids and Surfaces A: Physicochemical and Engineering Aspects*, *398*, 69–75.

Water Innovation Network for Sustainable Small Systems: A National Center for Innovative Small Drinking Water Systems. (2016). Retrieved from https://www.umass.edu/winsss/content/small-systems

Westerhoff, P., Chao, P., & Mash, H. (2004). Reactivity of natural organic matter with aqueous chlorine and bromine. *Water Research*, *38*(6),

Wijnja, H. (1999). *The Interaction of Carbonate and Organic Ions With the Adsorption of Inorganic Anions on Hydrous Metal Oxides*. The University of Connecticut.

Wijnja, H., & Schulthess, C. (2000). Vibrational Spectroscopy Study of Selenate and Sulfate Adsorption Mechanisms on Fe and Al (Hydr)oxide

Surfaces. *Journal of Colloid and Interface Science*, *229*(1), 286–297.

Wijnja, H., & Schulthess, C. P. (1999). ATR–FTIR and DRIFT spectroscopy of carbonate species at the aged γ-Al2O3/water interface. *Spectrochimica Acta Part A: Molecular and Biomolecular Spectroscopy*, *55*(4), 861–872.

Wijnja, H., & Schulthess, C. P. (2002). Effect of Carbonate on the Adsorption of Selenate and Sulfate on Goethite. *Soil Science Society of America Journal*, *66*, 1190.

Xu, Y., Axe, L., Yee, N., & Dyer, J. A. (2006). Bidentate complexation modeling of heavy metal adsorption and competition on goethite. *Environmental Science and Technology*, *40*(7), 2213–2218.

Yan, M., Wang, D., Ni, J., Qu, J., Chow, C. W. K., & Liu, H. (2008). Mechanism of natural organic matter removal by polyaluminum chloride: Effect of coagulant particle size and hydrolysis kinetics. *Water Research*, *42*(13), 3361–3370.

Yang, X., Roonasi, P., & Holmgren, A. (2008). A study of sodium silicate in aqueous solution and sorbed by synthetic magnetite using in situ ATR-FTIR spectroscopy. *Journal of Colloid and Interface Science*, *328*(1), 41–47.

Yu, G., Saha, U. K., Kozak, L. M., & Huang, P. M. (2007). Combined effects of tannate and ageing on structural and surface properties of aluminum precipitates. *Clays and Clay Minerals*, *55*(4), 369–379.